POLITECNICO DI TORINO

Corso di Laurea Magistrale

in INGEGNERIA PER L'AMBIENTE E IL TERRITORIO

Tesi di Laurea Magistrale

Satellite stereo data for DEM/DSM extraction

Relatore:

Prof. Piero Boccardo

Correlatore:

Arch. Constantin Sandu

Studente:

Giuseppe Mansueto

Anno Accademico 2018/2019

Abstract

The quite recent availability of satellite stereo pairs allows users to extract three-dimensional data that can be used in different domain of applications, such as urban planning, energy, emergency management, etc. This work aims to extract Digital Surface Models (DSM) from satellite stereo pairs acquired by three different satellites (Deimos-2, Pléiades-1A and WorldView-3) over the area of the city of Turin. The results are then assessed in term of geometric accuracy comparing them with a cadastral point height dataset, used as benchmark. The comparison in terms of difference height values (between the DSM and the benchmark), calculated on a set of sample points. Just two of the generated DSM guaranteed a high height accuracy level useful for the domain of application such as existing cartography update, emergency management, building damage assessment, roof slope and solar incoming radiation assessment. Further developments will investigate different blending techniques and software that could provide more accurate results.

Table of contents

1. Introduction

The development of the VHR (very high resolution) optical satellites, permitted to achieve a ground sample distance lower than 1 m. This increased the geo-referencing accuracy and the mapping capability and allowed in the last years an improvement in resolution of DEM, DTM and DSM (Hu *et al.*, 2016). A digital elevation model (DEM), often referred to as a digital terrain model (DTM), depicts bare earth, while a DSM represents the topography of the earth's surface including buildings and vegetation (*Fig. 1)* (Maune, 2011). The generation of DSM, through the use of high resolution stereoscopic satellite pairs, together with the correspondence of the images, allows more precise and economically more advantageous measurements of large land surfaces (Poon *et al.*, 2005). This thesis work aims to extract a Digital Surface Model (DSM) over the city of Turin from a satellite stereo pair acquired by three different satellites, comparing the result in term of geometric accuracy with a cadastral point height dataset.

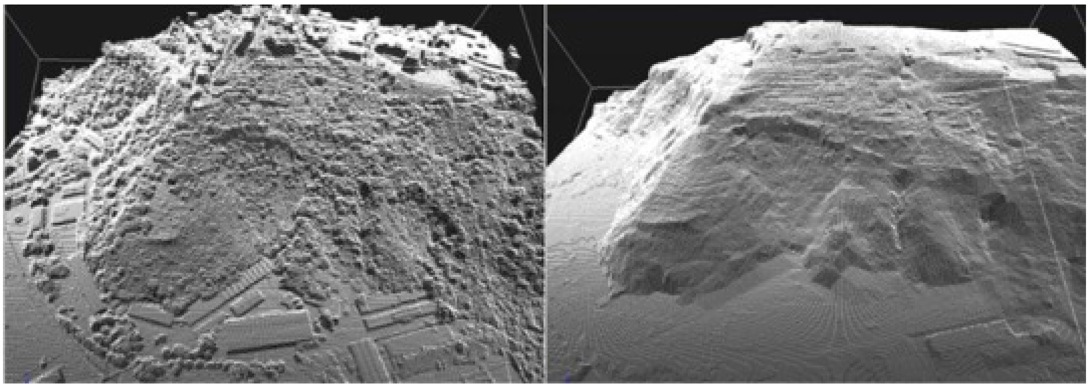

Figure 1 - Comparison between a DSM (left) and a DTM (right) processed from a Lidar scan of Naples area (Amato, 2015)

The survey, describes the common datasets and procedures for the DSM generation, explores the potential of stereoscopic images of Deimos-2, Pléiades-1A (in two and tri stereo mode) and WorldView-3 satellites for this purpose, assessing them from qualitative and quantitative point of view. The investigation was carried out processing the cityscape of Turin, regional capital of Piedmont in Italy, located at the geographic coordinates of 396630.87 East and 4991599.92 North, UTM (WGS84) Zone 32N. The dataset used is composed by VHR stereo imagery: for Deimos-2, Plèiades-1A acquired in panchromatic and for WorldView-3 in multispectral mode. The three satellites differ in acquisition resolution (ground sample distance) and WorldView-3 is the satellite with higher one (even in multispectral present higher resolutions than in the other satellites panchromatic images). Thus, it is expected that WorldView-3 guaranteed the best performance. The DSMs generation is been managed using OrthoEngine a software package available in PCI Geomatica 2018, using, as points for the collimation and orientation of the two images (three in the case of Pléiades-1A tri-stereo DSM), firstly an automatic collection of Tie points (TPs) and secondly adding to them a manual collection GCP (ground control points). After the comparison between the obtained products, noting that the DSM generated with the use of TPs only, the models were reported on the geoid, obtaining for each point a geoid referred height. The next phase was the characterization and evaluation of generated models, evaluating which of the DSMs guarantee the best representation of heights. The first step consisted in a qualitative analysis of the data, evaluating noise, sharpness in city canyons, ability in shaping the geometries and identification of details (vegetation, small objects on the ground). The second step instead concerned the evaluation of the altimetric accuracy of the models through the use of two different benchmarks (one ground height and the other gutter height referred).

Following there were outlined possible applications of DSMs extracted by satellite stereo pairs allows users to extract three-dimensional data that, with the help of 3D GIS tools, can be used in different domain of applications: existing cartography update, soil consumption analysis, urban green classification, evaluation on mobile network antenna positioning, emergency management, building damage assessment, roof slope and solar incoming radiation assessment.

2. DEM, DTM and DSM generation

"The term Digital Elevation Model (DEM), digital terrain model (DTM), and Digital Surface Model (DSM) are often incorrectly used as synonyms and a myriad of definitions exist in an attempt to distinguish these terms" (Saha, 2014). A DEM is defined as "digital cartographic representation of the elevation of the land at regularly spaced intervals in x and y directions, using z-values referenced to a common vertical datum" (Maune, 2011). Terrain bare-earth representations can be termed as either DEM or DTM (Saha, 2014), but DTM can be considered an upper level in comparison to normal DEM. This because in the DTM the discrimination characteristics of the terrain (breaklines, mass points, …) are better delineated, determining also an higher cost, related to the not automated generation of it (Maune, 2011).

DSM, instead, is a representation of the Earth's surface that includes all objects, both natural and anthropogenic ones (buildings, trees, power lines etc.), more suitable for 3D modeling, telecommunications management or forest management purposes (Saha, 2014). These 3D elevation models can be referred or to the mathematical ellipsoidal surface, reporting the ellipsoid heights, or to the geodic surface, showing the elevations of each point. An ellipsoid is defined as the surface generated by the rotation of an ellipse, with "$\propto$" as major semi-axis and "β" as minor semi-axis, on its own major axis *(Fig. 2)*.

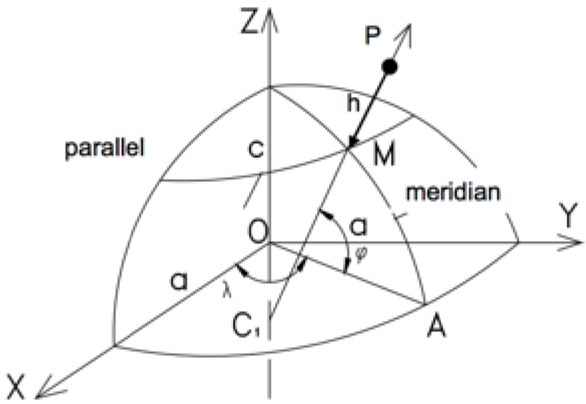

Figure 1 - The mathematical ellipsoid from which geographic coordinates (latitude and longitude) are referenced and from which ellipsoid heights are surveyed by GPS (Roggero, 2014)

The reference ellipsoid used in cartography is a smooth and mathematic surface, in which the geographic coordinate are the latitude (φ), measured in Nord or South degrees from the equator, and the longitude (λ), measured in East or West degrees from the Greenwich meridian. The heights, instead, are referred to GPS surveys, which normally adopt as reference ellipsoid the World Geodetic System of 1984 (WGS84) (Maune, 2011).

The geoid *(Fig. 3)* is defined as the average surface of the ocean, irregular level surface on which the gravitational potential is constant *(Roggero, 2014)*.

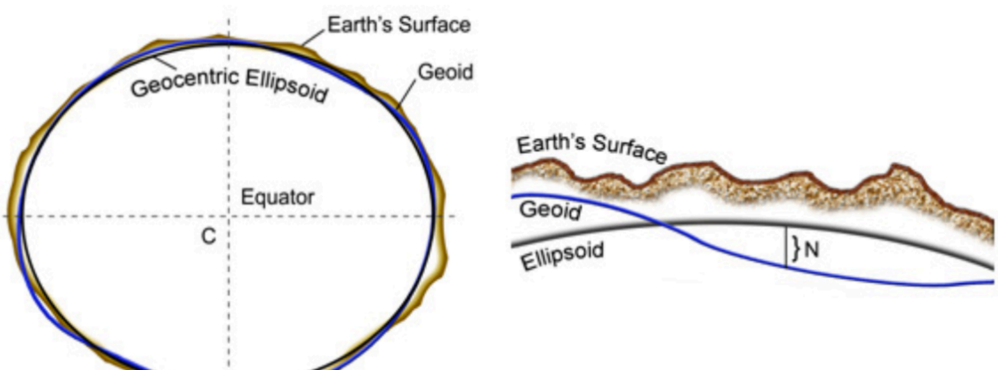

Figure 2 - Geocentric ellipsoid, geoid and earth surface in comparison (Maune, 2011)

The difference in altitude (N) between the geoid and the ellipsoid *(Fig. 4)* is defined as geoid ondulation, normally with local variations in the range of -106 m and +85 m. This is expressed mathematically as:

$$N = h - H$$

where:

- H, the elevation (also called orthometric height), is defined as the distance from the geoid measured on a plumb line;
- h, ellipsoid height, defined as distance between a point on the heart surface and the ellipsoid surface, measured by GPS on the perpendicular to the mathematical ellipsoid;
- N, geoid height (geoid ondulation), difference between h and H.

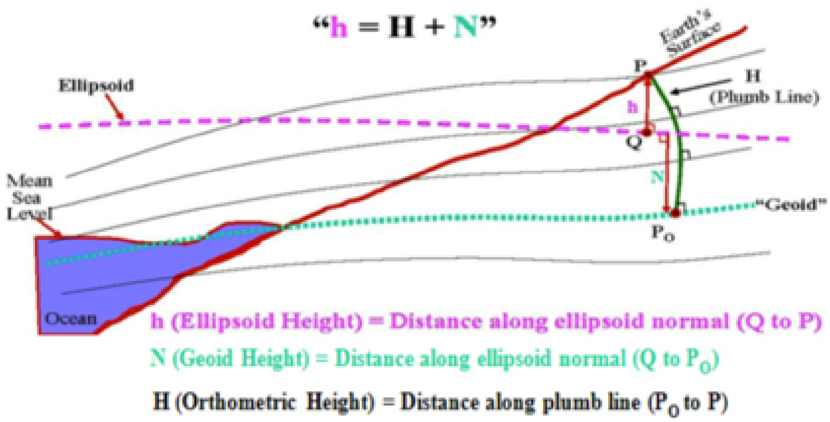

Figure 3 - Ellipsoid, geoid height and elevation in comparison (Maune, 2011)

2.1. Common procedures

There are many ways to achieve DTMs and DSMs, cartographic DTM, photogrammetry methods, LIDAR (Airborne light detection and ranging) technology, IFSAR techniques, generation from VHR stereo satellite images, and each of them present a different level of accuracy and resolution, depending on the sensor of the camera, its inclination and the distance from the ground.

2.1.1. Cartographic DTM

Digital mapping is often used as information base from which are extracted useful data for the production of digital terrain models (DTM). The operation is facilitated by the nature of digital mapping data: these are mostly vector data, in which each cartographic object is represented by a sequence of three-dimensionally referenced geo points, topologically organized and classified by categories. The creation of a database for a DTM takes place by extracting from a digital cartography all the elements that describe the altimetry, such as the single elevation points and the vertices of the polygonal contours, and interpolating them with an appropriate algorithm (TIN or other).

The DTMs produced in this way, especially if taken from large-scale digital mapping (1:5000), are used in many engineering applications, from the general design of civil and road works to the study of the evolution of hydrodynamic and geomechanical phenomena.

The procedure for creating cartographic DTMs follows these steps: from the ASCII files, that contain the geometries of the various sheets (normally at the 1:5000 scale), all the vertices that delimit the isolines are identified and extracted, as well as those that identify significant points for the altimetry. These objects are identified by codes that identify them as a direct, intermediate, auxiliary contours, or as an isolated dimensioned point of a photogrammetric origin. The elements thus selected, purified by the accessory codes, constitute a set of points which, appropriately interpolated (by TIN or other methods), allows the direct creation of the DTM.

On densely vegetated areas the aerial view of the terrain can be closed off for vast tracts; the cartographer finds himself in the impossibility of collimating points directly on the ground. The proportion of the land is determined, in this case, by subtracting from the measurable one the crown, a "plausible" value, variable according to the recognizable tree species. Due to this fact, the map shows a morphometric information of the terrain with quite varied precision: areas in which the plane-altimetric positions of the represented elements respect decimetrical tolerances, can mix seamlessly in areas where the topographical information have mere descriptive value, strongly penalized from the physical nature of the places (Barilotti *et al.*, 2014).

Faced with these problems, LIDAR technology emerges as an instrument capable of acquiring data directly on the ground to produce high quality digital surface models (DSM), from which to derive by numerical filtering and DTM classification of great precision and detail.

2.1.2. LIDAR (Airborne light detection and ranging) technology

LIDAR technology, presenting a higher accuracy, density and automation level in DSM with respect to a traditional photogrammetry, is common used for urban DSMs, for environmental protection aims and for the comparison with models with lower resolution *(Fig. 5 - 6).* Indeed, thanks to the use of lasers, it is possible to scan very large areas, reaching up horizontal coordinates and elevations of the terrain and most of the objects on it (trees, buildings, sidewalks, …) (Queija, Stoker and Kosovich, 2005). Its high productivity in acquisition of a crowded 3D points cloud in a short time range, allows LIDAR technology to develop different data structures variating in digital surface representation, accuracy and resolution: TINs, triangular irregular networks, and regular grids. Moreover, the doppler effect give the possibility to hole the vegetation, and so the capacity to determine the morphology of the natural terrain even if it is hidden (Shi, Zheng and Tian, 2009).

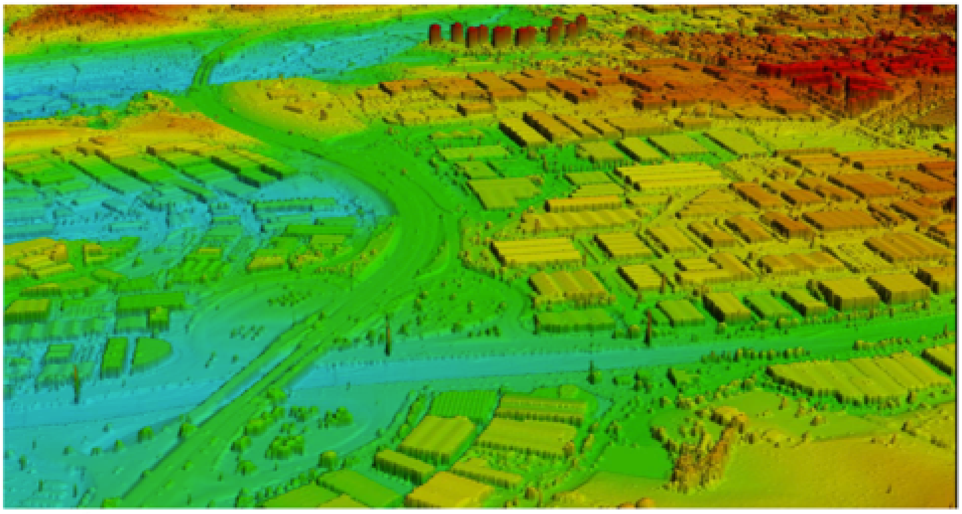

Figure 4 - DSM of Terrassa from LIDAR (InstitutfürMethodik der Fernerkundung (IMF))

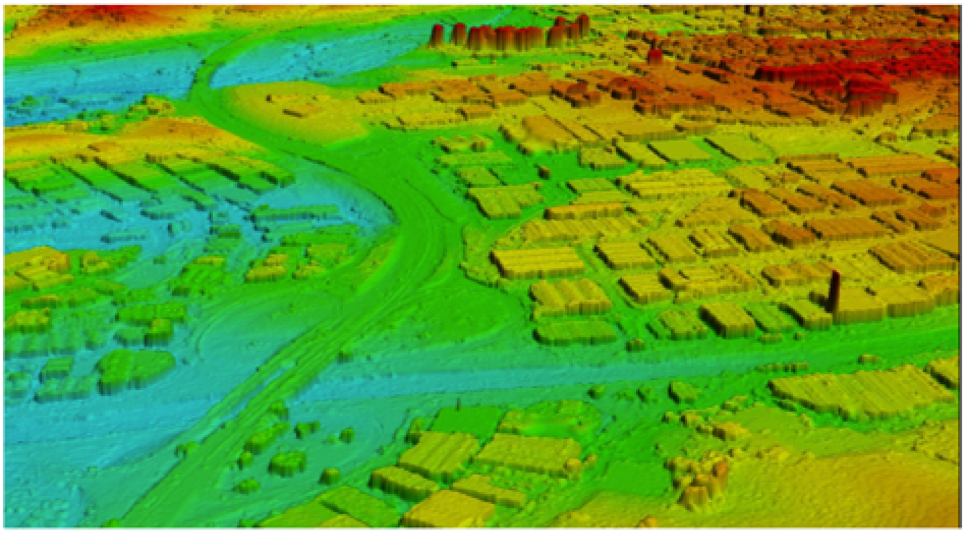

Figure 5 - DSM of Terrassa from Worldview-1 stereo satellite images (InstitutfürMethodik der Fernerkundung (IMF))

Depending on the type of application, the acquisition system can be airborne *(Fig. 7),* land-based or mounted on a dynamic terrestrial detection device.

The frequency of sampling allows the acquisition of a high number of points (several hundreds of thousands of points per second) per surface unit which, in relation to the scale of the survey, allows an extremely wide range of applications.

A scanning laser system, both aerial and terrestrial, is equipped with a laser range finder that determines the distance between the emission point (materialized by the rangefinder) and the point of reflection, which represents the generic point belonging to the terrain or to a possible structure, artifact or other. The rangefinder measures the time that the laser pulse takes to travel the round-trip distance between emission and reflection; distance is a function of the "flight time" and of the signal propagation speed, which in the air is the speed of light. The scanner not only measures the distance between the points, but also provides the relative or absolute coordinates of the reflection point.

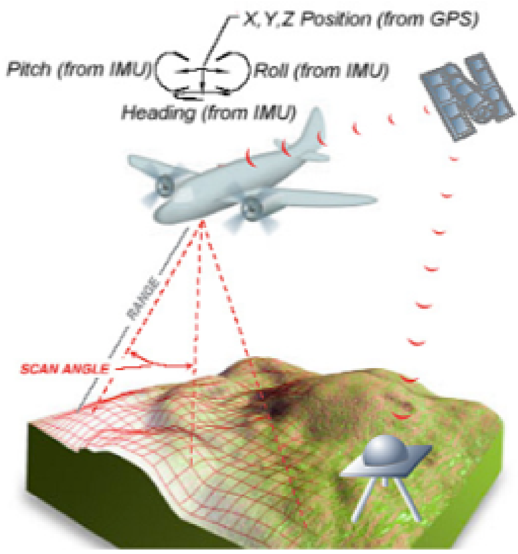

Figure 6 - LIDAR airborne acquisition system (Maune, 2011)

In this way, as a direct result of the measurement session, as said before, we will have a set of three-dimensional coordinates (real numerical model), referred to a very high number of points (point cloud) that are hit by the laser beam. The point cloud is the real digital description of the surface of the scanned object. Concerning the aerial Lidar, the georeferencing of the points is obviously more complex, since it must be taken into account the temporal space displacement of the plane and its oscillations around the own aces in flight. The problem is solved by connecting the Lidar sensor to an inertial navigation system (INS) and a satellite positioning system (GPS), installed on board, to determine the position and orientation of the aircraft in each instant. The system is also connected to GPS stations on the ground, placed on top of a specially designed geodetic network, to correct the position of the aircraft in post processing of data.

The georeferencing of the acquired model, as well as allowing to place the relief correctly in the space, and therefore to make all the necessary measurements and in-depth analysis, also allows the detection of the same objects or portions of territory at different times, thus making monitoring in the time.

A new widely tested application in this sense is the support that this method can provide in the field of geomechanical analysis, both in the planning and verification of on-site checks and in the preparatory measures and assessments for the design, for the securing of ridges and rock slopes. For the ridges, the correct reconstruction of the morphology of the terrain is also essential in the elaboration of simulation calculations, both in terms of trajectory (two-dimensional and three-dimensional) and energy (Amato, 2015).

The points detected can be classified in the post processing phase, because the "intelligence" of the survey is in the aftermath, that is possible to distinguish the points relating to the terrain, to the artifacts, to the vegetation, to form a metric survey *(Fig. 8)* and extract "geometric primitives" for solid modeling (Led and Diode, 2018).

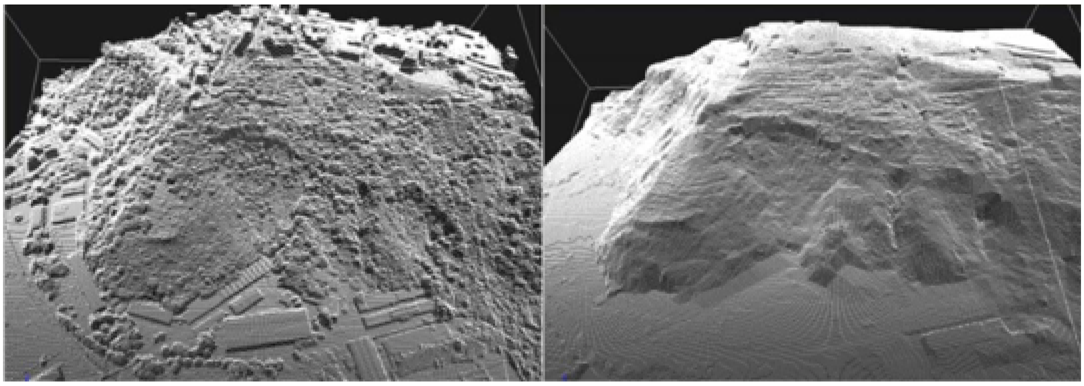

Figure 7 - Comparison between a DSM (left) and a DTM (right) processed from a Lidar scan of Naples area (Amato, 2015)

A significant improvement is achieved in the physical model of the places investigated, and information that is otherwise not perceptible by ordinary terrestrial and aerial survey methods often emerges.

The terrestrial methodology operates in a range of distances that, according to the instrumental types, can range from the sub-meter to the kilometric, and the accuracy generally varies from a few millimeters to a few centimeters, in relation to the instruments used and to the distance of the apparatus from the target to be detected.

For the aerial laser, the accuracy is generally decimetric, in the case in question the relief, compared with a topographic precision survey, presented a deviation of about 10-15 cm. With distance measurement, these instruments are generally able to measure also the amplitude of the return (reflectance) signal of each object-point at the proper frequency of the ray. This depends on the material that has reflected the radius, or even better on the characteristics at the time of the survey of the material. Since most laser scanners use near-infrared frequencies, reflectance will produce an infrared image pattern of the air or land survey performed (Amato, 2015).

2.1.3. IFSAR (Interferometric Synthetic Aperture Radar)

IFSAR technology uses two radar antennas installed on an aircraft used for overflights of the regions to be surveyed; this technique has the advantage of carrying out surveys of the earth's surface with a radar technique that is better than satellite, as well as being in three dimensions: with contained costs it is thus possible to reach accuracies comparable to those obtained with the use of satellites (from 5 meters to some tens of centimeters) depending on the slope of the ground (Mason and Data, 2008).

Looking at the two airborne in the figure 9, it is possible to notice that on the first one (on the left) is mounted a X-band radar, that looks just in front of the airborne, and that the second is improved by a further P-band radar and that is able to look in two different directions. Both of this IFSAR system produce DSMs from their X-band radar sensor, mapping vegetation, buildings and all the objects present on the terrain. In this way all the data regarding the shape of the terrain are missed. The second IFSAR system solve this problem using a second sensor, the P-band one, which is capable to penetrate all the objects on the top reflective surface.

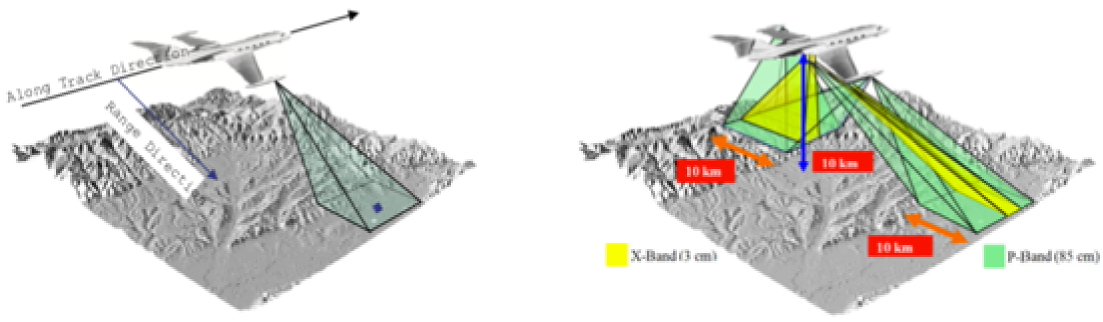

Figure 8 - two airborne using IFSAR sensors during data acquisition; the first (on the left) uses X-band radar, the second (on the right) is improved with both a X-band and a P-band radar (Maune, 2011).

As all technologies, IFSAR presents advantages, such as the possibility to use it in bad weather conditions (allowing to penetrate clouds) and the low cost of the survey, but also disadvantages. Indeed, layover, shadows or foreshortening can potentially cause the miss of some data *(Maune, 2011)*. It is also preferable, in order not to interfere with daytime air traffic and because the wave range is not within the visual spectrum, to make this surveys during the day (Mason and Data, 2008).

2.1.3.1. SRTM (Shuttle Radar Topography Mission)

The Shuttle Radar Topography Mission (SRTM), launched in the February of 2000, used the IFSAR technologies to create an unique dataset reporting more than the 80 percent of the Earth's land area. Thusly, thanks to this mission, it was born the first public near-global high resolution DEM, available for everybody (Berry, Garlick and Smith, 2007). Before this mission the best public dataset presented a GSD (a spatial resolution) of 1 km. Experimental researches were acted upstream the choice to test the accuracy of this method in all the situations and with different vegetation cover class, comparing the results it with other methods, like LIDAR techniques. The response of the preliminary studies evidenced a much better interpretation of the elevation, with respect to a overestimation of the elevation for the LIDAR, especially in densely vegetation environments (Shortridge, 2006).

2.1.4. VHR stereo satellite DSM generation

Satellite remote sensing has fundamental advantages such as, for example, the possibility of performing acquisitions at regular intervals, continuous monitoring of the area, or the possibility of acquiring data in developing territories. Given the great potential of panchromatic satellite images, various research projects have recently been launched on the interpretation and extraction of metric data from very high resolution stereo satellite couples (Nascetti, 2011). Stereo images are photographs of the same testfield but acquired with a short difference in time, and so presenting two different perspective views. Thanks to the stereo photogrammetry the perspective projection of the images is converted into an orthographic projection, obtaining a better depth perception.

The stereoscopic images, a VHR satellite stereo couple, enable the generation of digital model of the surface or of the terrain, mapping the elevations of a given area (Maune, 2011). The extraction of DSM from high resolution satellite stereo pairs is presented as a very advantageous alternative, thanks to the simplicity of data acquisition and the availability of numerous commercial software (such as PCI Geomatics, software used for the experimental part of this thesis) and algorithms able to extract 3D digital models.

For the extraction of DEMs from satellite images, various photographic calculations are necessary, two phases can be distinguished: the orientation of satellite images and the matching process. The orientation models can be divided into rigorous models and generic models. The firsts use a photogrammetric approach based on the collinearity equations, while in the second models the image coordinates are linked to the ground ones by polynomial relationships of which the coefficients are known (RPC).

Matching is the process that allows the recognition of homologous points between the two images, that the same points of the ground taken on the two frames. In this way we obtain a cloud of corresponding points in the two images and thus, knowing the acquisition geometry, we are able to construct the three-dimensional model of the terrain (Nascetti, 2011). This homologous point cold be distinguished in tie points (TPs) and ground control points (GCPs).

Once the images are collimated, the DSM can be generated. There is just another intermediate process before: the creation of Epipolar Images. “The epipolar geometry is the intrinsic projective geometry between two views. It is independent of scene structure, and only depends on the cameras' internal parameters and relative pose” (M. Thompson et al., 2017). The generation of these is fundamental and linked to the perception of the depth. With one camera, and then with one acquired stereo image, it’s not possible to appreciate the depth in the image. If we want to, we need two stereo images, with 2 different points of view. Considering one point in the first image, we know the position of it in the image space and we know that it is a projection of an object, but we can’t know how far it was from the camera when it was acquired. Now, if considering the same object acquired in the second image (that has another point of view), if it is not known its position in the image, it is needed a lot of work to link this to the one in the first image, obtaining the depth. The epipolar line, representing the geometrical space of all the possible projection of the rays, that link the object to the point representing it in the second image, into the second image, help in this research.

2.1.4.1. Tie and ground control points

As said before, a fundamental requirement in the stereo photogrammetric measurement is the knowledge of the position and the attitude of the camera at the moment of the image shooting. When it is not possible to directly determine all six external orientation parameters, a procedure called aerial triangulation (TA) is used. This is the traditional method for determining the external orientation of a frame of frames. The image coordinates of the frame and the object coordinates on the ground need to be posed in a relationship.

Based on the principle of collinearity, is constructed a system that relates the two coordinates, in order to determine the parameters of external orientation.

There are two categories of points:

- binding points (TP - Tie Points): points of which only the image coordinates are known, and which are measured automatically *(Fig. 10);* even if the object coordinates are not known it is possible to use them to the ground control over areas where you do not have ground control points (GCP).

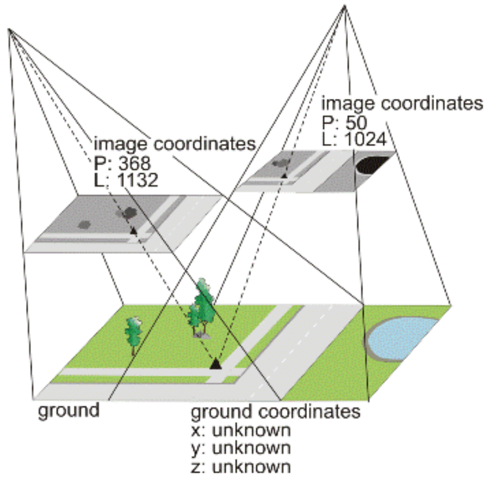

Figure 9 - Tie points (PCIGeomatics, 2019)

- support points (GCP - Ground Control Point): points of which both the image coordinates and the object coordinates are known. The image coordinates are measured manually by the operator, recognizing them on the individual frames, while the object coordinates are measured topographically by considering a system of geographic or projected coordinates.

Resuming, the TPs help to collimate and orientate the stereo photogrammetric couples and the GCPs rest the block on the geoid.

The GCPs need to be identifiable in both images and with known object coordinates. Their coordinates are usually determined topographically, it is possible to extract this information from existing cartographic maps (technical maps or orthophotos). In this case, particular attention must be paid to the quality of the measurements taken, because strongly influences the final result of the orientation (Dicar, 2015).

A fundamental aspect to take into account is the RMSE, Root Mean Square Error, average between the RMSE on the x and y axis, of each collected point. For a good collimation, this value needs to stay under a tenth of the pixels size of the image.

2.2. Dataset for DSM generation from VHR stereoscopic satellites images

The dataset is composed by civilian VHR stereo satellites images, which allows creating first-rate quality stereo geometry thanks to a convergence angle higher than 0.5, improving the DSM vertical accuracy. In addition, this type of satellites can acquire more than one image, with a difference inclination, in a low acquisition time difference (1-3 minutes), deleting the radiometric variation and facilitating the DSM generation. (Manuel Ángel Aguilar et al., 2013). The following chapters are made to describe the characteristics, performances and capture modality of the common used satellites for DSM generation.

2.2.1. Deimos-2

With a lifetime of at least seven years, Deimos-2 is a very-high (1 m in panchromatic at nadir) resolution stereo multispectral optical satellite purchased by UrtheCast company. Launched in the 19th of June 2014, its multispectral capability includes 4 channels in the visible and near infrared spectral range (red, green, blue and NIR). The satellite is equipped with a push-broom VHR camera with 5 spectral channels (1 panchromatic, 4 multispectral), improved by the fast and precise rotation of the platform which hold it. Its sun-synchronous orbit at a mean altitude of 620 km, with a local time of ascending node of 10h30, allows an average revisit time of two days worldwide (one day at mid-latitudes).

DEIMOS-2 has four imaging modes: single strip imaging, multi-pointing imaging, single-pass stereo imaging and tessellation imaging:

- Single Strip Imaging: 12 km wide and up to 1,400 km long image. The satellite has a ±45o across-track tilting capability (being ±30o the nominal range);
- Multi-pointing Imaging: DEIMOS-2 can perform multi-pointing *(Fig. 11)* imaging, switching from one target to another with minimum idle time;
- Single Pass Stereo Imaging: Two acquisitions of the same area in the same orbit, with different pitch angles. Images are 12-km wide and up to 200 km long. The viewing angles are different for the two images, in order to allow the generation of 3D models;
- Tessellation Imaging: Two acquisitions of the same area in the same orbit, with different pitch and roll angles. Images are 24-km wide and up to 200 km long (composed from the acquisition of two adjacent strips, 12-km wide each, and captured with a lag of a few seconds);

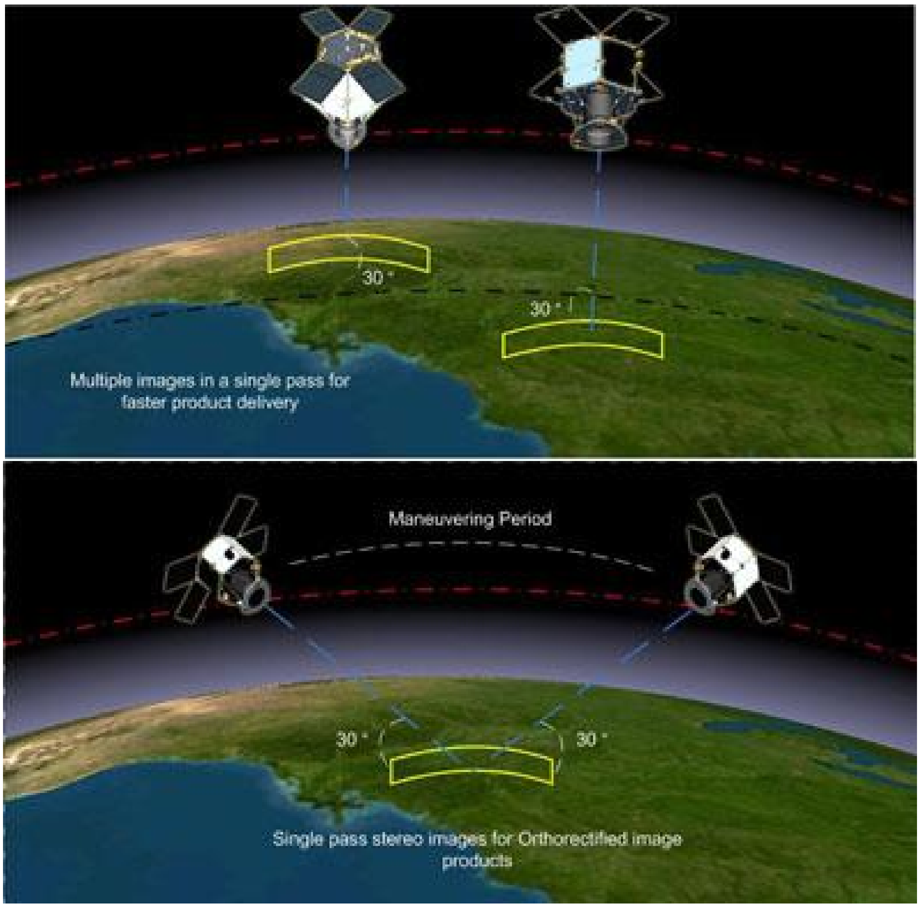

Figure 10 - Deimos-2, comparison between multi-pointing imaging and stereo pass imaging modes (Galileo *et al.*, 2015)

The control, download, processing and data storage of the acquired images is administered by Deimos Imaging, that in order to guarantee at least one contact with the satellite to each orbit has four ground stations and a better response time (Boecillo (Spain), Kiruna (Sweden) and Inuvik (Canada)).

This satellite is typically used for agriculture health control, pasturage management, evaluation of dryness cases, urban planning or coastline control (Galileo et al., 2015).

2.2.2. Pleíades-HR

Pleiades-HR *(Fig. 12)* is a very-high (0.5 - 0.7 m in panchromatic at nadir) resolution stereo multispectral optical satellite constellation composed by two spacecraft purchased by CNES (Space Agency of France) company. The first of the two was launched in 2009 (Codou *et al.*, 2016).

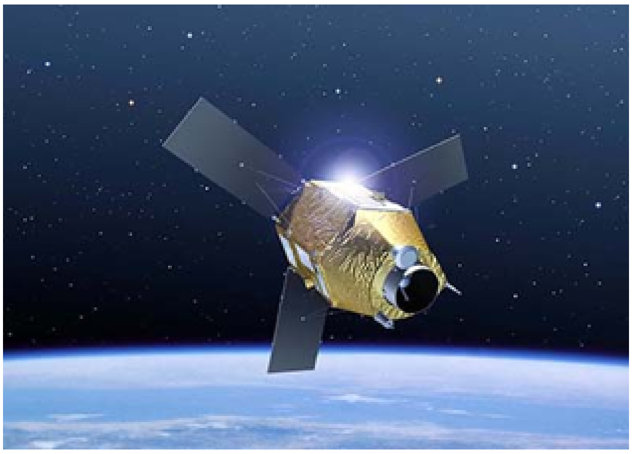

Figure 11 - Pleiades-1A satellite sensor (Satellite imaging corporation)

The satellite is equipped with a VHR camera with four spectral bands (blue, green, red, and IR), able to reach up an image location accuracy of 3 meters (CE90) without ground control points, with the possibility to improve it to 1 meter using GPSs. Its sun-synchronous orbit at a mean altitude of 694 km, capable of acquiring high-resolution stereo imagery in just one pass, and can accommodate large areas (up to 1,000 km x 1,000 km) (Airbus Defence & Space, 2013).

One of the aims of this mission is the provision of provision of so-called "level-2 products" to customers consisting of a panchromatic image with a merged multispectral image orthorectified on a DTM (Digital Terrain Matrix) (Codou *et al.*, 2016).

The download of the acquired images can be requested from Pléiades constellation satellites less than six hours before they are acquired, irreplaceable function in situations where the expedited collection of new image data is crucial, such as crisis monitoring" (Satellite imaging corporation) (Airbus Defence & Space, 2013).

Pléiades-HR afford also a tri-stereo terrain data generation approach, which differs from conventional stereo data generation through the application of two oblique and one near-nadir viewing of the terrain, as opposed to just two oblique views *(Fig. 13)*; which provides the ideal solution for accurate 3D modelling. This is especially relevant in areas of high relief variation, including dense, high-rise urban landscapes, where the tri-stereo image coverage (2 x oblique and 1 x nadir) image combination significantly minimizes the problem of data 'loss error' areas in the final Digital Surface Model (DSM). This can result in a reduction of ± 75% of "hidden area objects", which can arise with conventional 2 x oblique image coverages, as a result of object lean and view obscuring effects Pléiades tri-stereo mode, acquired from the same orbit during the same pass, is particularly favorable for reaching the required metric accuracy because images are radiometrically and geometrically very homogeneous, which allows a very good radiometric matching for relief computation. The final terrain datasets consisted of 1 meter GSD resolution DSM, and a derived (equivalent resolution) Digital Terrain Model (DTM), with vertical (LE90) absolute and relative accuracies of ≤ 1.5 and 1 meters respectively; and horizontal (CE90) absolute and relative accuracies of ≤ 1.5 and 1.5 meters respectively. A significant advantage to the overall objectives of the project was that the tri-stereo data acquisition was able to acquire both the 2 x oblique and 1 x nadir imagery *on the same day*, so that there was a direct link between the modelled topography and the derived land-cover/use dataset, mapped from the nadir image" (M. Thompson et al., 2017).

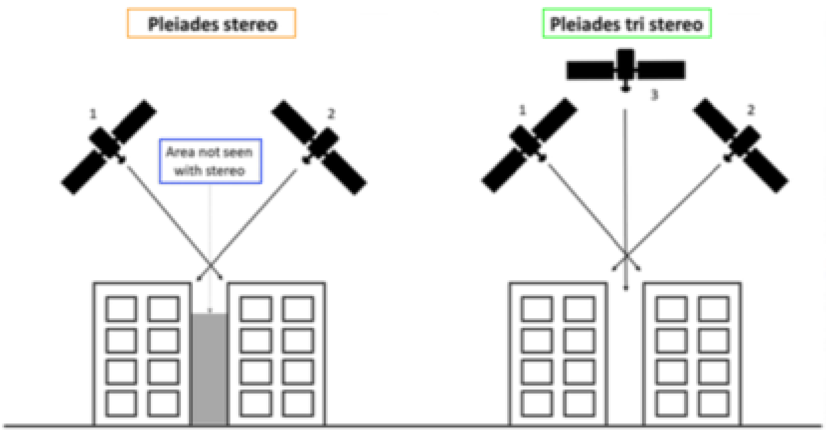

Figure 12 - Comparison between stereo and tri-stereo Pleiades acquisition (Panagiotakis *et al.*, 2018)

2.2.3. Cartosat-1

Cartosat-1 *(Fig. 14)* is a high (spatial resolution of 2.5 meter and cover a swath of 30 km) resolution stereo multispectral optical satellite build by ISRO (Indian Space Research Organization) company. Launched by the PSLV on May 5, 2005 at Sriharikota (India). The satellite is equipped with two panchromatic cameras that take black-and-white stereoscopic pictures in the visible region of the electromagnetic spectrum, mounted in such a way that near simultaneous imaging of the same area from two different angles is possible. Its sun-synchronous orbit at a mean altitude of 617 km, with a local time of ascending node of 10h30 and an orbital repeat cycle of 116 days. The acquired images, firstly stored in a 120 Gb solid state recorder, are then transmitted to ground stations when the satellite is in the visible zone.

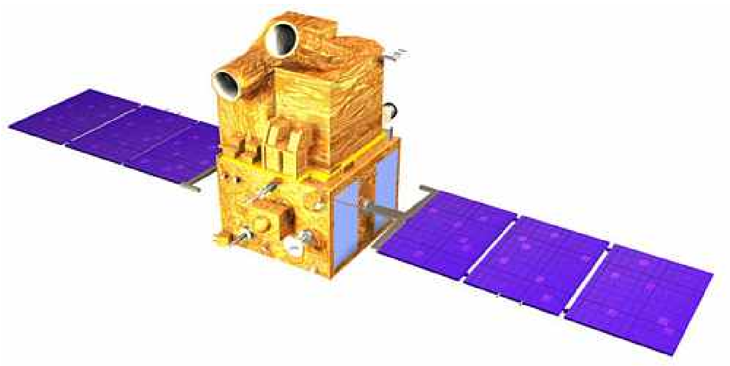

Figure 13 - Cartosat-1 satellite sensor (Image Copyright © ISRO)

This satellite is typically used for large scale mapping applications and stimulate newer applications in the urban and rural development, land and water resources management, disaster assessment, land cover change detection, relief planning and management, environmental impact assessment and various other Geographical Information Systems (GIS) applications (Satellite imaging corporation, 2016).

2.2.4. DigitalGlobe Inc. VHR satellite constellation

This satellite constellation *(Fig. 15)*, composed by Worldwiew-1, Worldwiew-2, Worldwiew-3, Worldwiew-4 (no longer operating due to a malfunction) is the DigitalGlobe Inc. very-high resolution stereo multispectral optical satellite constellation.

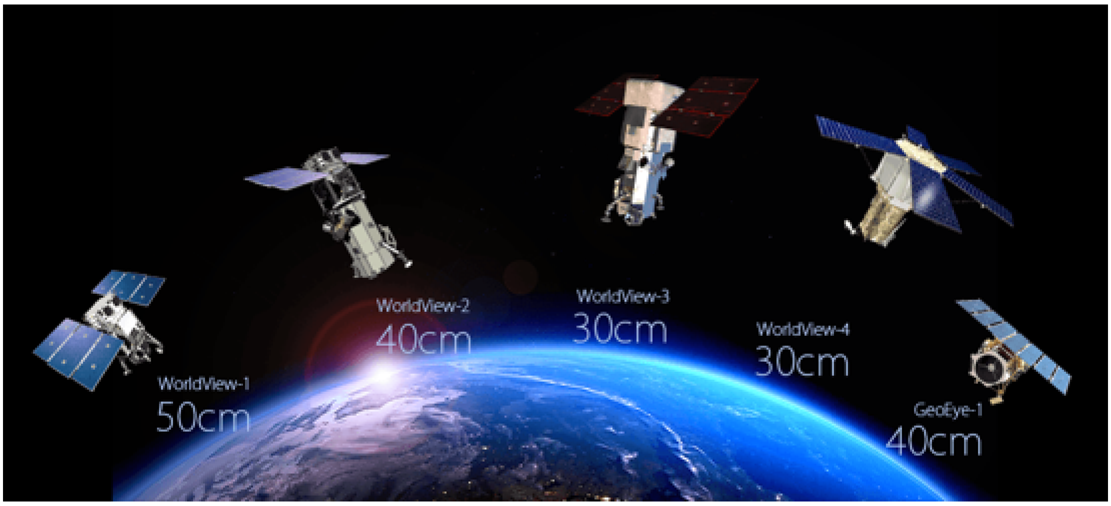

Figure 14 - WorldView satellite constellation and Geoeye-1

2.2.4.1. Geoeye-1

Geoeye-1 *(Fig. 16)* is a very-high (50 cm in panchromatic mode and 2 m in the four multispectral bands) resolution stereo multispectral optical satellite purchased by DigitalGlobe company. GeoEye-1 shows a remarkable agility that allows it to acquire rather large areas in stereoscopic mode: in this way pairs of images with similar acquisition conditions are obtained, particularly valid for the extraction of Digital Terrain Models (DEM).

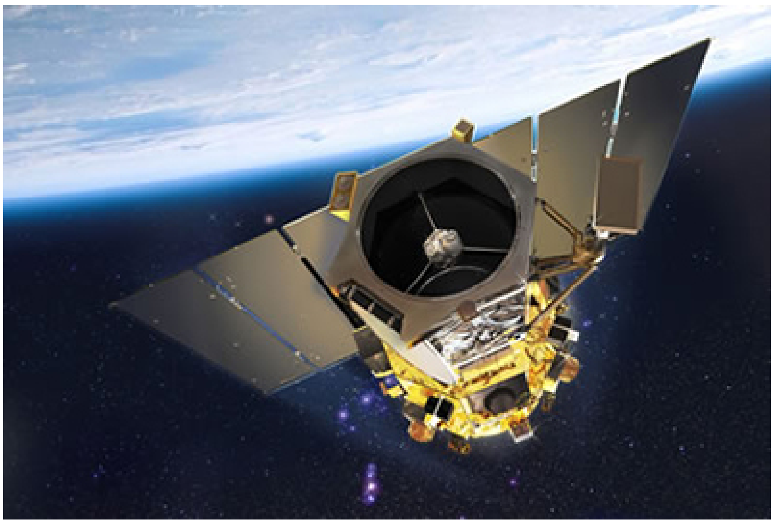

Figure 15 - Geoeye-1 satellite sensor (Satellite imaging corporation, 2016)

Launched in the 6th September 2008, its multispectral capability includes 4 channels in the visible and near infrared spectral range (red, green, blue and NIR). The satellite is equipped with a VHR camera with 5 spectral channels (1 panchromatic, 4 multispectral), improved by the fast and precise rotation of the platform which hold it. Its sun-synchronous orbit at a mean altitude of 770 km, with a local time of ascending node of 10h30, allows an average revisit time of three days worldwide following a polar orbit (Satellite imaging corporation, 2016). Geoeye-1 present a location accuracy of 5 meters (CE90) without ground control points, with the possibility to improve it to 3 meter using GPSs.

The planimetric accuracy offered by GeoEye-1 allows the user to map natural and anthropogenic objects directly on the image acquired with an error of less than 3 meters compared to their actual position on the earth's surface.

This satellite is typically used for defence and national security, air and sea transport, petroleum products and gas, cartography and location-based services, risk management and environmental monitoring and natural resources aims (Ita *et al.*, 2019).

2.2.4.2. WorldView satellite constellation (WV1, WV2, WV3)

WorldView-1, WorldView-2 and WorldView-3 was launched respectively in 2007 (with 50 cm of resolution in panchromatic mode), in 2009 (providing 46 cm of resolution in panchromatic mode and 1,85 m in eight multispectral bands) and in 2014, with PAN resolution at 0.31 m and multispectral one at 1.24 m.

WorldView-3, launched November 11, 2016 at 10:30 a.m., is the latest in a constellation of commercial high-spatial resolution Earth imaging satellites developed by DigitalGlobe Inc. It is equipped with a VHR camera with 29 spectral channel: 1 panchromatic, 8 multispectral, 8 SWIR bands (from 1.2 to 3.7 m of special resolution), 12 CAVIS bands ("Clouds, Aerosols, Water Vapor, Ice, and Snow" at 30 m resolution for atmospheric compensation), improved by the fast and precise rotation of the platform which hold it. All of them are sun-synchronous orbit with a local time of ascending node of 10h30 (Kruse, Baugh and Perry, 2015).

Worldview satellites are well known for *"the agility of the satellites not only makes the revisit period shortened but also enriches the satellite working mode to a large extent. The agility provided by the CMG devices makes the stereo imaging process flexible. There are primarily two situations for the along-track stereo area collection, i.e. multiple-view stereo and stitched stereo. Both utilize the attitude maneuvers ability of satellite, the former acquires stereo-images of the same target area from at least triple view angles, while the latter aims at achieving a wide ground coverage by acquisition of several stitched stereo-pairs, alleviating the restriction in swath width of sensor due to the enhancement of spatial resolution. Taking the situation of dual stereo-pairs for instance, the stereo area covering a size of 26.6 km by 112 km at maximum is available. As shown in the figure, there are mainly four imaging periods. After completing a period forward push-broom scanning to attain an image strip (Fig. 17 (a)), the satellite moves forward with reverse attitude maneuvers immediately in the pitch direction and meanwhile changes the satellite pointing direction through side swaying, in this way capturing the second image strip (Fig. 17 (b)) which is adjacent and overlapped with the first one with a translational distance smaller than swath width of sensor; then, with continuous reverse maneuver long the orbit and also a certain angle of side swaying, the satellite carries out a period forward push-broom scanning again over the first strip to form as a stereo-pair (Fig. 17 (c)); next, the satellite carries out forward push-broom* *scanning again over the second strip to form as another stereo-pair (Fig. 17 (d)); finally, the two stereo-pairs with a certain overlapping area cross the orbit are obtained"* (Hu *et al.*, 2016).

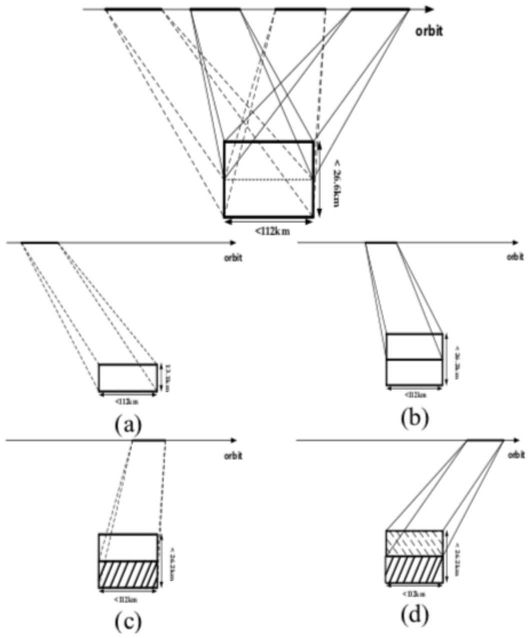

Figure 16 - Demonstration of the stitched stereo imaging mode (the situation of dual stereo-pairs)

2.3. Application domain

The application domain of Digital Elevation Model is strictly related to its data processing level. It is possible to distinguish 5 levels of detail:

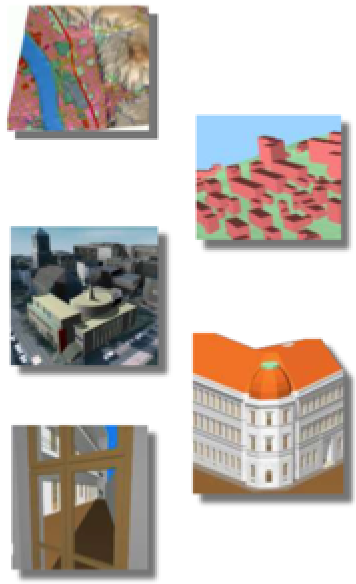

Figure 17 - Different LOD in DSM

- LOD 0 - Regional model: 2.5D DTM;
- LOD1 - City/Site model: "block model", characterized by the absence of rooftops on the buildings;
- LOD2 - City/Site model: textured, with a differentiated roof structures;
- LOD3 - City/Site model: "rendering", detailed architecture model;
- LOD4 - Interior model: "walkable", architecture model more detailed than LOD3.

The last three, as it is possible to see in the figure 18, are models which require an higher processing level, necessary in architecture fields. Instead, the first two are more suitable for civil/environmental application.

Focusing on the environmental domain, LOD0/1 DSM could be a valid instrument both in cities and countryside evaluations:

- Emergency risk analysis: evaluation of flood risk, landslide monitoring, numerical modelling if river beds (Amela, Agostino and Soffia, 2011), vulnerability explosion analysis, etc…;
- Evaluation of city interference factors: noise dispersion simulation, etc…;

- Energetic city evaluation: taking into account the volume of the building its possible to estimate the energy consume or the number of potential photovoltaic panels, etc…;
- Archeologic analysis, as indirect surveys, for the interpretation of complex stratigraphic situation of excavated sites (Archeologica, Studio and Edilizia, 2017);
- Mobile network signals analysis: evaluation of the best points (the higher one) in a given area, for the installation of mobile network antennas;
- Base map for automated guidance car (future application).

3. Study site and dataset

In this chapter will be described the study site area and the used dataset, focusing on each satellite testfield area, resolution and characteristics during the acquisition of it.

3.1. Turin

The city of Turin, regional capital of Piedmont in Italy, is located at the geographic coordinates of 396630.87 East and 4991599.92 North, Zone 32T, referring to the UTM (WGS84) coordinate system (*Latitude and longitude / GPS-coordinates*) *(Fig. 19).* This Italian city, crossed by Po and Dora rivers, with an average height on mean sea level of 239 m and an extension of 130,17 Km2, is centred in front of Susa Valley, surrounded by the western Alpine arch and Superga Hill (www.aboutturin.com).

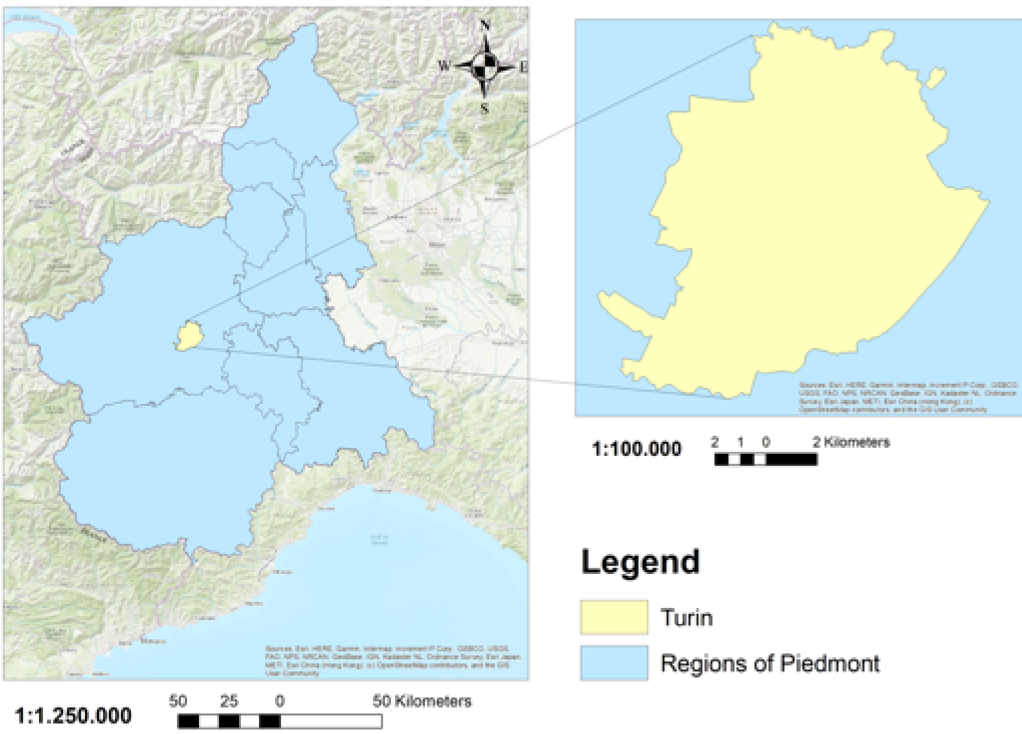

Figure 18 - Study site focus, Turin and Piedmont

3.2. Dataset

The dataset is composed by seven VHR stereo satellite images, two from DEIMOS-2, two from WORLDVIEW-3 and a triplet from the tri-stereo satellite PLÉIALDES-1A.

All the images exhibit a low processing data level, with basic geometric and radiometric elaboration. There were used panchromatic pictures because of their higher GSD resolution; the only exceptions are the multispectral images of WorldView-3. In the attachments *(Att. 1)* is reported a comparative table resuming the characteristics of the 3 satellites

As we can see in the tables *(Tab. 1 - 4 - 8)*, the frames coming from the same satellite presents the same date and a difference of 2/3 minutes in acquisition time, in order to preserve the same solar irradiation which, prevent from shadows-linked errors. Comparing the images from two different satellites, instead, the acquisition date and time don't mach.

The image 20 *(Fig. 20)* and the tables 2 - 3 - 5 - 6 - 7 displays the VHR stereo satellite images, utilized to generate the DSMs*,* in dimension and orientation in the space (base map). It is evident that if the target is to generate a DSMs of a larger area, it will be used as dataset Deimos-2 (highest geometric resolution). On the contrary, if we prefer a better resolution it is suggested to use Worldview-3 dataset, with a GSD (Ground sample distance) of 0.34 m. Pléiades-1Atwo stereo dataset take place in the middle of the two cases: it is a good choice both in radiometric (GSD is 0.5 m) and geometric resolution. At any rates the best choice remain the use of the triplet of Pléiades images, which allow to reach the best DSM result.

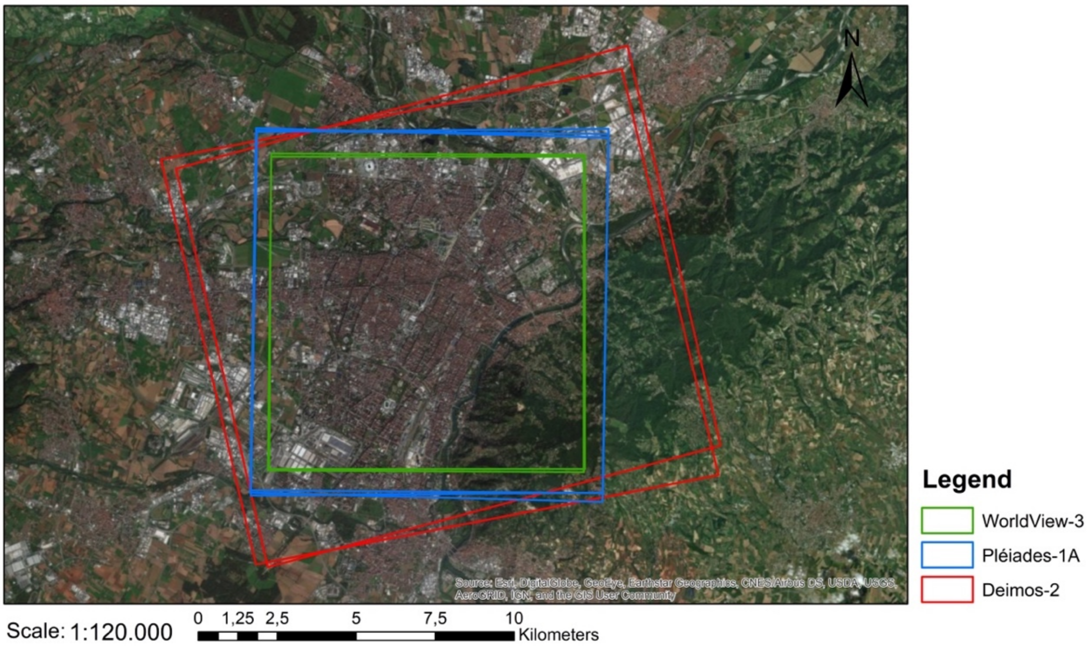

Figure 19 - Location of satellite imagery in Turin testfield. Red: Deimos-2 scenes, blue: Pléiades-1A triplet images, green: WorldView-3 scenes

Table 1 - Characteristics of Deimos-2 panchromatic images (Deimosimaging)

Image ID	DEIM_PAN_L1B (1)	DEIM_PAN_L1B (2)
Acquisition date	2018-07-11	2018-07-11
Acquisition time (GTM)	10:04:50	10:06:34
Type	Stereo-Pan	Stereo-Pan
Incidence angle (DEG)	4	1.4
Sun azimuth(DEG)	133.93	134.68
Sun elevation(DEG)	60.60	60.85
Columns	11712	11712
Raws	8604	8604
Framed area (km^2)	196.3898	196.3898
Bands	1	1
Pixel resolution at nadir (m)	1	1

Table 2 - Dataset frame of DEIM_PAN_L1B (1) (Deimos-2)

X	Y
7.5641867(DEG)	45.1055150(DEG)
7.7452614(DEG)	45.1413350(DEG)
7.7843992(DEG)	45.0302580(DEG)
7.6042639(DEG)	44.9917350(DEG)

Table 3 - Dataset frame of DEIM_PAN_L1B (2) (Deimos-2)

X	Y
7.5566631(DEG)	45.1126700(DEG)
7.7410007(DEG)	45.1409810(DEG)
7.7825677(DEG)	45.0251200(DEG)
7.5976073(DEG)	44.9989050(DEG)

Table 4 - Characteristics of Pléiades-1A panchromatic images (Airbus defence and space)

Image ID	DS_PHR1A (1)	DS_PHR1A (2)	DS_PHR1A (3)
Acquisition date	2018-04-27	2018-04-27	2018-04-27
Acquisition time (GTM)	13:24:06	13:23:08	13:32:55
Type	Stereo-Pan	Stereo-Pan	Stereo-Pan
Along the track incidence (DEG)	10.37	15.13	15.11
Across the track incidence (DEG)	-5.93	-4.69	-4.59
Sun azimuth (DEG)	153.99	153.99	153.99
Sun elevation (DEG)	56.02	56.02	56.02
Columns	21482	21340	21887
Raws	22356	21296	22736
Framed area (km^2)	128.35707	128.35707	128.35707
Bands	1	1	1
Pixel resolution at nadir (m)	0.5	0.5	0.5

Table 5 - Dataset frame (latitude and longitude) of DS_PHR1A (1) (Pléiades-1A)

X	Y
N045°07'08"	E007°35'44"
N045°07'10"	E007°44'13"
N045°01'02"	E007°44'14"
N045°00'58"	E007°35'44"

Table 6 - Dataset frame (latitude and longitude) of DS_PHR1A (2) (Pléiades-1A)

X	Y
N045°07'13"	E007°35'44"
N045°07'10"	E007°44'14"
N045°00'54"	E007°44'14"
N045°00'59"	E007°35'44"

Table 7 - Dataset frame (latitude and longitude) of DS_PHR1A (3) (Pléiades-1A)

X	Y
N045°07'06"	E007°35'44"
N045°07'14"	E007°44'13"
N045°01'03"	E007°44'14"
N045°00'52"	E007°35'44"

Table 8 - Characteristics of WorldView-3 multispectral images (WorldWiew dataset files)

Image ID	S2AS	S2AS
Acquisition date	16-12-2017	16-12-2017
Acquisition time (GTM)	11:05:21	11:06:16
Type	Stereo-Multispectral	Stereo-Multispectral
Across the track incidence (DEG)	-25.0	-26.1
Sun azimuth (DEG)	175	175.2
Sun elevation (DEG)	21.6	21.6
Columns	33333	33333
Raws	33333	33333
Framed area (km^2)	99.4446	99.4446
Bands	3	3
Pixel resolution at nadir (m)	0.3	0.3

4. Data processing and analysis

For processing the stereo satellite data was used PCI Geomatics, specifically OrthoEngine. Using this software we can generate DSM referred to the ellipsoid height or to the elevation (distance from the geoid measured on a plumb line).

In the following chapters it is showed in details the used procedure, schematized in figure 21, to determine the obtained DSMs.

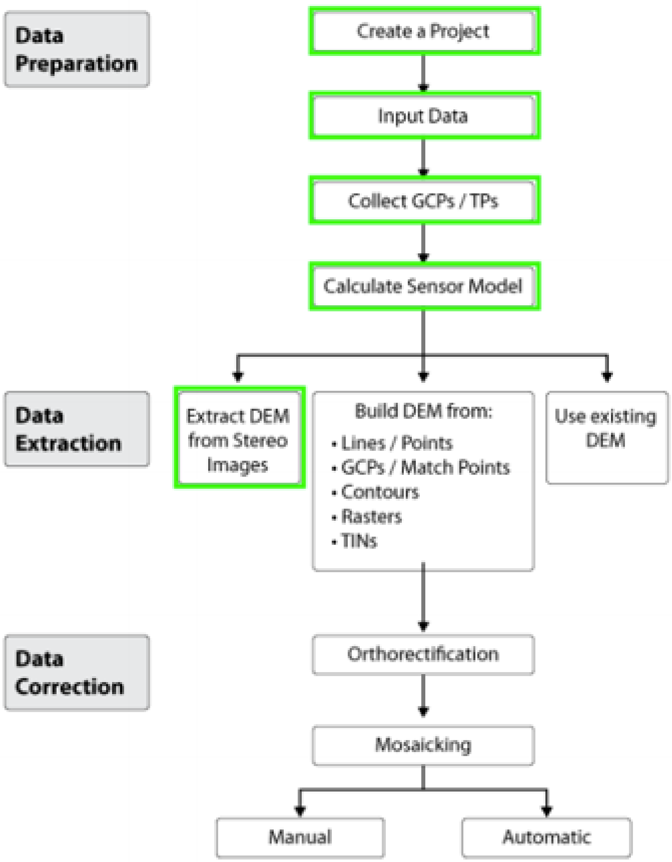

Figure 20 - Geomatica PCI, OrthoEngine process (Geomatica)

4.1. Ellipsoid referred DSM (extraction with Tie points)

Considering, as example, the two VHR stereo satellite images of Turin acquired by Worldview-3, started PCI Geomatics, we will proceed in the OrthoEngine section *(Fig. 22)*.

Figure 21 - PCI, starting the OrthoEngine processing

The first step is to create a new project, imposing as math modelling method the "Rational function" for the "Optical satellite modelling" *(Fig. 23)* and setting up the projection, in order to define a geographic reference system for the DSM *(Fig. 24)*. The geographic system chose is the UTM-WGS84 32N system and the pixel spacing correspond to the resolution of the image (for WorldView-3 is 0.34 in multispectral).

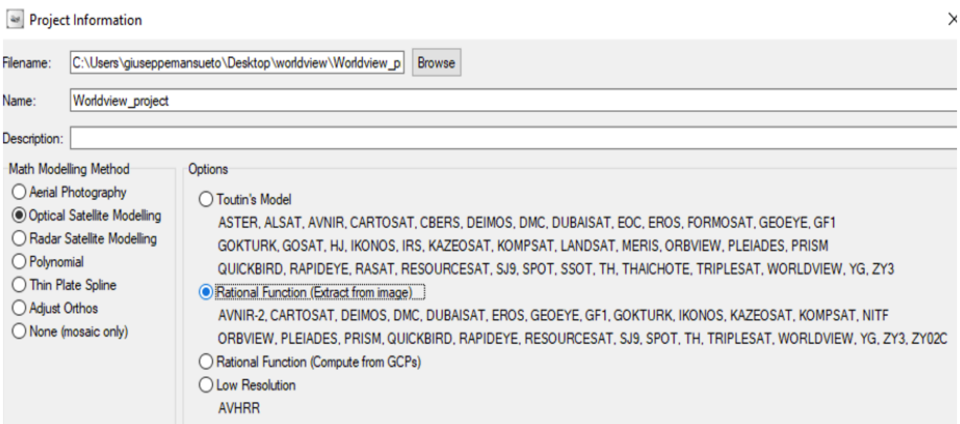

Figure 22 - OrthoEngine, setting up the project information

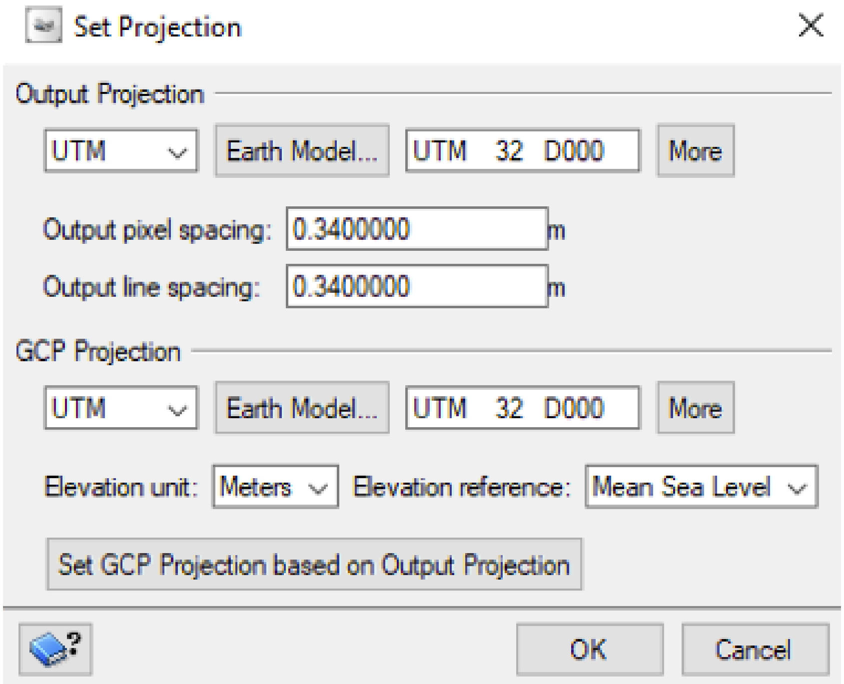

Figure 23 - OrthoEngine, setting up the projection values

The subsequent step is to insert the data (VHR stereo satellite images) using as input the metadata file (.IDM extension) , creating the overviews and saving each of them in a new folder *(Fig. 25 - 26 -27).*

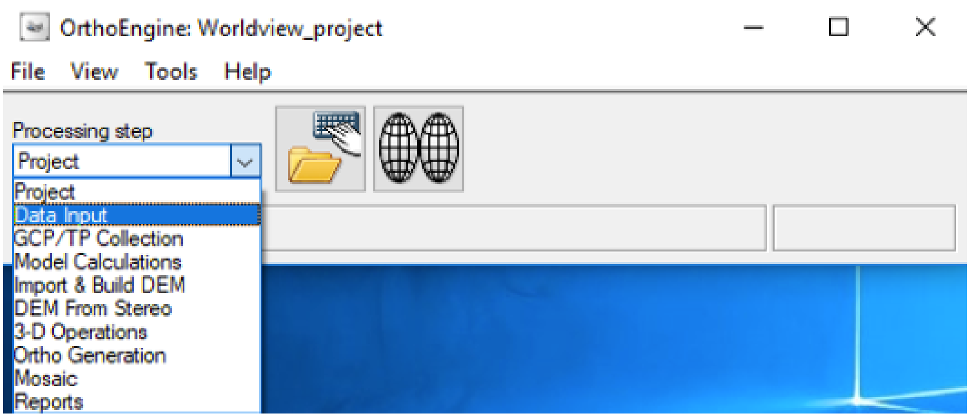

Figure 24 - OrthoEngine, inserting the dataset

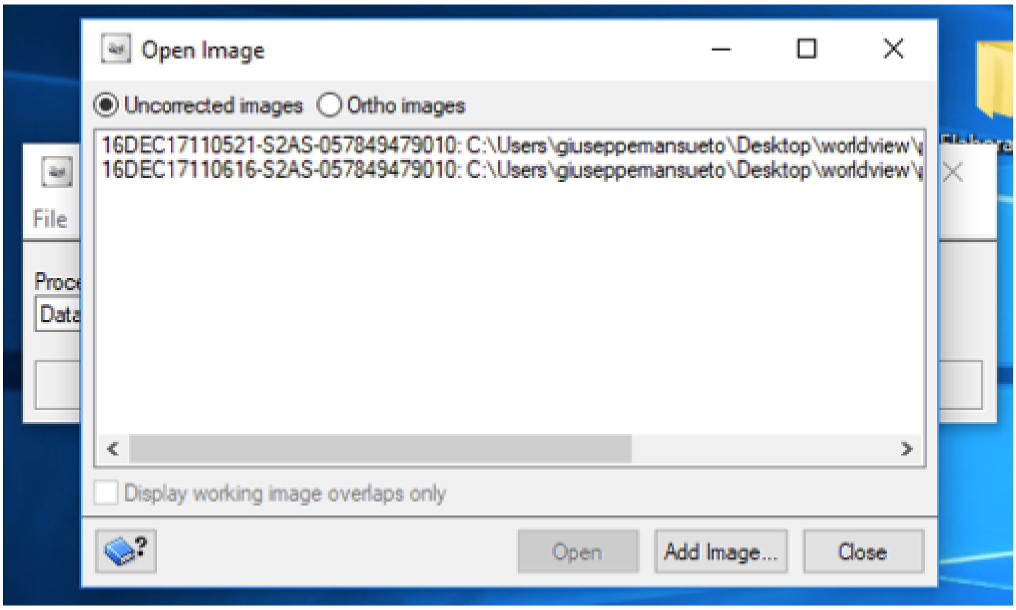

Figure 25 - OrthoEngine, dataset

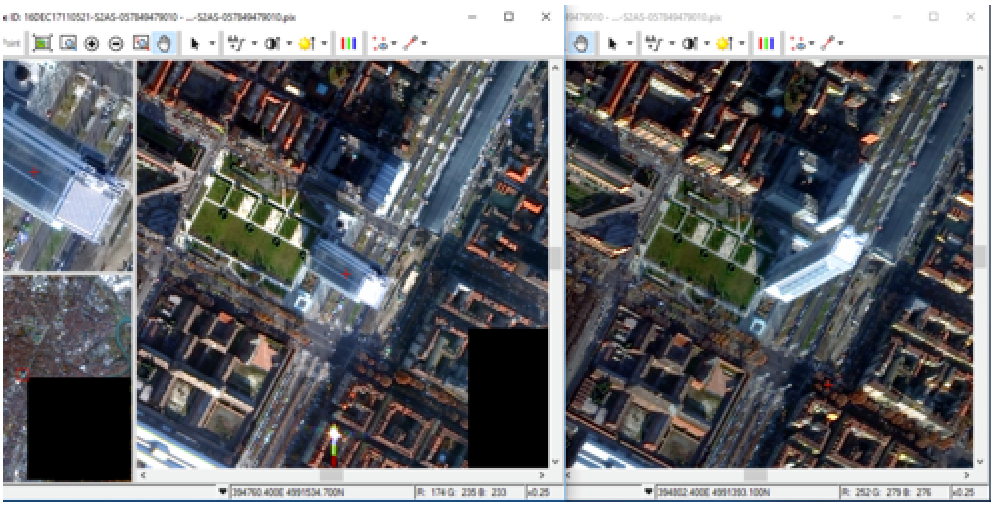

Figure 26 - Views from the two different stereo images

Knowing that the two imported data were acquired from 2 different points of views, due to the different position of the satellite along the orbit, we need to establish some point in order to collimate them *(Fig. 28)*. There are two ways to reach the point:

1. Collecting TIE points, points of which are known just the image coordinates, in the overlap area of the two images (as we did in this case).
2. Collecting GCP points, points of which both image and object coordinates are known, thanks to the support of the regional technical maps that contain

information about quotes and geographic coordinates. This process will be explained better in the following chapter (3.2).

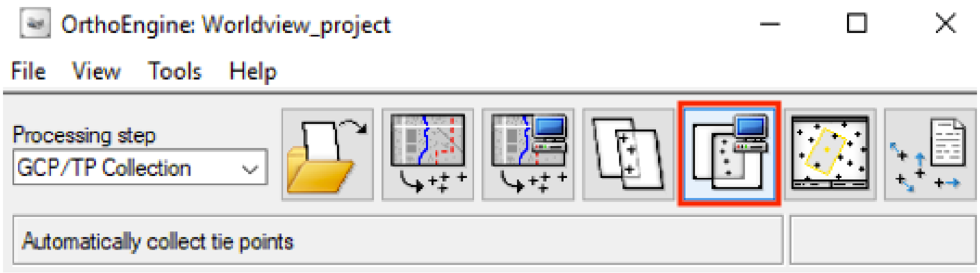

Figure 27 - OrthoEngine, automatic collection of Tie points

Considering the first way, before starting the automatic collection of Tie points, we need to set up some parameter's values *(Fig. 29)*

- "Trial per point" (fixed on 3) is number of iterations the program will do to collect the tie points;
- "Minimum acceptance score", fixed on 0,75;
- "Sample source method", setup on Susan algorithm;
- "Search radius" (fixed on 100), area in which the Susan algorithm can find the tie points;
- "Elevation search strategy".

A fundamental aspect to take into account during the image processing are the physical boundaries of the image ("changes in the local intensity of an image due to object boundaries, changes in surface orientation or material properties") (Gao, Zhu and Guo, 2012), which are always characterized by the presence of noises caused by signal transmission problems or corrupted pixels in the camera sensors.

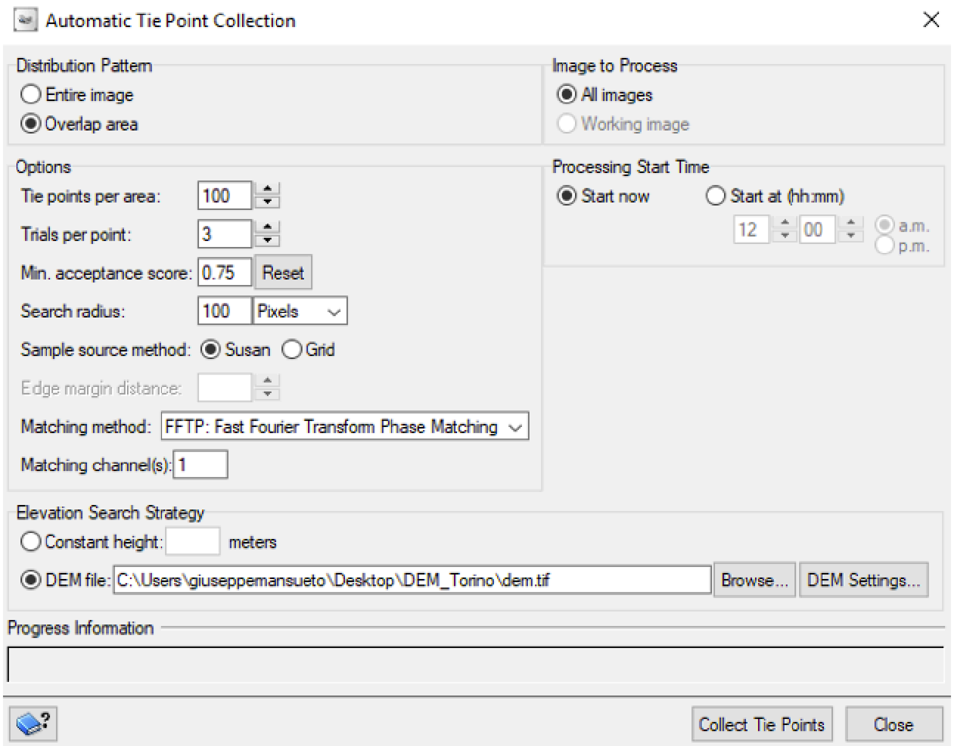

Figure 28 - OrthoEngine, setting up automatic Tie points collection options

In order to obtain a better edge map, the SUSAN algorithm (Smallest univalue segment assimilating nucleus) is the best choice in image processing because, in only one pass over the input image, can come upon the boundary and corners of the image, removing the usual isolated impulse noises. SUSAN works starting with USAN pixels (already corrected): a circular filter is moved on the image *(Fig. 30)* and if the difference in intensity between a pixel inside the circle and the nucleus of the circle is under a given limit value, that pixel assume the intensity of the nucleus itself. It is possible to write:

$$S(ro) = \sum_{r \in N(r_0)} C(r_0, r)$$

Where $C(r_0, r)$ is defined as:

$$C(r_0, r) = \begin{cases} 1 \ if \ |f(r_0) - f(r)| \le T \\ 0 \ if \ |f(r_0) - f(r)| > T \end{cases}$$

where r_0 and r represent, respectively, the positions of the nucleus and of any other point within the mask; $f(r_0)$ and f(r) denote the corresponding intensities; T is the threshold of brightness difference.

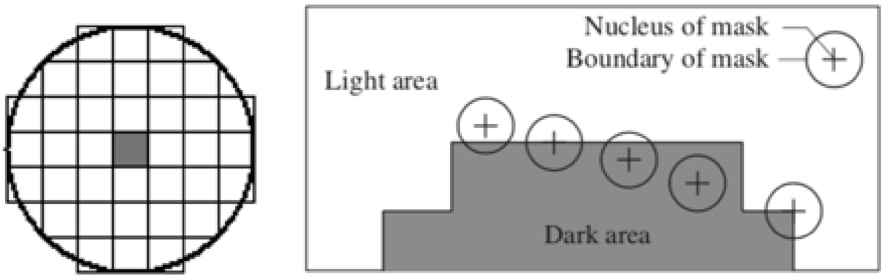

Figure 29 - 37 pixels circular filter (on the left) and 5 circular filter differently displaced in an image (on the right) (Gao, Zhu and Guo, 2012)

After this pixel correction it is possible to create the SUSAN algorithm:

$$R(r_0) = \begin{cases} G - S(r_0) & if \ S(r_0) < G \\ 0 & other \ cases \end{cases}$$

Concerning the elevation search strategy, a SRTM DEM, set up in some elevation parameters *(Fig 31),* was used as base. Fixed all this background contents, starting the collection of the Tie points, as it is possible to see, PCI will detect their image coordinates *(Fig. 32)*.

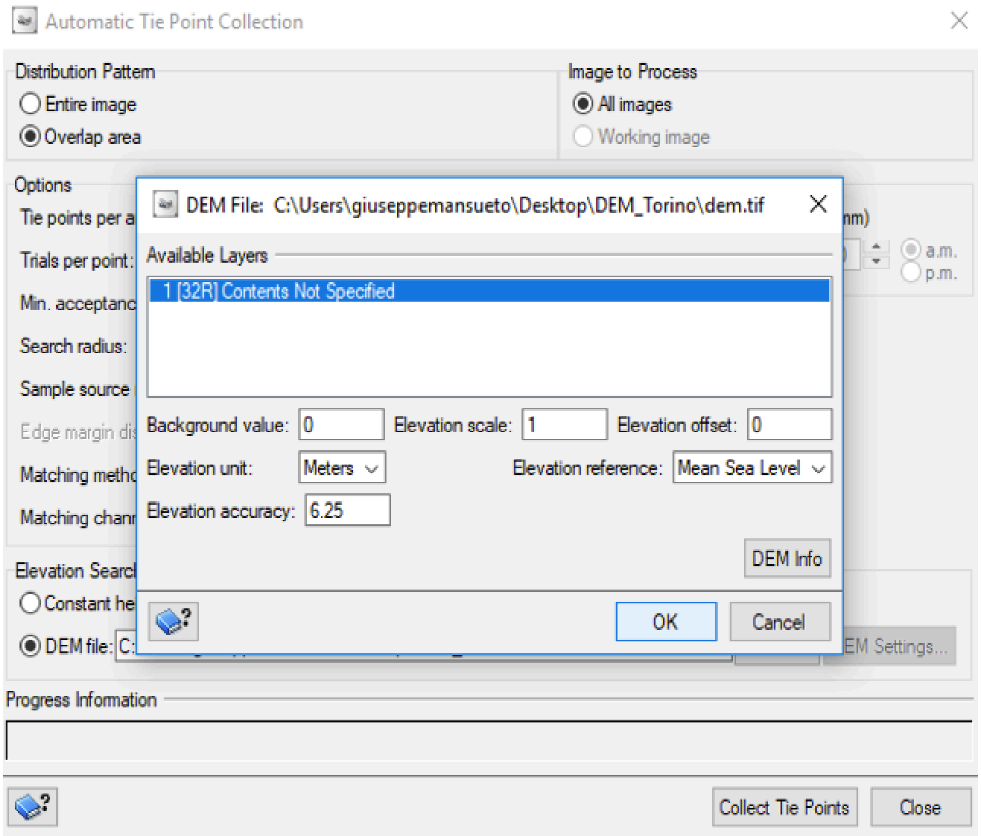

Figure 30 - OrthoEngine, automatic Tie point collection, setting the SRTM DEM parameters

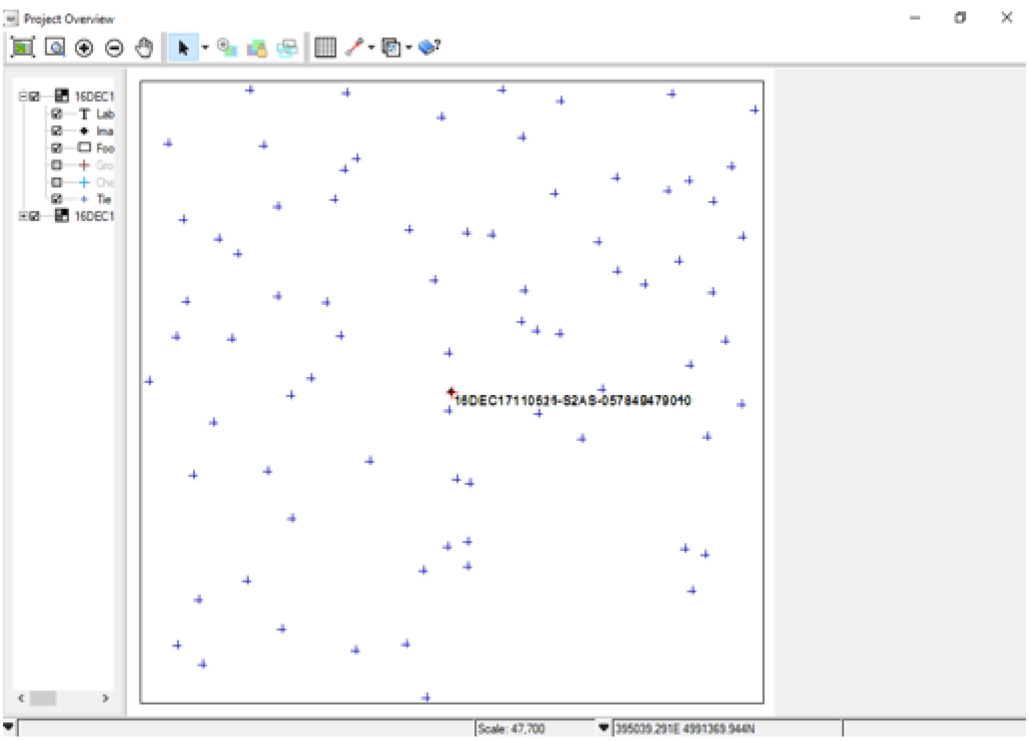

Figure 31 - Collected Tie point in the imagery space

The important aspect to take in account is that not all the collected tie points "valid" for the collimation of the two images. The program could have made some errors of evaluation. According to this, we have to check up in the "Residual report" section *(Fig. 33)*, the global RMSE, Root Mean Square Error, (average between the RMSE on the x and y axis) of all collected tie points. This value needs to be a tenth of the pixels size of the image, then in this case RMSE needs to stay under 0,1.

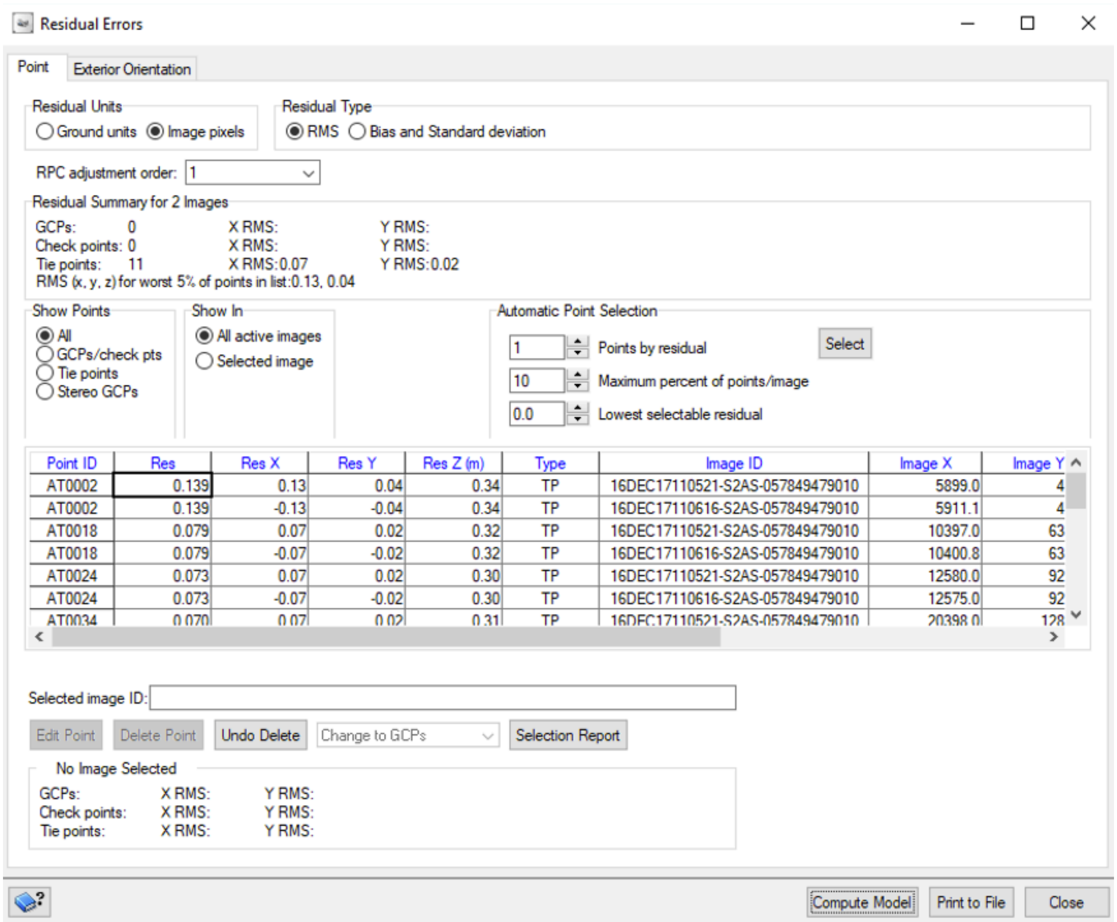

Figure 32 - OrthoEngine, Tie points collected report

The last processing step is the generation of the DEM itself ("DEM from stereo"), but before we need to create the Epipolar Images *(Fig. 34 - 35)*.

Figure 33 - OrthoEngine, Creation of Epipolar image

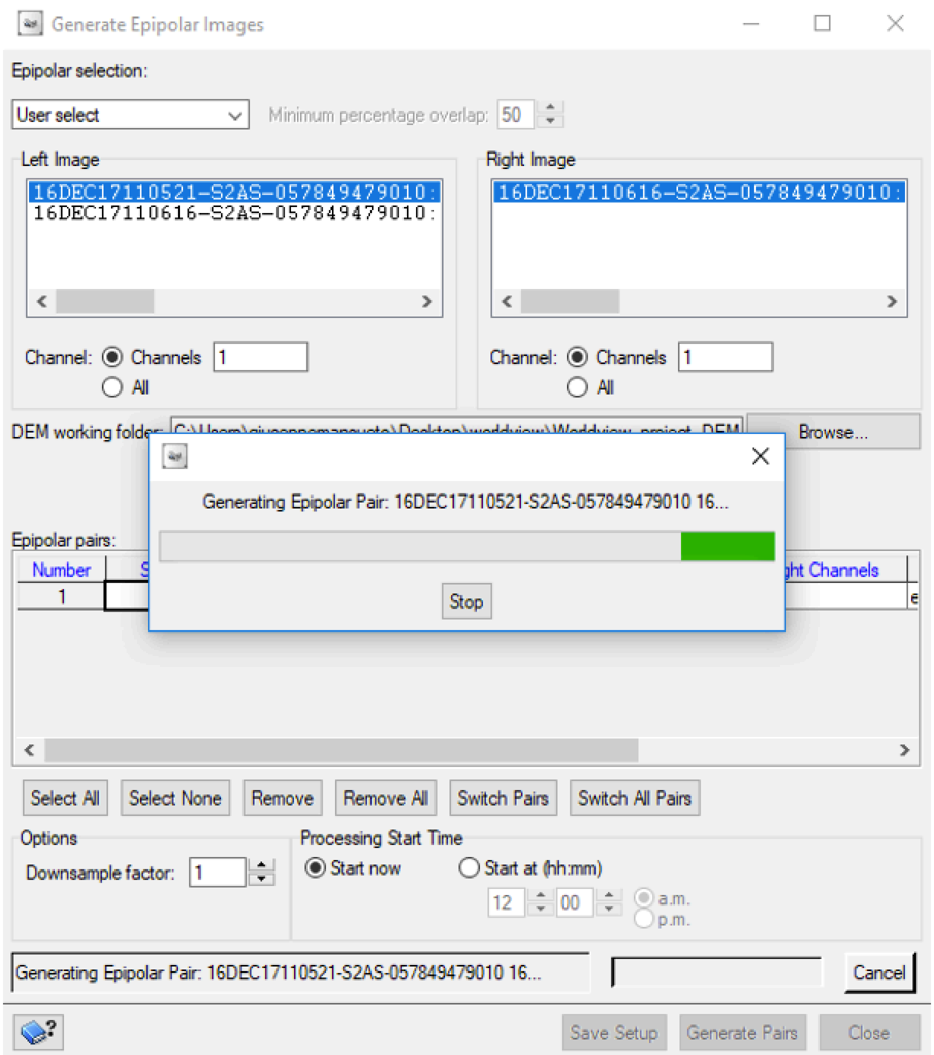

Figure 34 - OrthoEngine, Epipolar images generation

Afterwards the generation of the Epipolar images, it's possible to process the Geocoded DSM *(Fig. 36 - 37)*. Imposing a halved resolution (with respect to the satellite's one), a low smoothing filter and as terrain type a hilly one, the obtained result of the process is a good quality DSM, referred to the ellipsoid, thus each point will be reporting the ellipsoid height. It is important to point out that the resolution of the generated DSMs is always the half of the used dataset one.

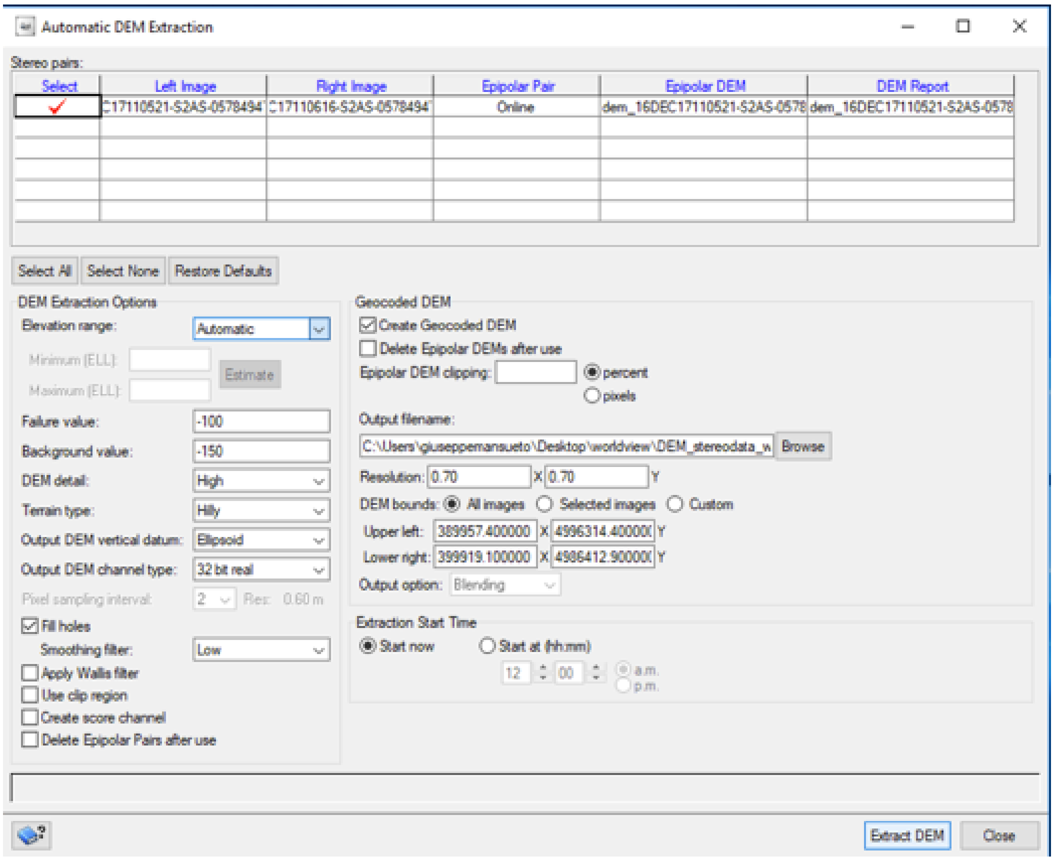

Figure 35 - OrthoEngine, generation of Geocoded DSM

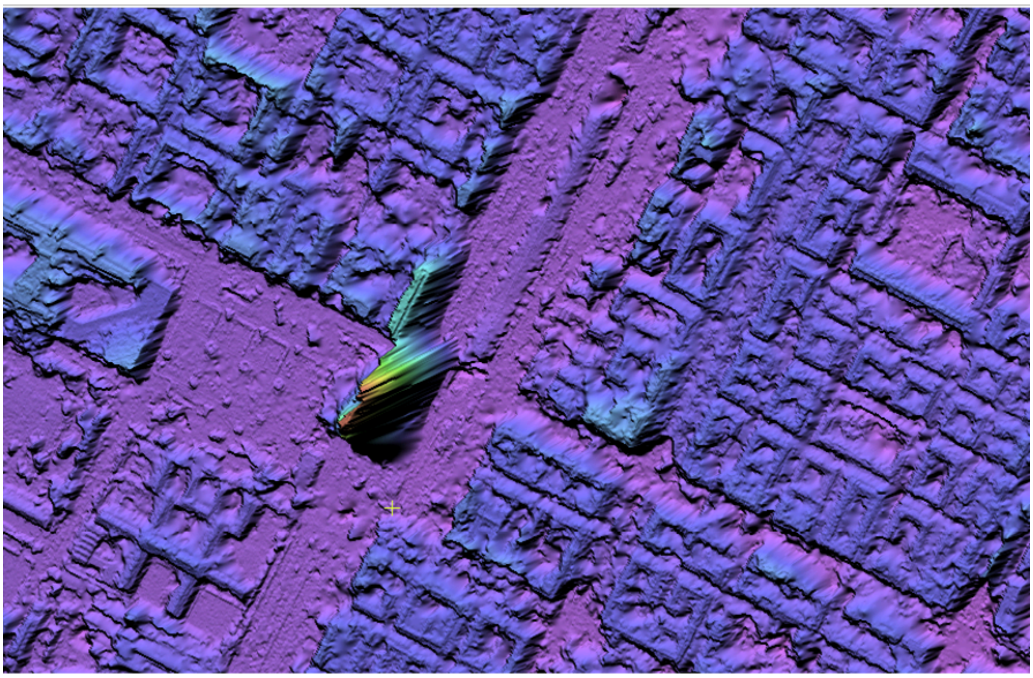

Figure 36 - Generated DSM from WorldView-3 stereo satellite couple (elevations goes from violet to red)

4.2. Geoid referred DSM (extraction with Tie and Ground Control Points)

The DSM digitalization process using GCPs (Ground Control Points) is almost the same of the one with Tie points. In this case, in addition to collecting the Tie points, there is a manual collection of Ground control points (at least four) *(Fig 38)*. In this case, the Tie points were used to collimate the images, the Ground control points function, instead, was to orient and rest the block on the geoid. This further collection of GCPs improve the precision of the algorithm that will associate to each pixel a height.

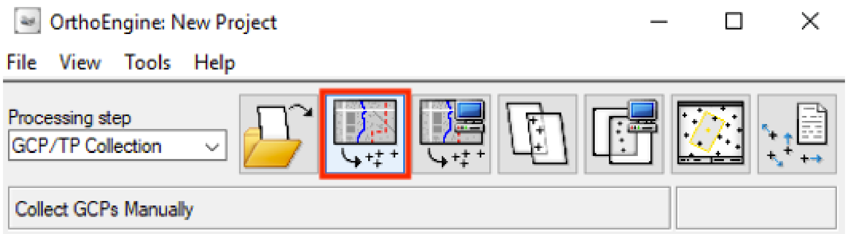

Figure 37 - OrthoEngine, GCPs manual collection

Looking for GCPs in the two images *(Fig. 39)*, the most important thing is to find an appropriate location to match them (intersection of 2 lines, a corner, a shape on the ground, etc...) in order to reach a low RMSE and to obtain the best orientation between the images. It is also important that these points are well distributed in the tested area. “If the two images do not line up during the DSM Extraction process, the output elevation layer may have high levels of error” (PCI, 2013).

The inserted geographic parameters (latitude, longitude and mean sea level elevation) *(Fig. 39, Tab. 9 - 10)*, used to georeferencing the GCPs, were extracted from regional technical maps of Turin, based on UTM-WGS84 32N system. WGS84 (acronym of World Geodetic System 1984) is a geodetic, worldwide geographic coordinate system based on a reference ellipsoid developed in 1984. The WGS84 system does not have an official cartographic representation associated with it, but the UTM (universal transverse projection of Mercator) representation is commonly used, which takes the name UTM-WGS84. It is derived from the Mercator projection, of the earth's surface on a plane, based on a reticulum, a Cartesian system that joins the angular system of latitude and longitude *(personal notes from Geomatica course, M. Caprioli)*. All the GCPs used for the generation of WorldView-3, Pléiades-1A two and tri-stereo DSMs are reported as attachments *(Att. 2 - 3)*.

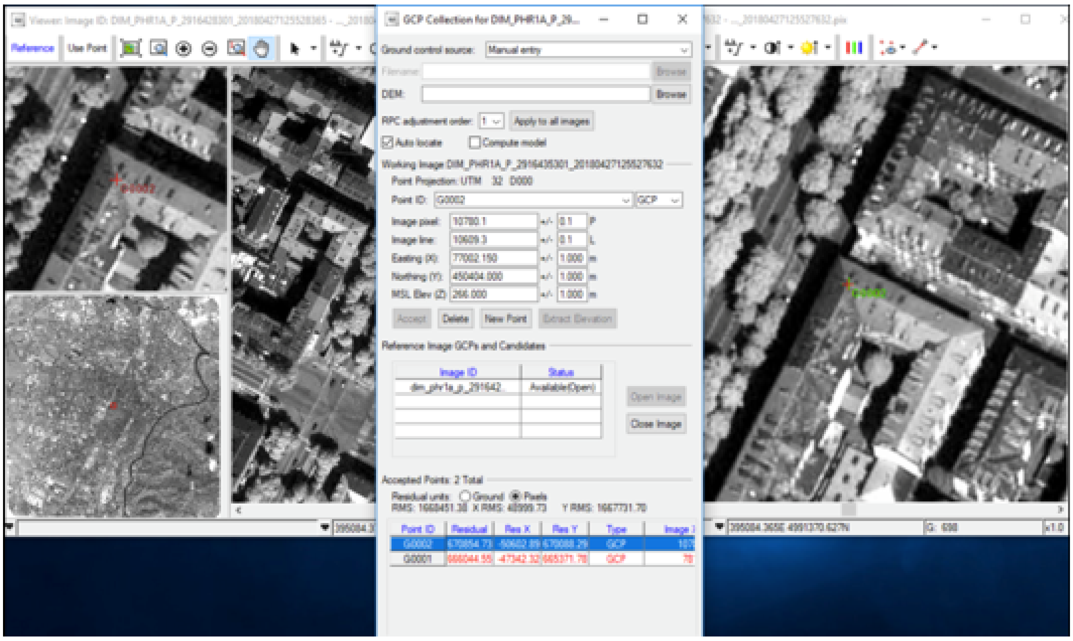

Figure 38 – OrthoEngine, GCPs collection, research of prominent points

Table 9 - GCPs coordinates (UTM WGS84 32N) and values of RMS for Pléiades-1A generated DSM

Point ID	Image pixel	Image line	Easting (X)	Northing (Y)	MSL Elev. (Z)	RMS (X,Y)
GCP1	7145.8	2643.8	393156	4995764	258	2.33
GCP2	18770.8	9646.5	399011	4992201	217	1.91
GCP3	11839.1	7305.7	395506	4993403	236	1.38
GCP4	2487.1	20180.2	390640	4986993	257	0.94

Table 10 - GCPs coordinates (UTM WGS84 32N) and values of RMS for WorldView-3 generated DSM

Point ID	Image pixel	Image line	Easting (X)	Northing (Y)	MSL Elev. (Z)	RMS (X,Y)
GCP1	21630.3	4099.8	396534	4995153	237	1.23
GCP2	19825.2	28122	396004	4987953	219	2.35
GCP3	17934.8	10903.9	395427	4993113	234	0.16
GCP4	14379.4	16072.3	394350	4991557	250	2.00

The obtained final DSM *(Fig. 40)* is not referred to ellipsoid anymore but to the geoid, reporting the elevations in meters on sea level.

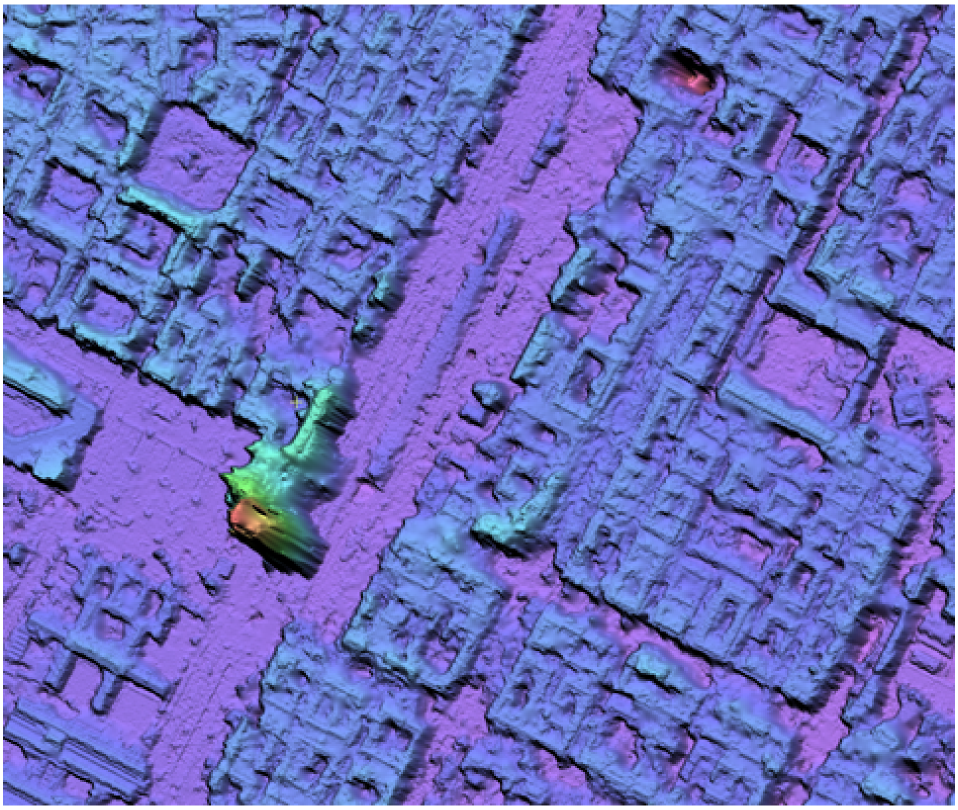

Figure 39 - Generated DSM from WorldView-3 stereo satellite couple (with use of GCP), elevations goes from violet to red

4.3. Geoid referred DSM (extraction with Tie points)

As it will be better explained in the next chapter, the previous processing methods (chapter 4.1 and 4.2) did not bring to a perfect result. For this reason, it was decided to carry on another processing session using Tie points only, and referencing them on the mean sea level. In the PCI operational procedure, it is just necessary to change in the DSM automatic extraction section the ellipsoid option in m.s.l. (*Fig. 41).*

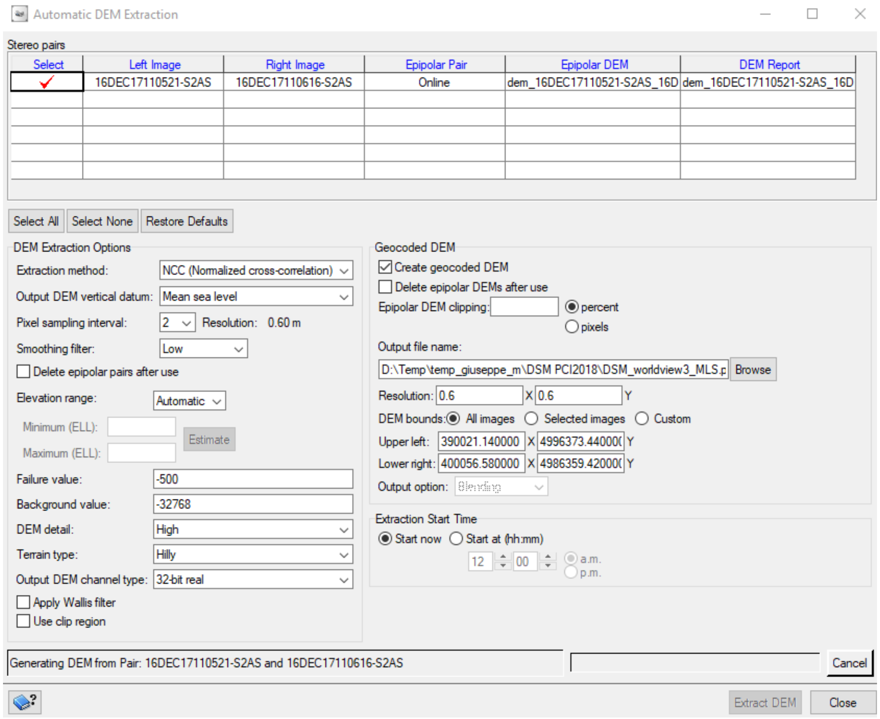

Figure 40 - OrthoEngine, generation of geocoded DSM on m.s.l.

The extracted DSM *(Fig. 42)* shows a much higher precision in collimation and orientation on the geoid with respect the DSM generated with GCPs.

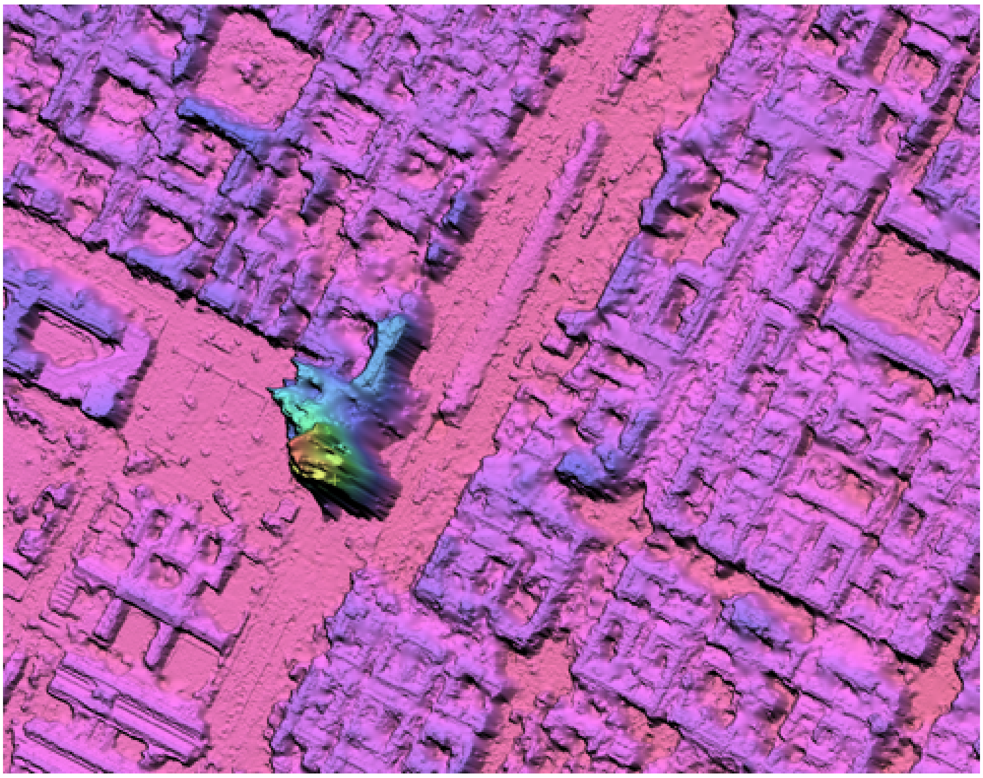

Figure 41 - Generated geoid referred DSM from WorldView-3 stereo satellite couple (with use of TPs), elevations goes from violet to red

5. Results and discussion

In this chapter there will be showed up the obtained results, assessing them from a qualitative and quantitative point of view. The first analysis consist in a qualitative analysis of the data, evaluating noise, sharpness in city canyons, ability in shaping the geometries and identification of details (vegetation, small objects on the ground). The second assessment, instead, concerned the evaluation of the altimetric accuracy of the models through the use of two different benchmarks (one ground height and the other gutter height referred).

5.1. Qualitative analysis of the produced DSMs

Starting from the analysis of Deimos-2 DSM extracted with TPs, with a spatial resolution of 2 m, it is clear that it cannot be used for any kind of analysis purpose in a city area. As it is possible to see in the figure 43, the cityscape presents a lot of issues related to noise and false elevation spikes. The majority of the errors come out on the road network or in streets with narrow canyons, due to moving objects and shadow effects.

The buildings elevation accuracy, because of the low resolution of the images from which it was extracted, in comparison with the other satellite extracted DSM, is very poor and does not permit to identify or distinguish the shape of the object on the ground. Looking at the second frame *(Fig. 44)* of the Deimos-2 DSM, focusing on the more rural hilly part of the city, it is possible to understand the elevation of the area in the complex, but not the details. For these reasons and for the difficulty in the identification of good GCPs, in the prospective of a better product, it was decided to not carry on a DSM with GCPs using Deimos-2 imagery dataset.

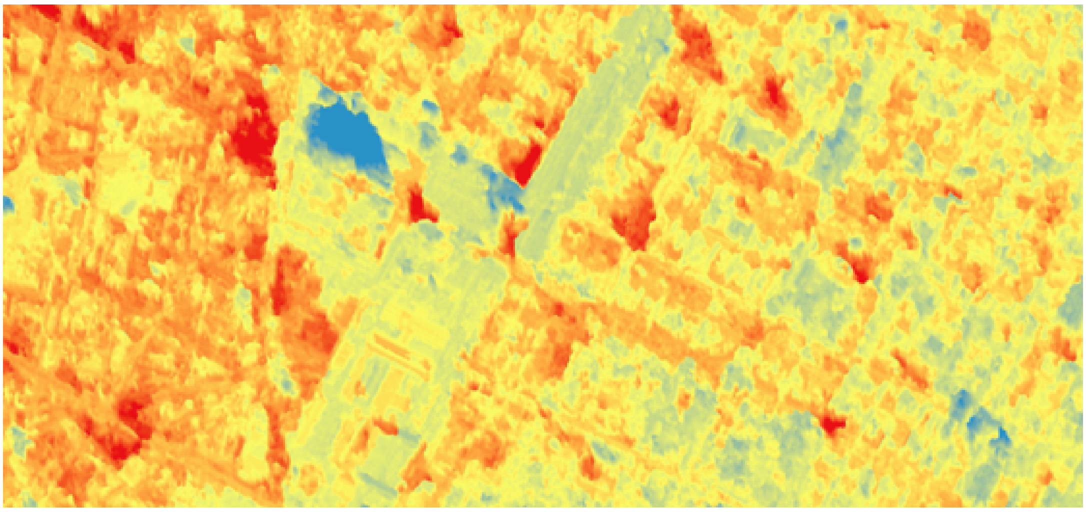

Figure 42 - Deimos-2 extracted ellipsoid DSM

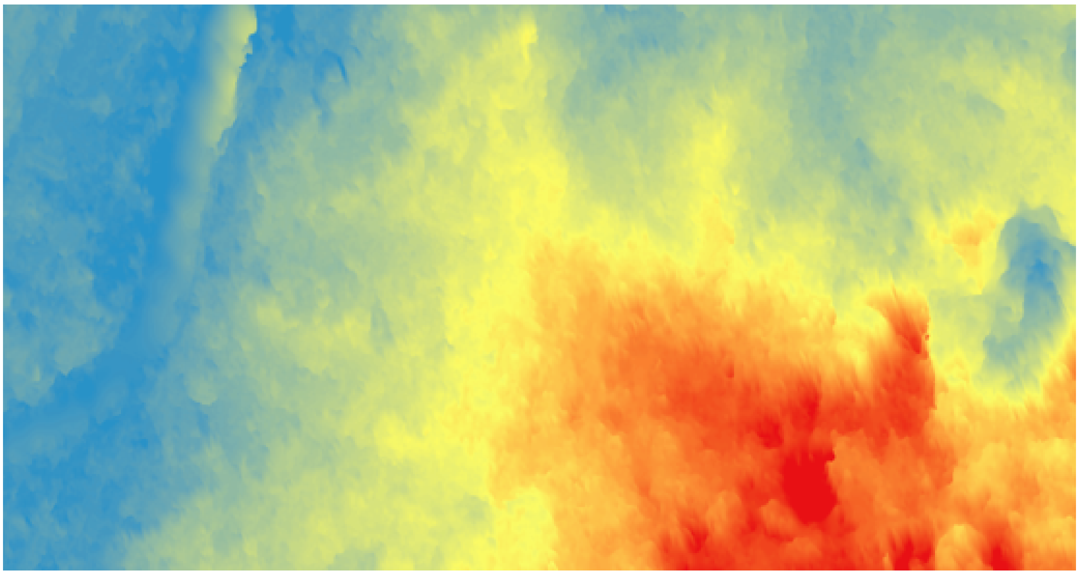

Figure 43 - Deimos-2 extracted ellipsoid DSM, hilly part of Turin

Moving to the ellipsoid DSMs obtained from Pléiades-1A and WorldView-3 dataset, one quickly realizes that the results are clearly superior to the Deimos-2 one. The main reason is that these satellites shows, as said before, a higher resolution (0.34 WV3 and 0.5 Pléiades-1A). In the figure 45 are reported three frames of Pléiades-1A two-stereo, Pléiades-1A tri-stereo and WorldView-3 ellipsoid DSMs (obtained using TPs for the collimation of the model) of a limited area of the city of Turin. From a first qualitative analysis it is possible to report that the best quality belongs to Pléiades-1A two-stereo DSM, followed by Pléiades-1A tri-stereo DSM and WV3 DSM. It was take into account this testarea for the presence of many different “objects” and cityscapes useful for the evaluation, rimmed in black in the figure 45.

The first circle focuses on a skyscraper, the “Grattacielo Banca Intesa San Paolo” locate between Cit Turin and Cenisia district of the city of Turin. Looking at the focus 1, zooming on the skyscraper with a scale of 1:6000, it is well shaped just in Pléiades-1A DSMs, in particular the two-stereo one better shaped the South-West front and the tri-stereo, instead, better sculpt it in the complex, catching also the steps and some trees in front of the East front. WorldView-3 result present a scrolling of the skyscraper, probably due to its shadow in the time of the acquisition. In the second circle *(Focus 2)* is surrounded a big 90’s century building, “Officine Grandi Riparazioni” located in Cenisia district of Turin. Focusing on the roof, its shape is not represented faithfully in the WorldView-3. Both Pléiades-1A DSM shows a good result; the two-stereo DSM better represents the roofs flaps, exhibiting that the external part of the roof is higher than the central one. The tri-stereo one, instead, better defines the details in the North-West part. The last focus concentrate to the evaluation of two canyon of cityscape, one located in “Corso Galileo Ferraris” *(Focus 3)*, in Crocetta district, and one in “Via Monginevro” *(Focus 4)*, in Cenisia district. As in the first case, Pléiades-1A with tri-stereo mode DSM reach up a higher quantity of details in the scene, outlining also the trees in the middle of “Corso Galileo Ferraris”. Although this ability to delineate details could be essential for the identification of the vegetation, this work is targeted to the correct determination of the buildings and ground heights in the city. The two-stereo Pléiades DSM delineate the streets shaping them completely, without the noise found in the tri-stereo one and without the building overlaps present in WorldView-3 DSM, which also in this case looks weak in comparison to the others. Moreover, it is important to remember that the elevations reported in the various focus *(Focus 1 - 2 - 3 - 4)* are heights referred to the ellipsoid, thus not referred to the sea level.

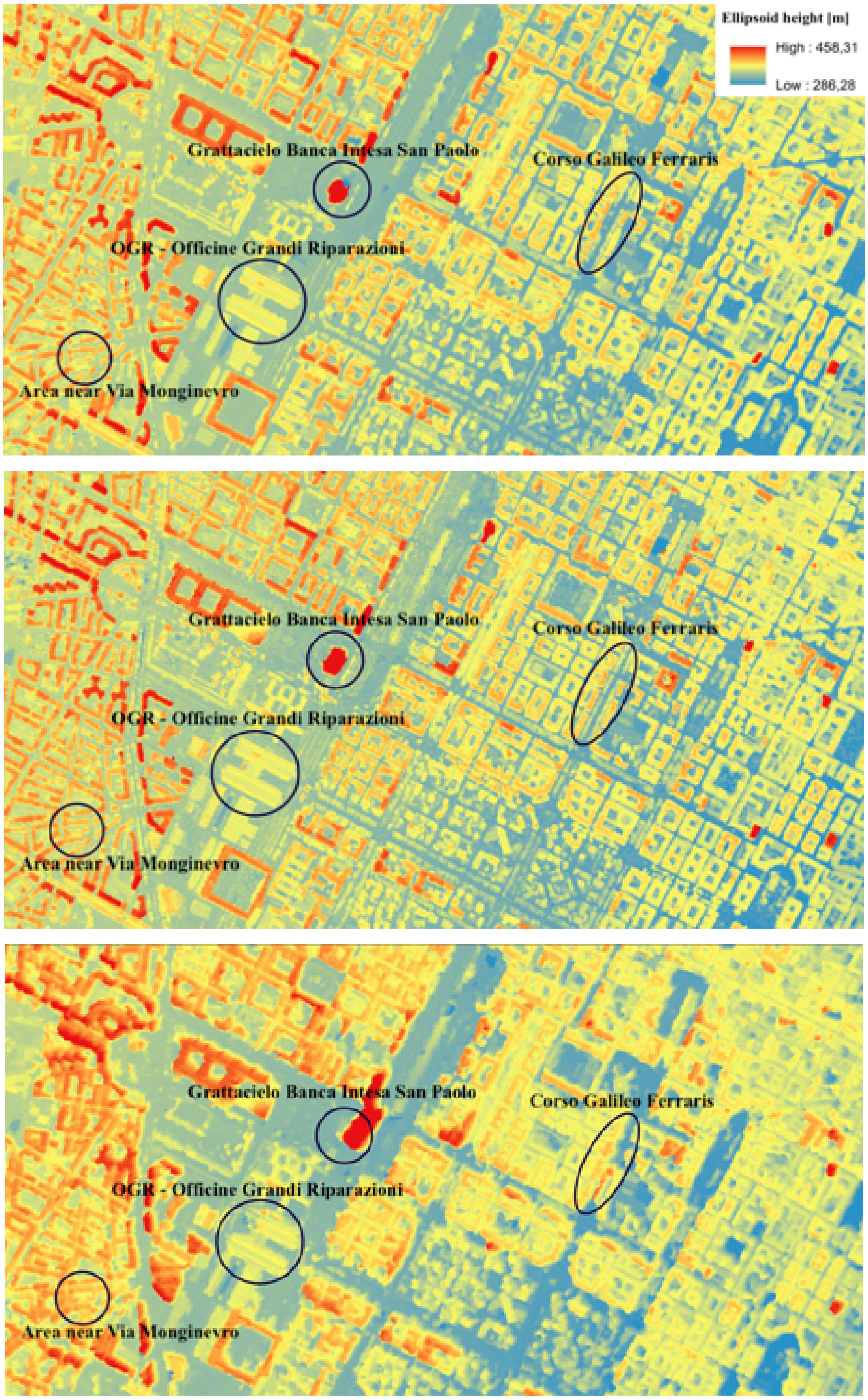

Figure 44 -Visual analysis over a limited urban area, in order: Pléiades-1A 2stereo, Plèiades-1A 3stereo and WV-3 extracted ellipsoid DSMs

Ellipsoid DSM - Focus 1: Grattacielo Banca Intesa San Paolo, TO

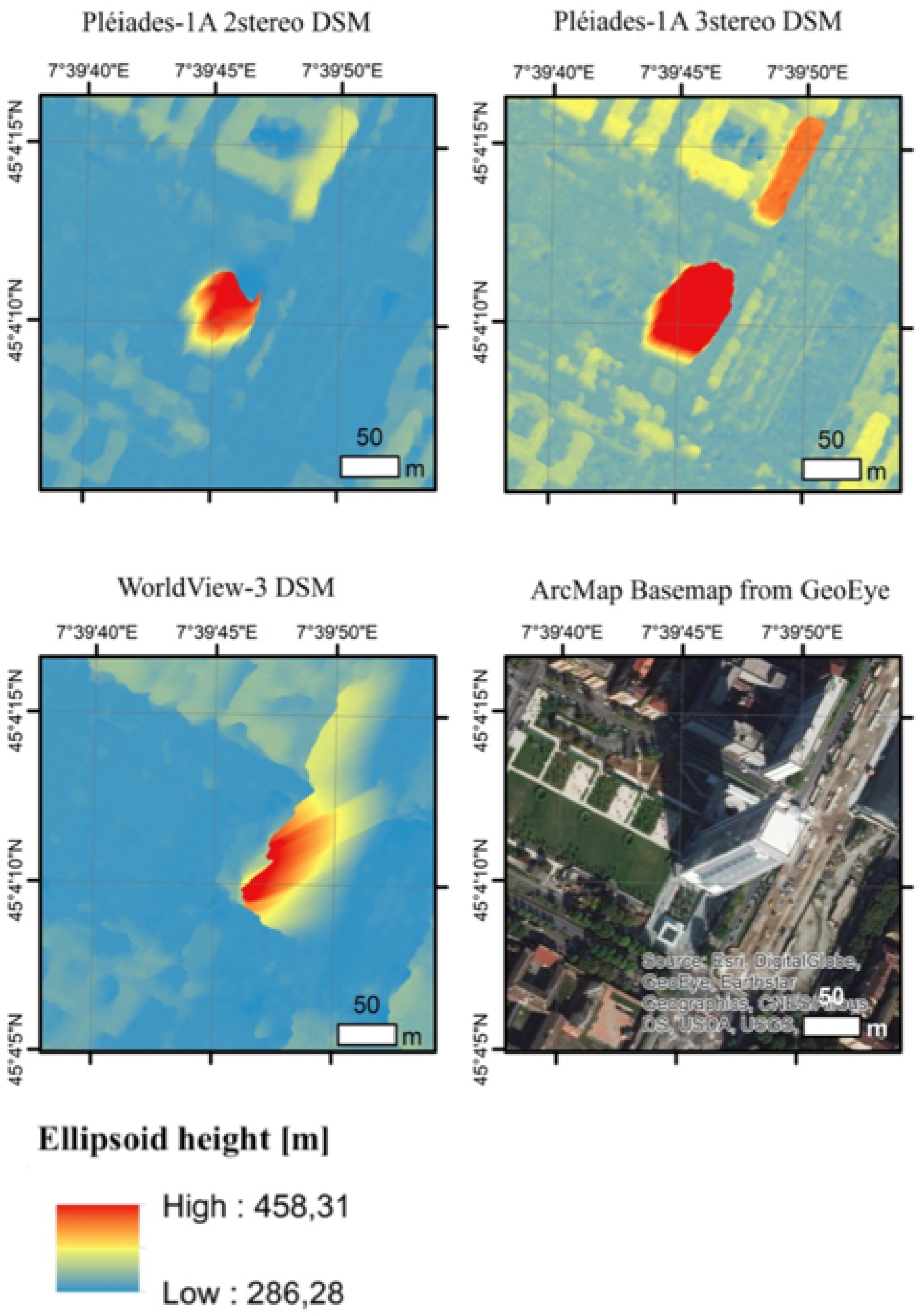

Ellipsoid DSM - Focus 2: Officine Grandi Riparazioni, TO

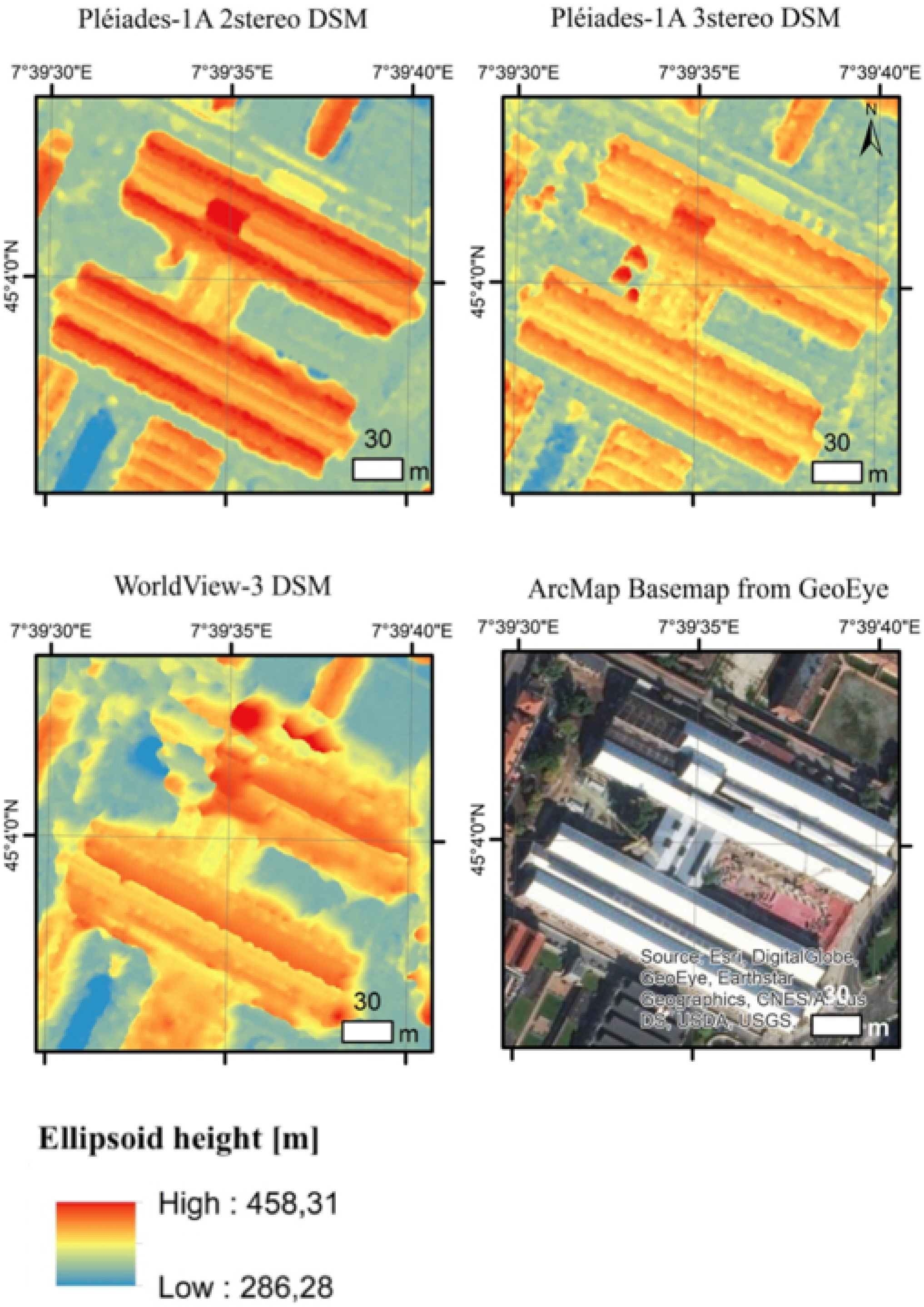

Ellipsoid DSM - Focus 3: Corso Galileo Ferraris, TO

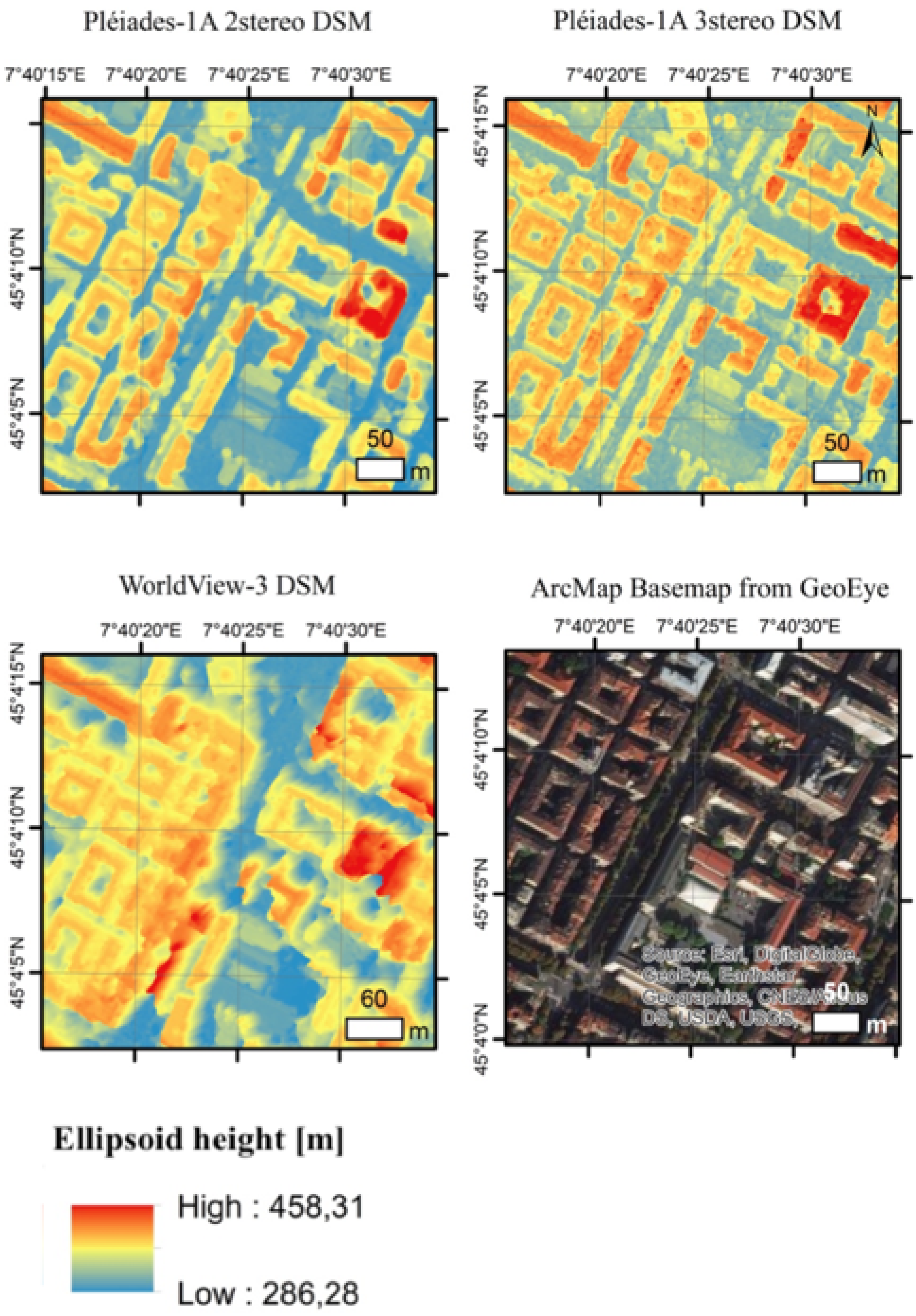

Ellipsoid DSM - Focus 4: Near Via Monginevro, TO

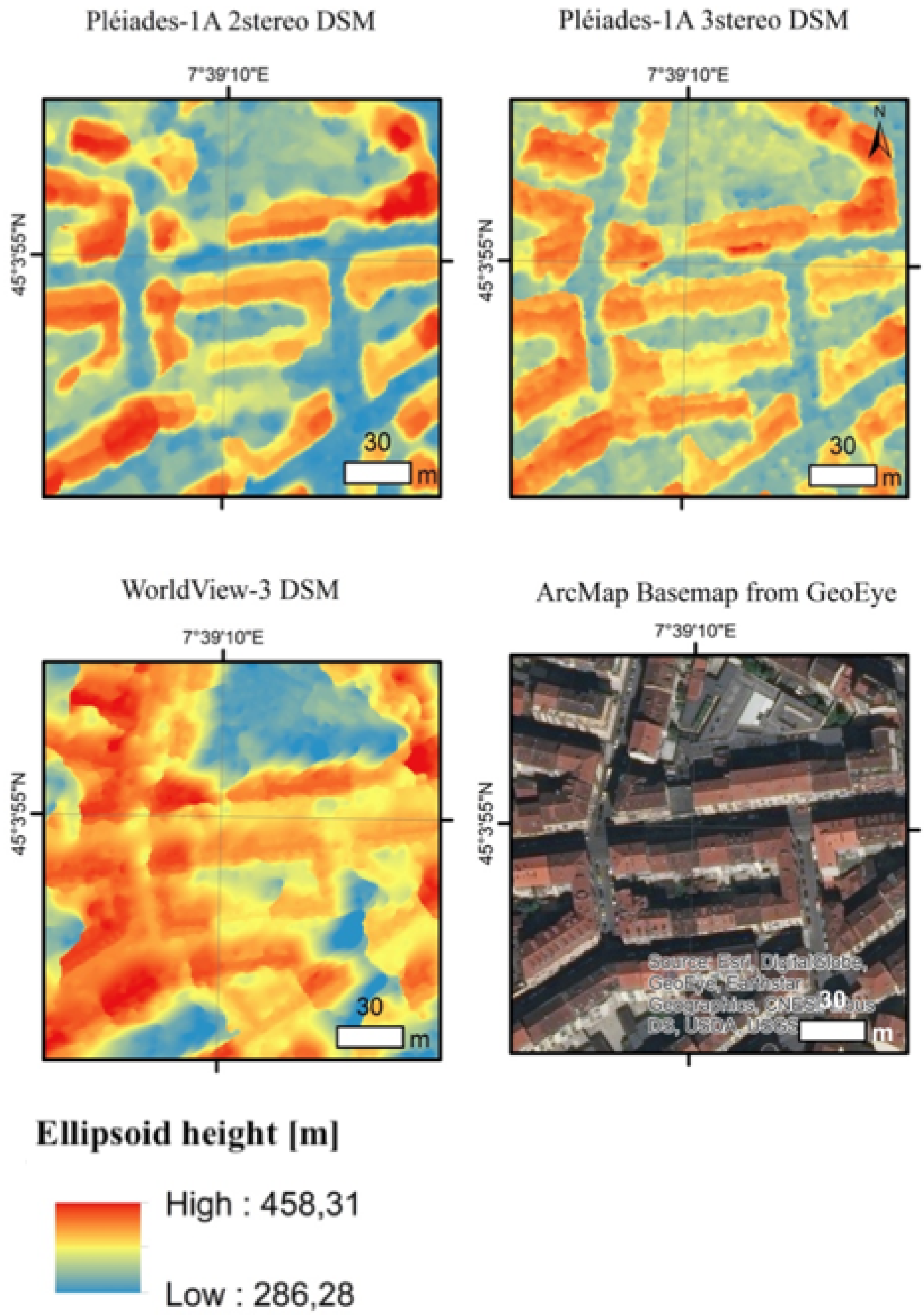

After the analysis of the cityscape, the analysis focused on the hilly part of Turin *(Fig. 46)*. In this case the differences in quality, in the three DSMs, are not so evident as before. WorldView-3 presents a good behaviour in reporting the difference in height of the hilly terrain, but is not able to outline well both the Po river course and the roads located on the hill. Both Pléiads-1A DSMs, instead, well shape these elements. In this case Pléiades-1A with tri-stereo mode DSM made some mistake in the river processing, maybe due to the fact that the concentration of TPs in this area is low, generating some height peaks in it.

Despite it was expected to find the best results in Pléiades tri-stereo DSM, looking at the outputs, we can assert from the qualitative evaluation, that the DSM produced using the two-stereo mode of Pléiades-1A is the best one.

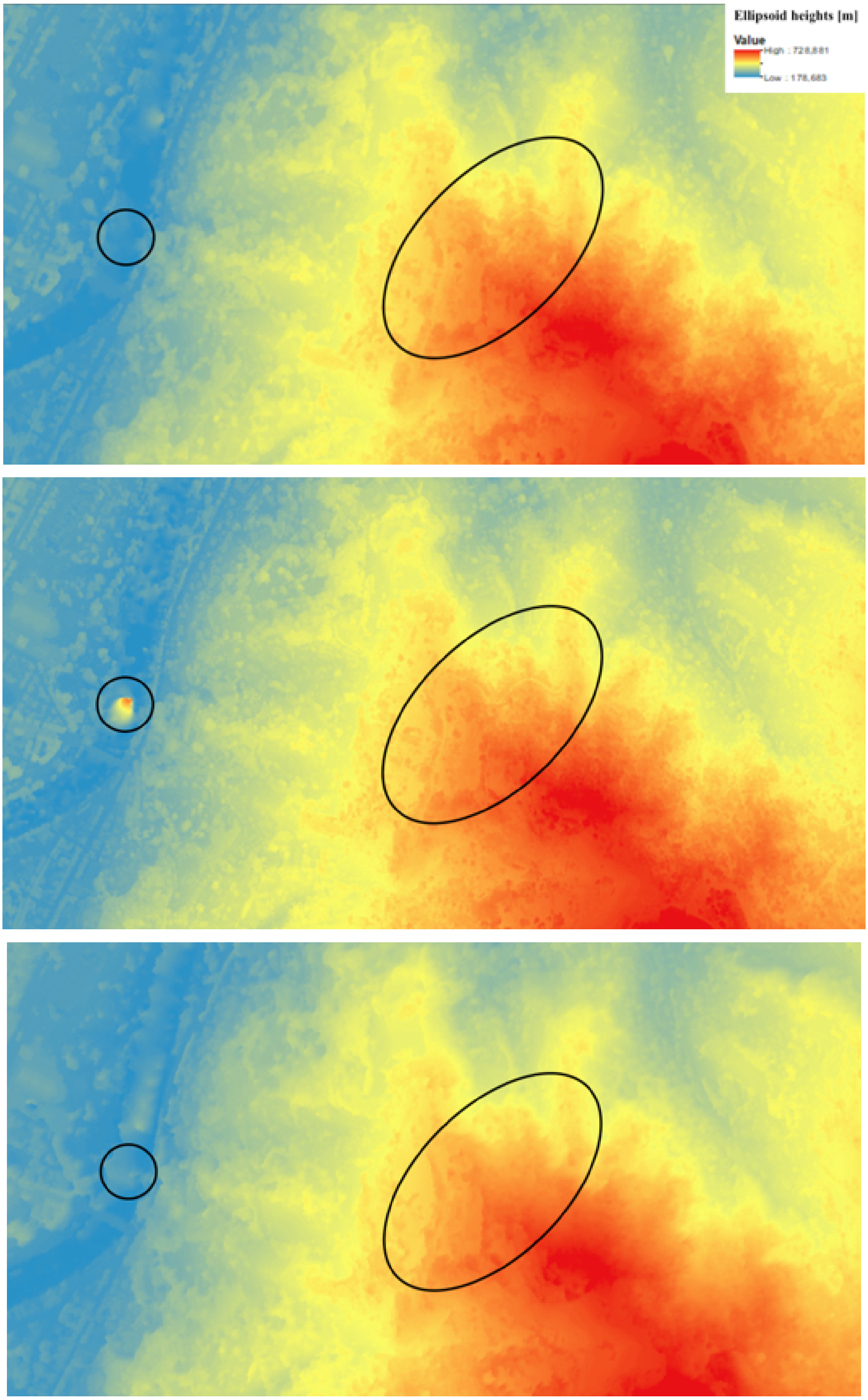

Figure 45 - Visual analysis over a limited urban area, in order: Pléiades-1A 2stereo, Plèiades-1A 3stereo and WV-3 extracted ellipsoid DSMs, hilly part of Turin

As point out before, the heights of the previous DSMs where referred to the ellipsoid, but it is needed to report the heights to the geoid, in order to obtain the heights on the mean sea level. In the direction of this purpose, as saw in the chapters 4.2 and 4.3, there were extracted DSMs geoid referred, firstly using together TPs and GCPs and then utilizing just TPs.

In the figure 47, 48 and their focus *(Focus 5 - 6)* are showed two cityscape frames of the DSMs for each satellite. Moreover, it was decided to focus this qualitative analysis just on Pléiades-1A tri-stereo and WorldView-3 products, with the intent to find better results with respect to the other obtained on the ellipsoid.

In WorldView-3 DSMs *(Focus 5)* the main differences are in the north part: one is the representation of the skyscraper "Banca San Paolo" and the other is the north entrance of "Porta Susa" station. Both are better reported in the DSM generated with TPs: the skyscraper is better shaped, and the entrance of the station present an height different from the roof of the station itself (the real one).

Look at the Pléiades-1A tri-stereo DSMs (*Focus 6)* the conclusion it is the same, that is that the DSM generated with TPs delineate better the objects. Indeed, in DSM generated with GCPs the skyscraper presents a foreshortening and, looking at the streets in the focus, the canyons are not always well represented, exhibit in some cases an overlap of the heights near buildings on it.

Besides this visual consideration, in all (WV-3 and Pléiades-1A) the GCPs DSMs there is a geometrical error, which consist in a wrong collimation and orientation of the block. This problem is not present in the TPs DSMs. This error can be related to the RMS of the points *(Chapter 4.2, tab. 9 - 10, Att. 2 - 3)*, indeed using ground control points (which in most of the cases presents a RMS higher than the TPs) it was increased the total RMS.

In conclusion, the best method to report the heights on the geoid is the one explained in the chapter 4.3, the one that uses Tie points.

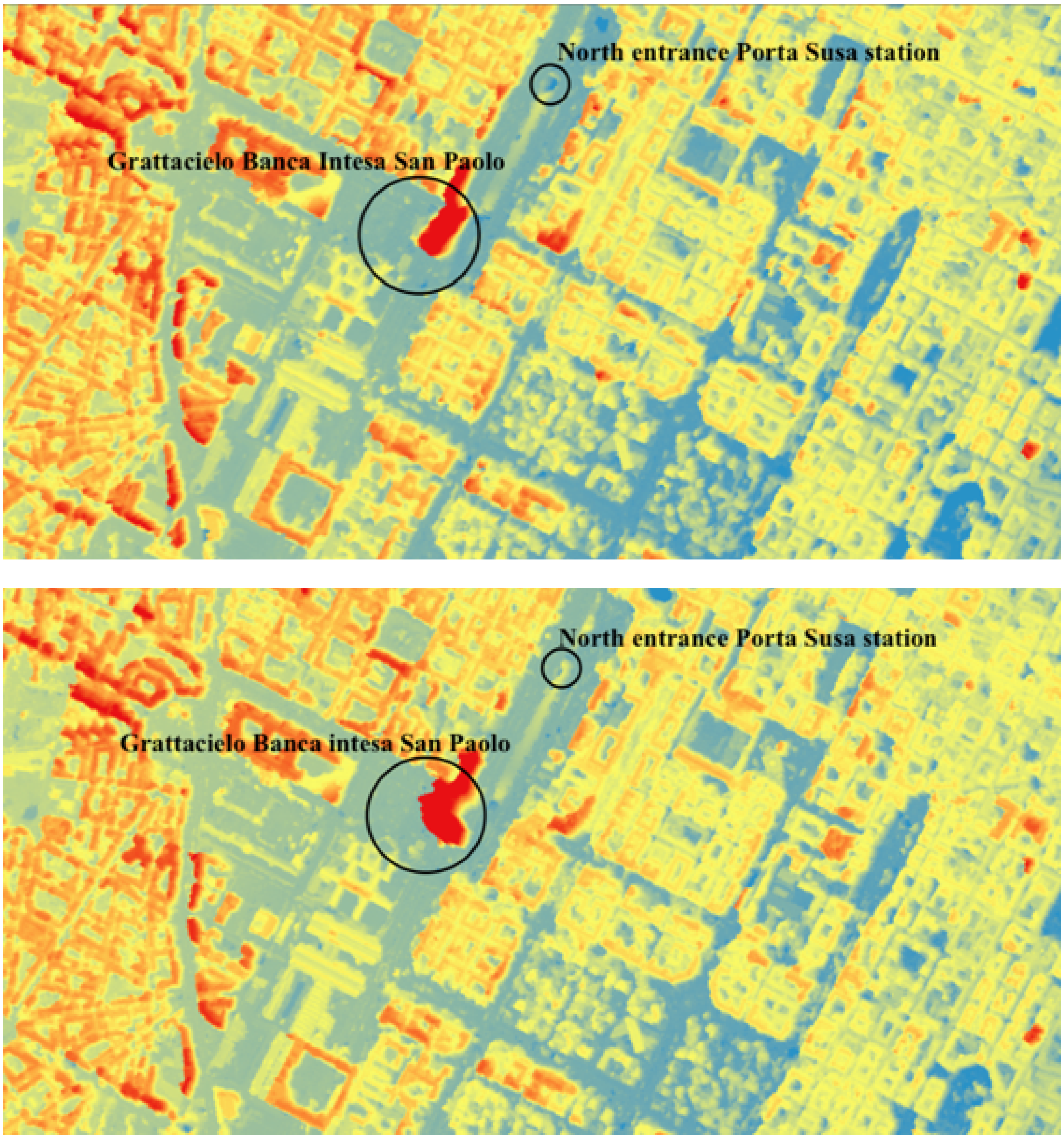

Figure 46 - Visual analysis over a limited urban area, in order: "WV3 TPs" (geoid) and "WV3 TPs + GCPs" (geoid) extracted DSM

Focus 5 - Comparison between WorldView-3 "TPs DSM" and "TPs + GCPs DSM"

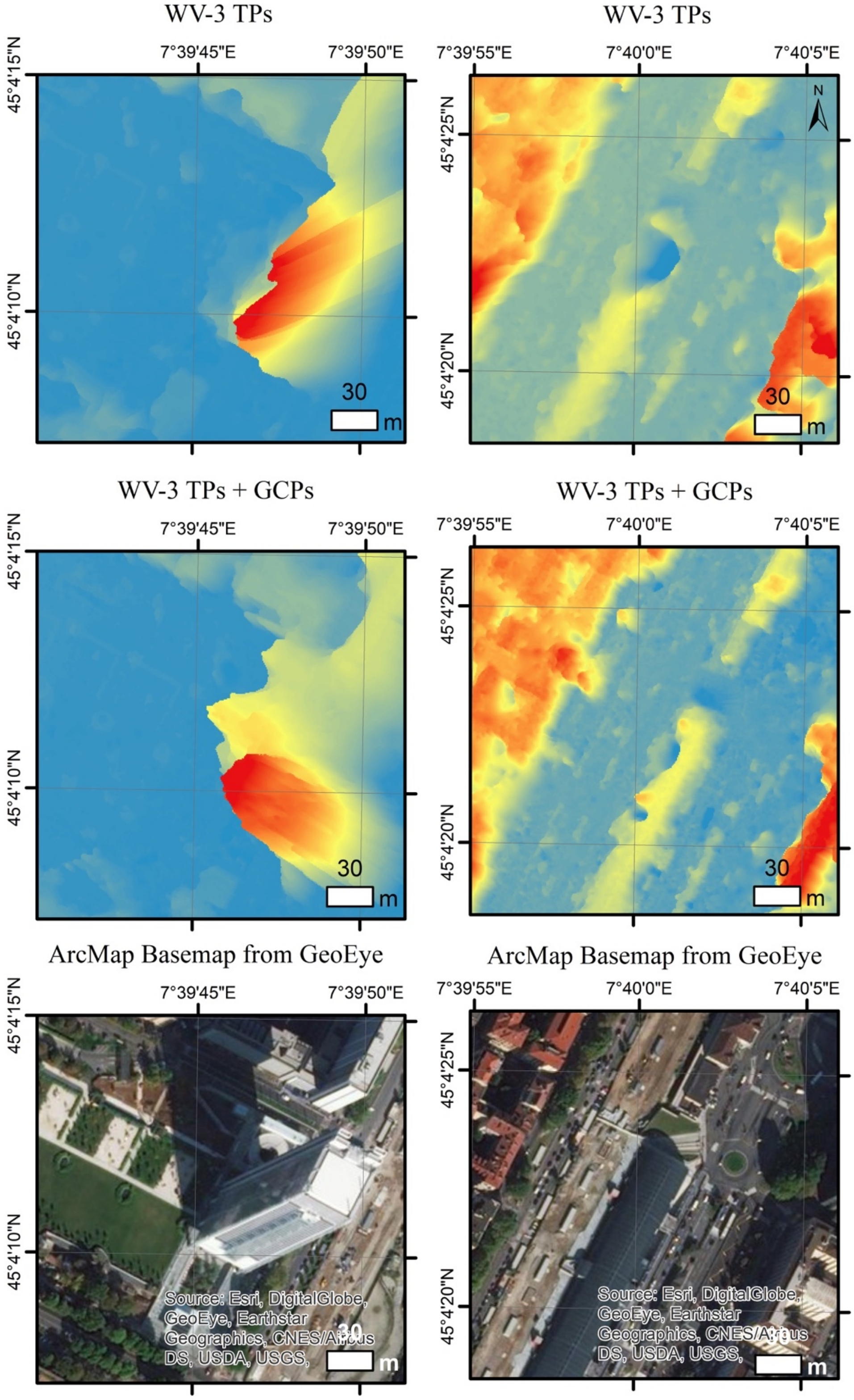

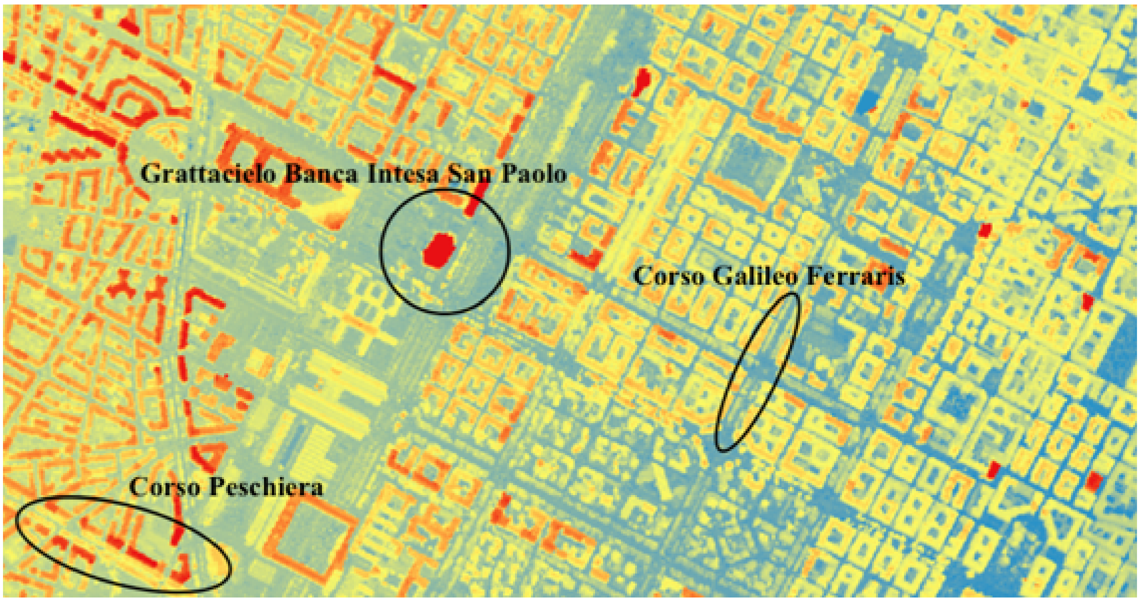

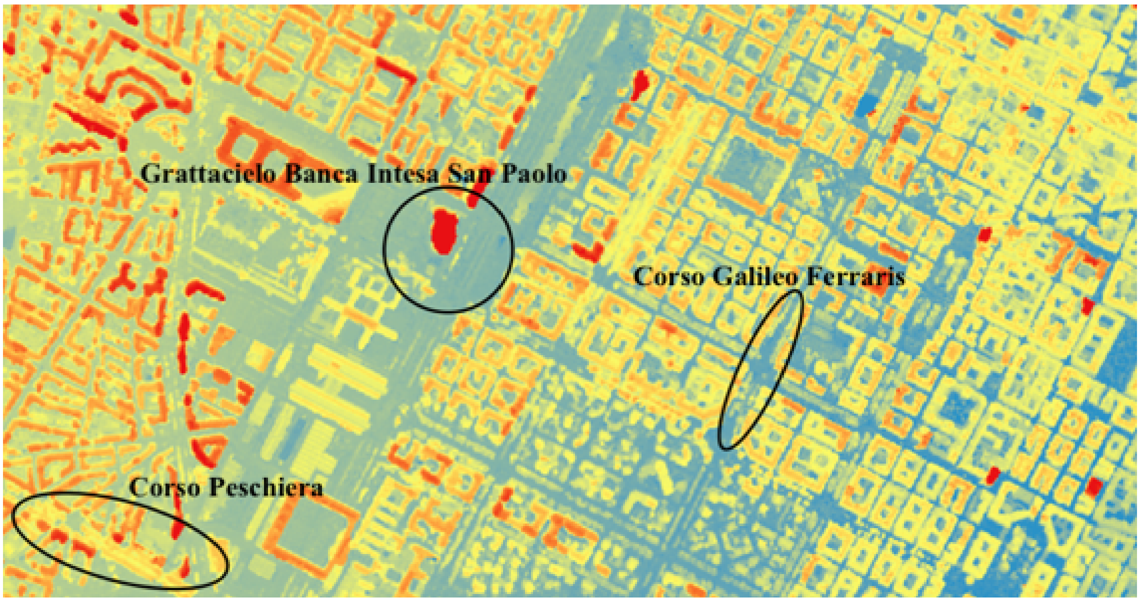

Figure 47 - Visual analysis over a limited urban area, in the order: "Pléiades-1A 3stereo TPs" (geoid) and "Pléiades-1A 3stereo TPs + GCPs" (geoid) extracted DSM

Focus 6 - Comparison between Pléiades-1A 3st "TPs DSM" and "TPs + GCPs DSM"

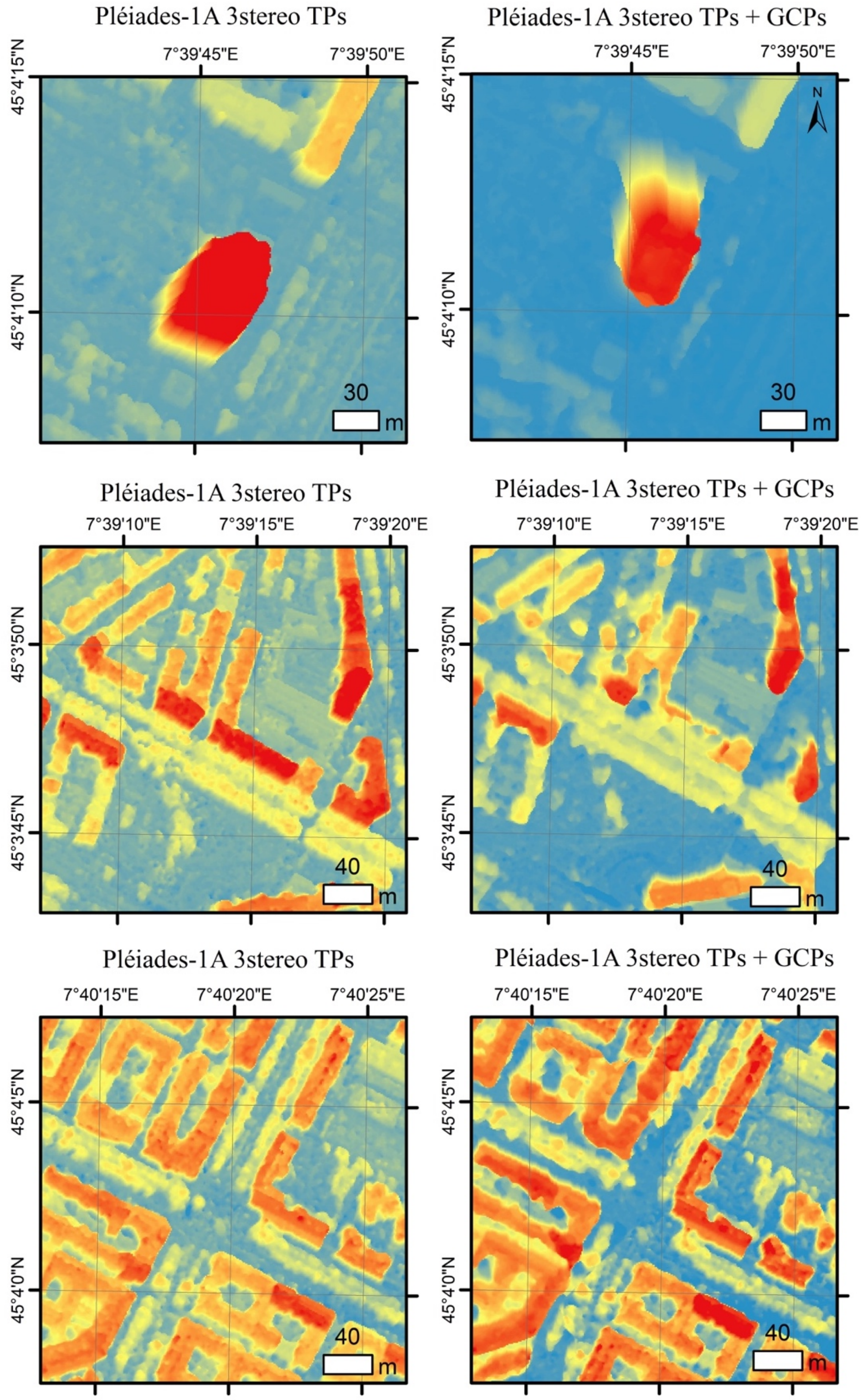

5.2. Benchmark and DSM Accuracy

5.2.1. Creation of the benchmarks

From now on (in the next chapters) the term DSM mean DSM geoid referred and height, the height on mean sea level.

In order to evaluate the accuracy of the obtained DSMs, it was necessary to find an untroubled dataset to employ as benchmark (reporting the correct geoid heights of Turin). These data, borrowed from LARTU (Urban and territory analysis and representation laboratory), report the heights of marked points (mainstay, trustworthy, network vertex and stable reference points) and volumetric units, in a vectoral extension. The geographic projected coordinate reference system of this dataset, Gauss Boaga - Monte Mario Italy, was different to the DSMs one, UTM WGS84 32N. For these reasons it was necessary: firstly to convert the coordinate reference system and secondary to transform the extension of the files in raster (extension of the DSMs). For the first step, the shape files were converted in coordinate system UTM WGS84 using the data management tool "Project" of ArcMap *(Fig. 49),* setting as input data the LARTU files (e.g. in the fig. 49 "000160_PUNTO_STABILE_DI_RIFERIMENTO"), as output coordinate system UTM WGS84 32N and as transformation the transformation from Monte Mario Italy to UTM-WGS84.

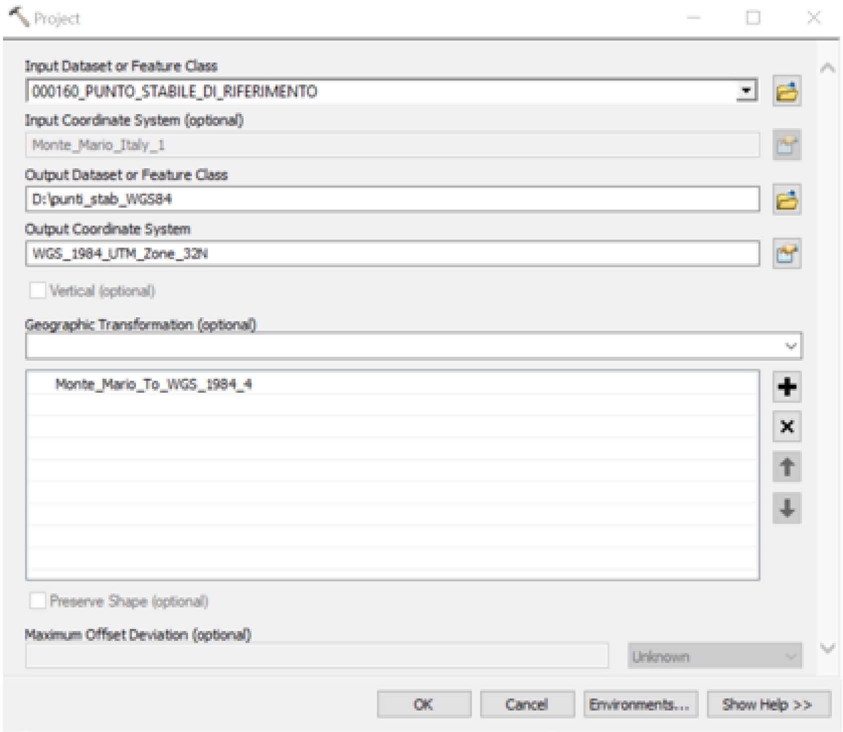

Figure 48 - ArcMap Project tool

Once obtained the LARTU data (benchmarks) in the same system of the DSMs, it was possible to proceed to the conversion of them from a vector extension into a raster one. While vector elements are based on geometries (points, polylines and polygons) to represent the real world, the raster data consist of pixels contain a value that represents the conditions of the area covered by the cell. The marked points files were converted using “Point to raster” *(Fig. 50)* and the volumetric one using “Polygon to raster” (Fig. 51) tools of ArcMap. As it is possible to see the “Cellsize” value in both the conversion tools was fixed on 0.3, as a smaller cell size guarantees a match of just one cell of the DSM in the further subtractions, avoiding an overlap with more than one (and consequently more than one value of height). There were generated: a raster reporting in the pixel cells the values of ground heights (from now on “ground raster”) and a raster reporting in the pixel cells the values of gutter heights of the buildings (“gutter raster”). This transformation of the benchmark permit to subtract them to the DSMs.

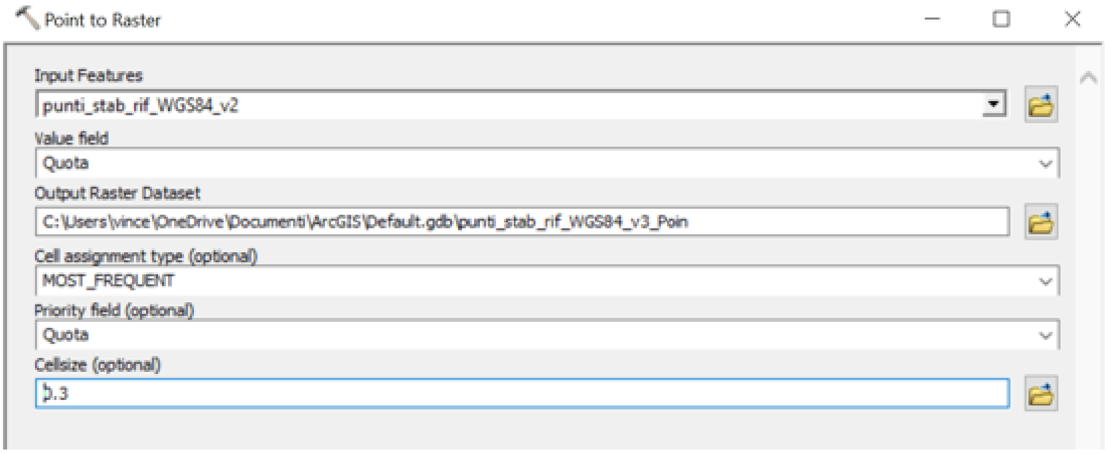

Figure 49 - ArcMap Point to Raster tool

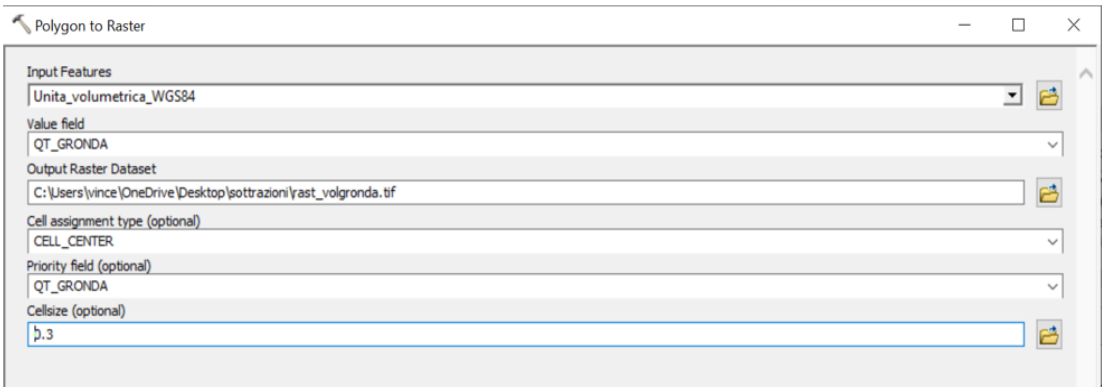

Figure 50 - ArcMap Polygon to Raster tool

In the interest of a correct analysis of the height, it was necessary to delate the edges of the DSMs. This part has an anomalous height value, dictated by a common error made by the satellite during the acquisition. It was choosed and clipped an area of the city common for both the satellites. Thus, the DSMs was been clipped by “Clip” ArcMap tool *(Fig. 52)*. In the figure 53 is reported an important setting detail, for avoid a possible translation of the clip (misaligning the reference system and the consequent match with the refenced points): going in Environment and then processing extent, it is needed to set as base of the snap the DSM that is wanted to clip.

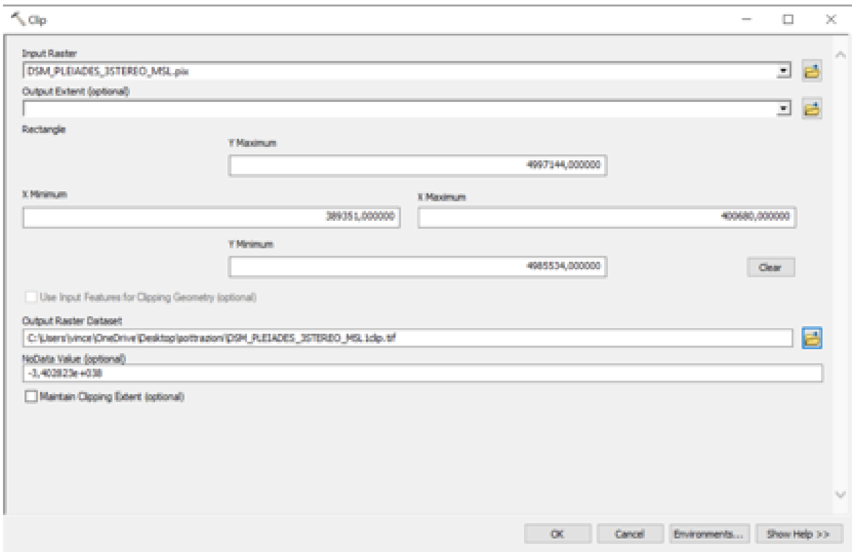

Figure 51 - ArcMap Clip tool

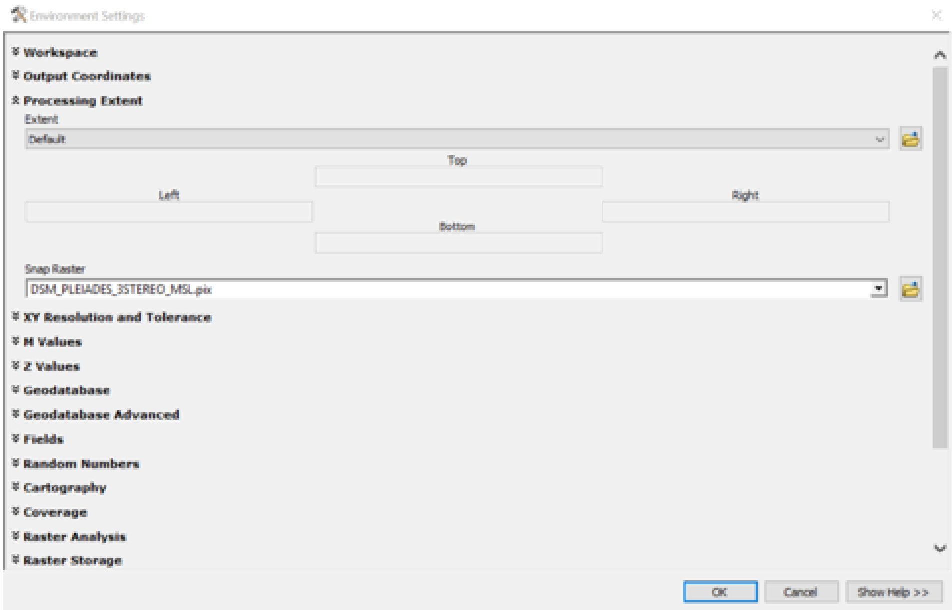

Figure 52 - Processing extent settings, Environment options, ArcMap Clip tool

Terminated the clipping operation, the next step was executing, via the "Minus" command *(Fig. 54)*, the subtraction of the benchmarks (marked points and reference volumetric units raster) to the DSMs.

Figure 53 - ArcMap Minus tool

5.2.1.1. Benchmarks for ground heights assessment

The three obtained products (once for each DSM, WV3, Plds tri-stereo and Plds two-stereo), generically named in this section "difference ground raster" represent in each pixel the difference in ground height between a DSM and the "ground raster". In the figure 55 is showed the perfect overlap of the "Pléiades-1A tri-stereo difference ground raster", "ground raster" and "Plèiades-1A tri-stereo geoid DSM"; as it is possible to visualize the subtraction, work just for the pixel of the DSM which have a corresponding pixel in the "ground raster". In the figure 55 are also reported the correspondent heights of all the overlap pixels, in which the height of the "difference ground raster" pixel result 11 m. This value, as it will be said in the following chapter, is an example of the DSM mistake, made in the digitalization phase of that point.

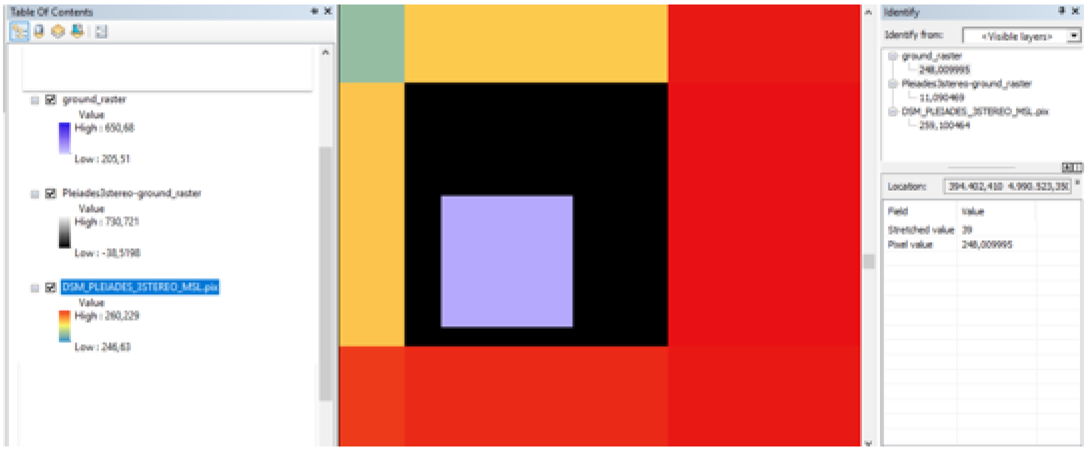

Figure 54 - Visual output of the Minus tool application, " Pléiades tri-stereo difference ground raster" pixel (violet), overlapped to "ground raster" (black) and "Pléiades tri-stereo DSM"

In order to extract the statistics related to the heights value it is necessary to carry out a "Raster to point" *(Fig. 56)* on the "difference ground raster", obtaining a vector extension file, generically called "difference ground vector". This operation was done for all the three raster dataset.

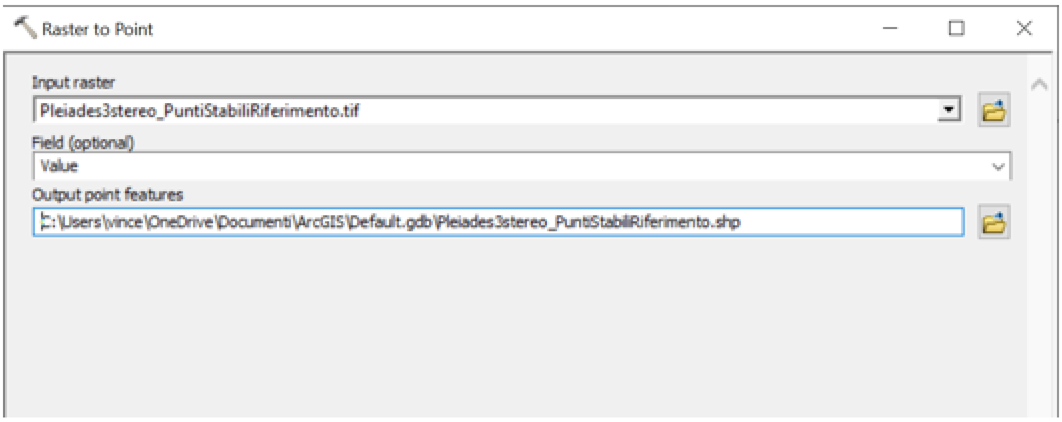

Figure 55 - ArcMap Raster to point tool

The more is low the difference in height, the more the value of the "difference ground raster" tends to zero. If the difference tends to 0 the DSM results are considered more accurate.

5.2.1.1. Benchmarks for gutter heights assessment

As for the “difference ground raster”, the processed products are three (once for each DSM, WV3, Plds tri-stereo and Plds two-stereo), generically named “difference gutter volumetric raster” represent in each pixel the difference in gutter height between a DSM and the “gutter raster”. In the figures 57 and 58 is showed the perfect overlap of the “Plèiades-1A tri-stereo difference gutter volumetric raster”, “gutter raster” and “Plèiades-1A tri-stereo geoid DSM.

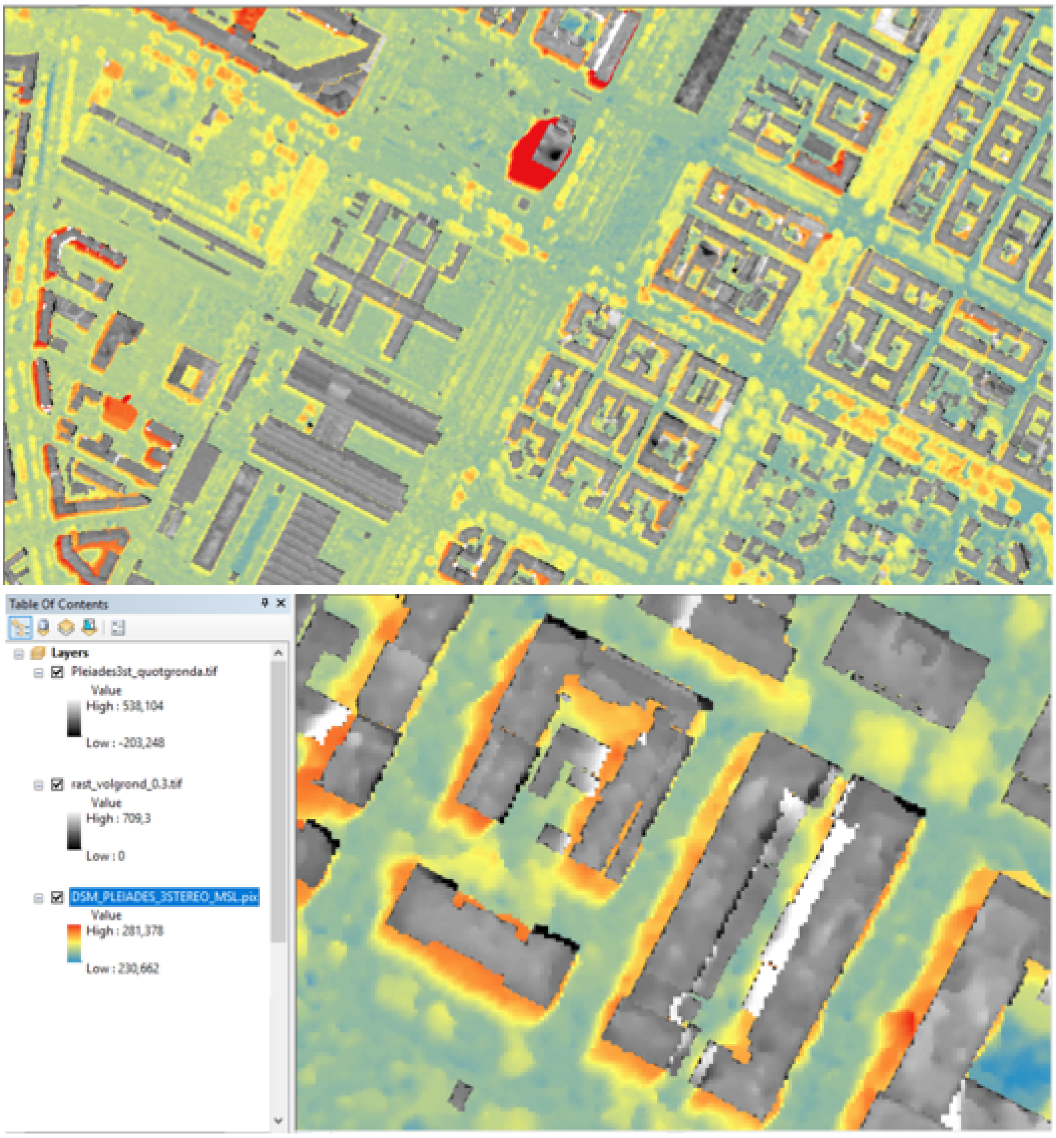

Figure 56 - Visual output of the Minus tool application " Plèiades-1A tri-stereo difference gutter volumetric raster", overlapped to "gutter raster" and "Pléiades tri-stereo DSM"

Figure 57 - Detail: " Plèiades-1A tri-stereo difference gutter volumetric raster" pixel (the grey one in the center), overlapped to "gutter raster" (black) and "Pléiades tri-stereo DSM" (all the other colors)

In order to extract the statistics related to the heights, also in this case it is needed a transformation of the three rasters in vector points extension files, generically defined as "difference gutter volumetric vector".

5.2.2. Discussion benchmark results

It was decided to carry on the heights analysis on the vector points datasets (three "difference ground vector" and three "difference gutter vector" outlining a test area respectively of 27,6 km^2 and 2,4 km^2 common for both the satellite acquisition frame. In the figure 59 it is reported as example the test area within the "difference ground vector" points form the Plèiades-1A two-stereo subtraction, against the background of Pléiades-1A two-stereo DSM. In the figure 60 it is reported the area within the "difference gutter vector" points form the Plèiades-1A two-stereo subtraction, against the background of Pléiades-1A two-stereo DSM.

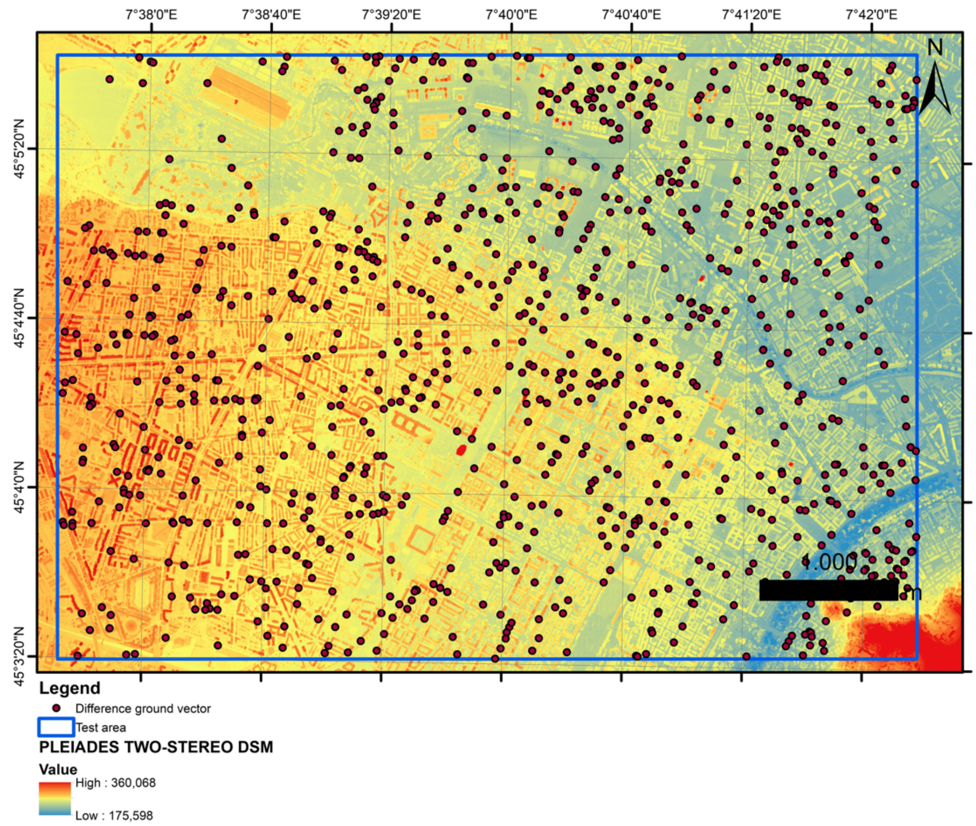

Figure 58 - Test area, inside "difference ground vector" points Pléiades-1A tri-stereo referred, Pléiades-1A tri-stereo DSM on the background

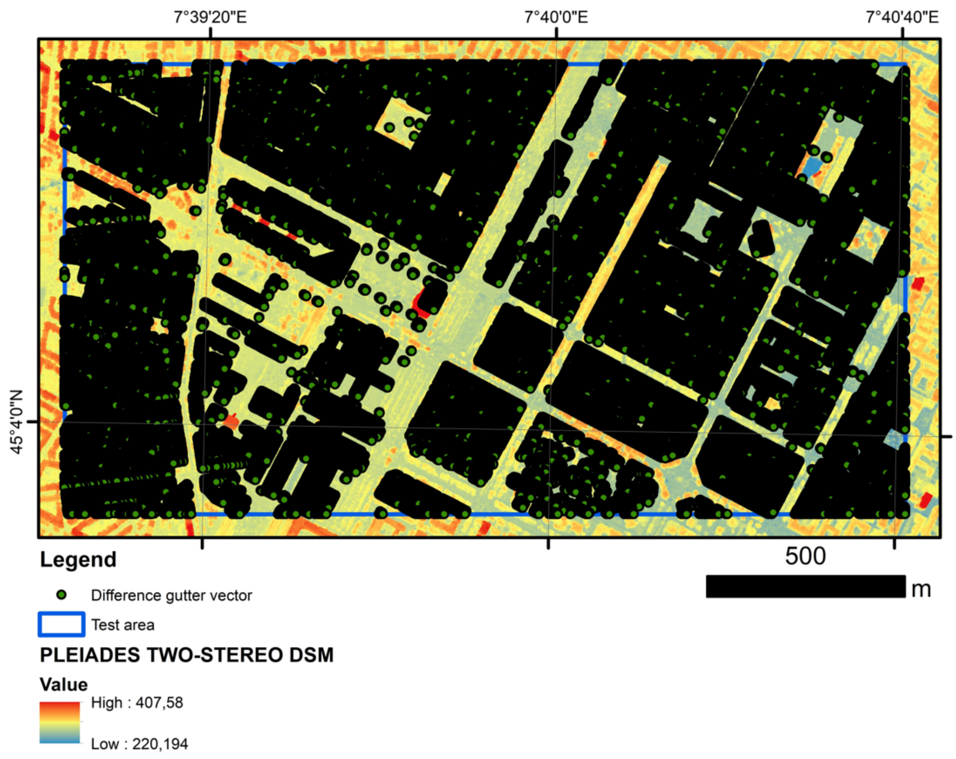

Figure 59 - Test area, inside "difference gutter vector" points Pléiades-1A two-stereo referred, Pléiades-1A tri-stereo DSM on the background

5.2.2.1. Results using ground heights benchmarks

At this point it was subtracted to the DSMs the benchmarks raster referred to the ground heights (“ground raster”), obtaining the raster representing the difference in heights “difference ground raster” and transformed it in a vector product “difference ground vector”. From these files, through a “select by location” command, there were selected the points falling in the test area. From these points were extracted the statistics, reporting their count (number of elements), the minimum and the maximum, mean, sum and standard deviation above all their heights *(Fig. 61 - 62 - 63)*. All the values are also resumed in the table 11.

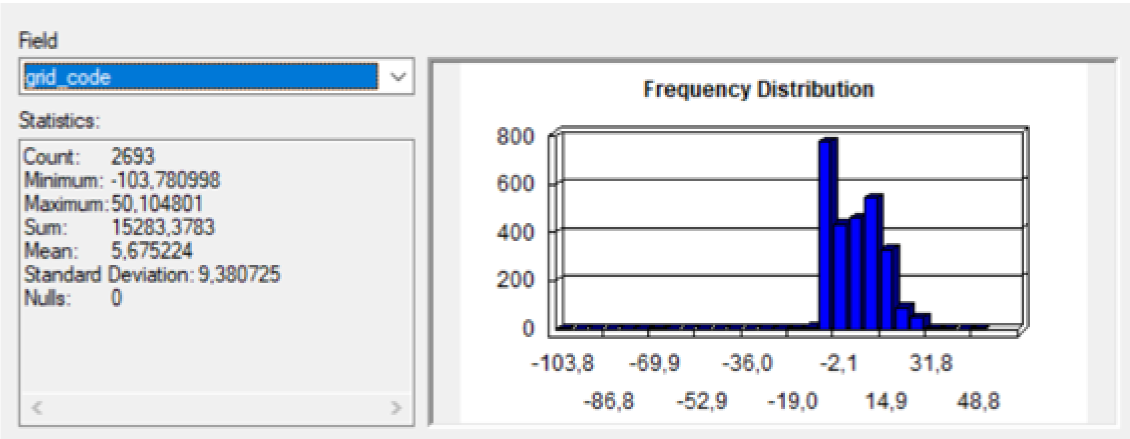

Figure 60 - Statistics ground heights WorldView-3 DSM minus "ground raster" (ArcMap)

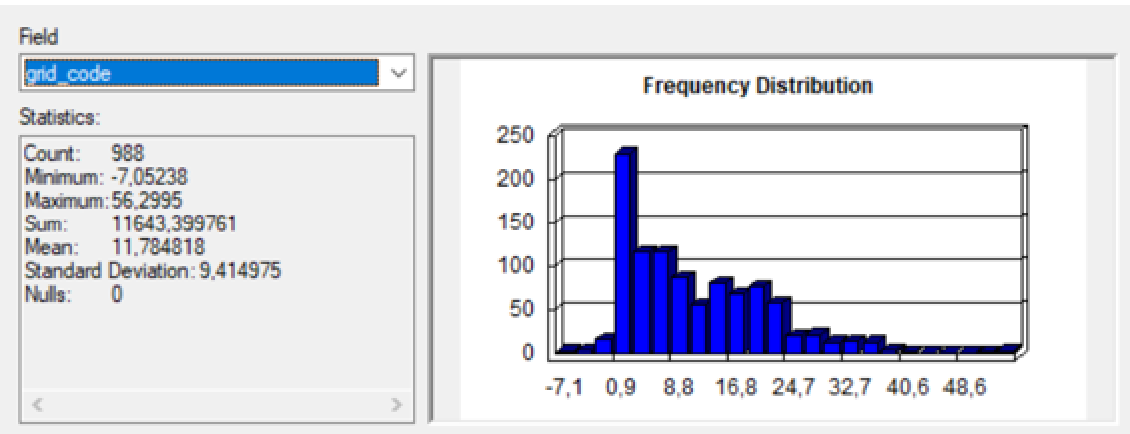

Figure 61 - Statistics ground heights Pléiads-1A two-stereo DSM minus "ground raster" (ArcMap)

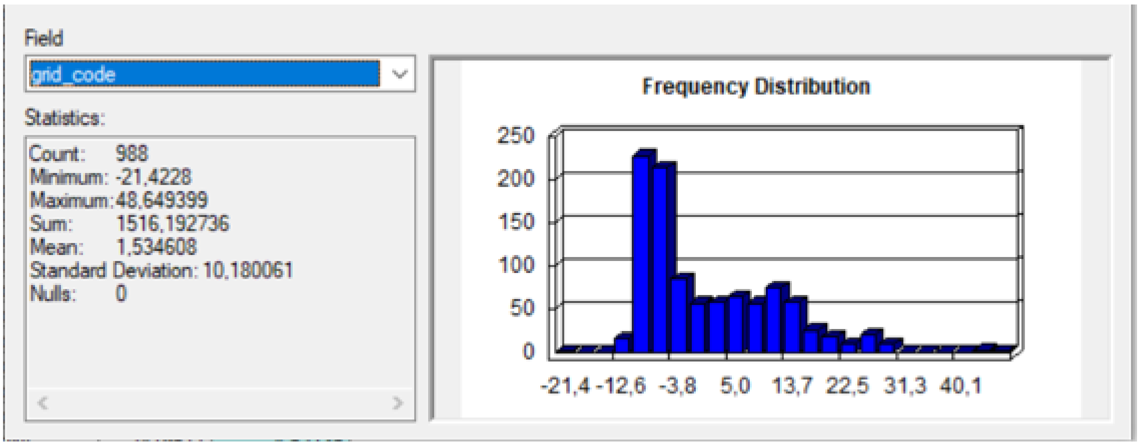

Figure 62 - Statistics ground heights Pléiads-1A tri-stereo DSM minus "ground raster" (ArcMap)

Table 11 - Summary table of the statistics referred to the height ground differences

	WorldView-3	Pléiades-1A two-stereo	Pléiades-1A tri-stereo
Count	2693	988	988
Min [m]	-104	-7	-21
Max [m]	50	56	47
Sum [m]	15283	11643	1516
Mean [m]	5.7	11.8	1.5
St. deviation [m]	9.4	9.4	10.2

The analysis was conduct on a sample of 2693 points for WorldView-3 and 988 points for Pléiades-1A (each representing a height difference). Being a difference between the heights of the DSM and the real heights, the models reach the perfection for value of difference that tends to zero.

Looking at the statistics referred to all the sample *(Tab. 11)* it is possible to notice that the standard deviation (express the variability of the distribution) presents in all the models very high values, which in the case of Pléiades-1A tri-stereo is also very far from the mean value. It was therefore wanted to investigate the causes that led to these phenomena. Thus, there were chose 6 sample points presenting an abnormal (too far from zero) ground height difference value and 3 a correct one, from Pléiades-1A tri-stereo sample; then they were analyzed *(Focus 7 - 8 - 9).* The causes found are applicable to all the models. The anomalies are related to two effects:

a) High positive difference values (Focus 7), perspective geometric distortions due to the inclined view angle of the satellite acquisition, found where the point (which in the reality is on the ground/street) fall in the DSM on a roof, then the DSM present the height of the roof and the point the ground one;

b) High negative difference values *(Focus 8),* when the DSM for the foreshortening or the presence of shadows (usually in the city canyons) has wrong digitalized the ground, underestimating the height value. In this case the point fall on the DSM in a "hole", in which the DSM present a really low height and the point the real one of the ground.

In the Focus 9 instead, it is possible to appreciate, that the height difference values tend to 0. All this sample points have in common the being not shot by the foreshortening effect and being perfectly on the ground. Another additional effect that is not observable in the DSM, is the mistake caused by the presence of object on the streets (e.g. vehicles, dehors, stalls, etc.) during the acquisition of the images, bringing to an overestimation of the heights. For this reason, this kind of analysis are normally conducted in areas with little traffic. Since we did not compare the result with a very high precision models (LIDAR) it is not possible to carry on the analysis in the rural areas of the city. Therefore in the next chapter the focus will be on the roof (gutter) heights analysis.

Focus 7 - Sample points that present height difference abnormal values in Pléiades-1A tri-stereo

Sample point 1 (height difference = 48,64 m)

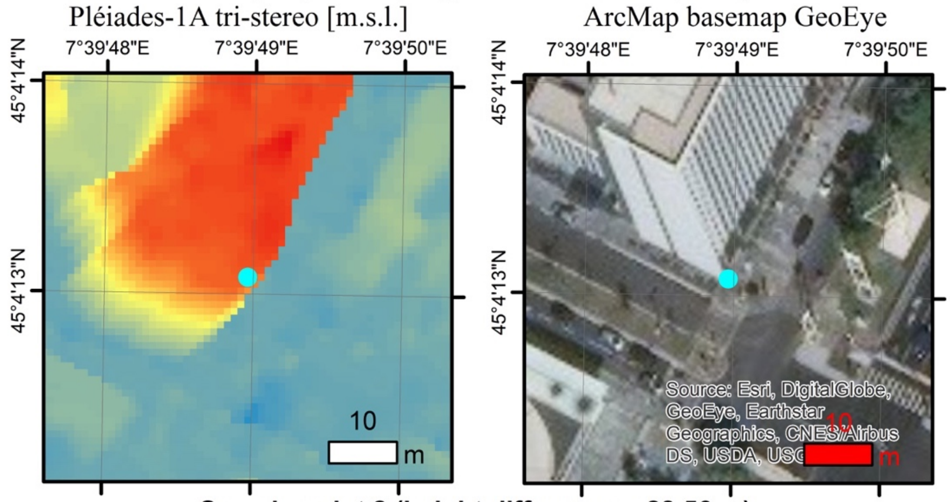

Sample point 2 (height difference = 28.56 m)

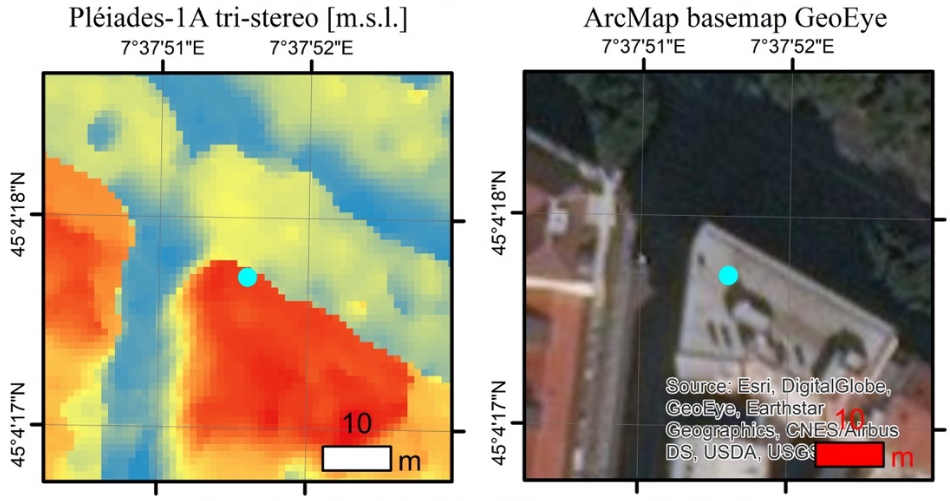

Sample point 3 (height difference = 14.48 m)

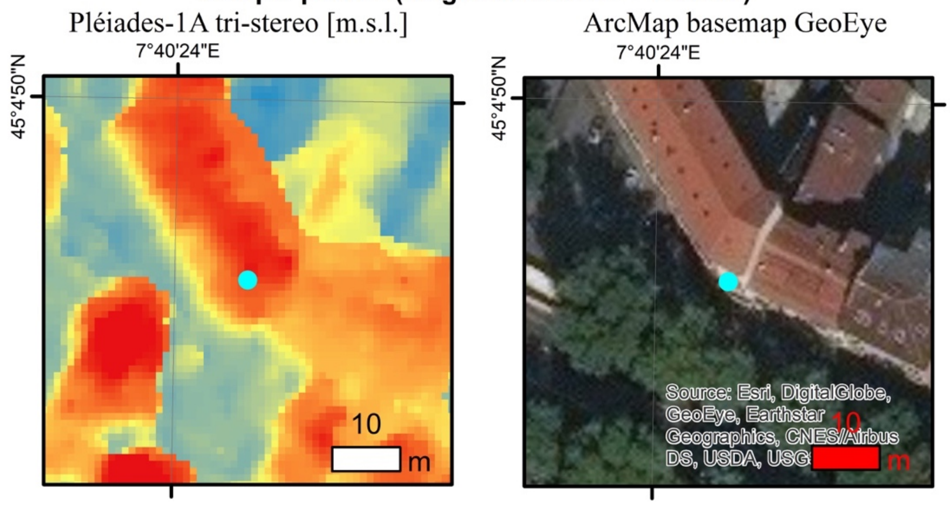

Focus 8 - Sample points that present height difference abnormal values in Pléiades-1A tri-stereo

Sample point 4 (height difference = -21.42 m)

Pléiades-1A tri-stereo [m.s.l.]

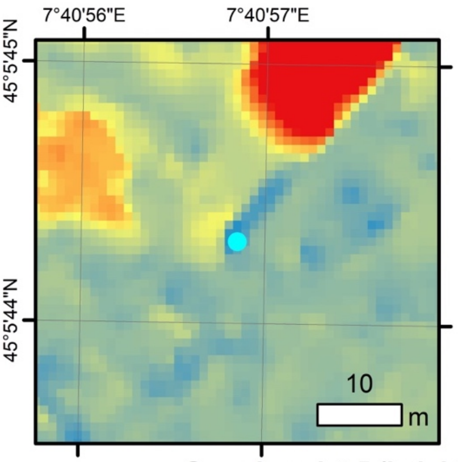

ArcMap basemap GeoEye

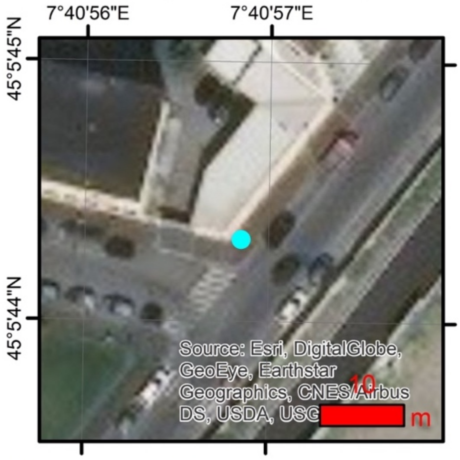

Sample point 5 (height difference = -10.19 m)

Pléiades-1A tri-stereo [m.s.l.]

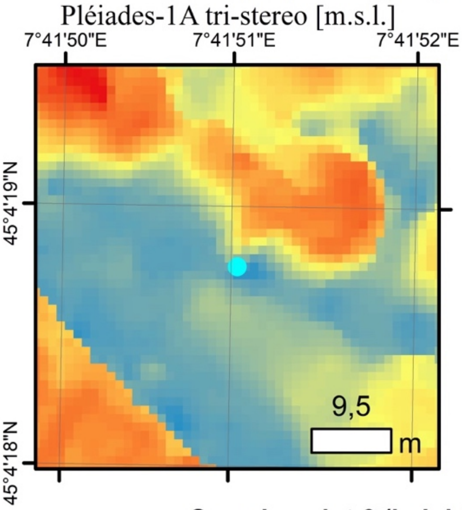

ArcMap basemap GeoEye

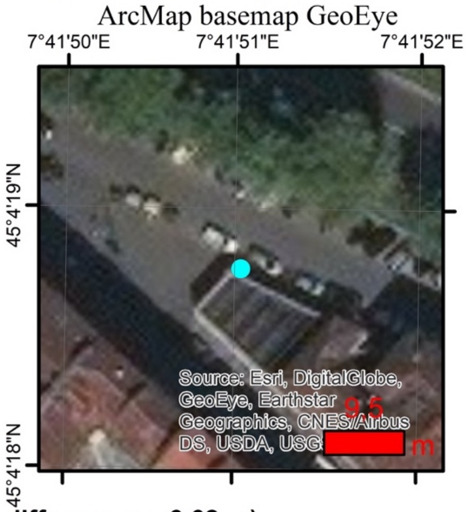

Sample point 6 (height difference = -6,62 m)

Pléiades-1A tri-stereo [m.s.l.]

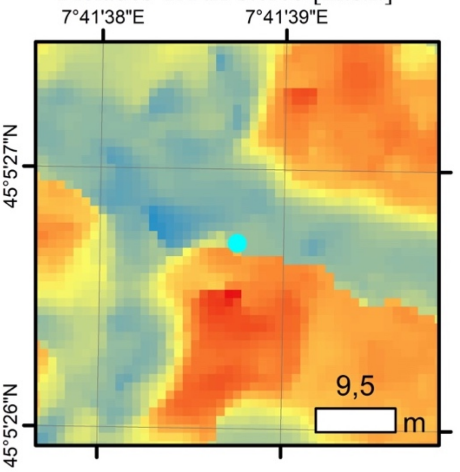

ArcMap basemap GeoEye

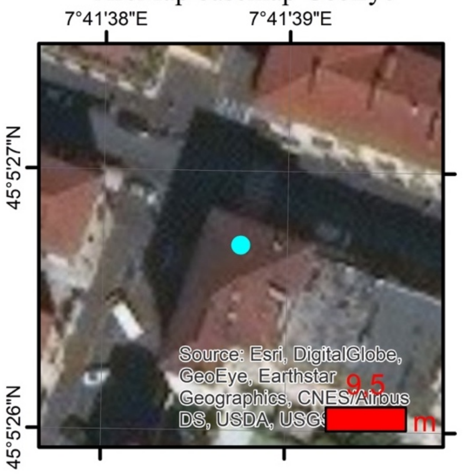

Focus 9 - Sample points that present height difference correct values in Pléiades-1A tri-stereo

Sample point 7 (height difference = 0.24 m)

Pléiades-1A tri-stereo [m.s.l.]

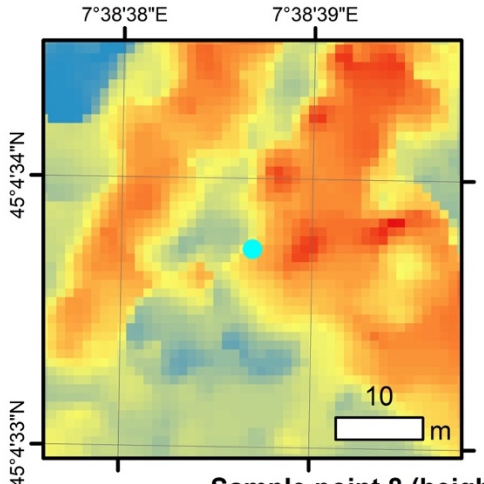

ArcMap basemap GeoEye

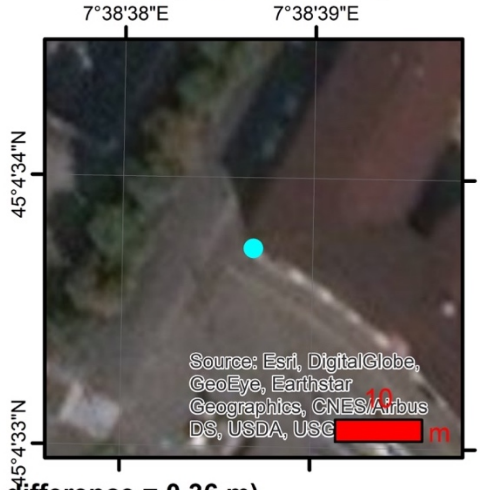

Sample point 8 (height difference = 0.36 m)

Pléiades-1A tri-stereo [m.s.l.]

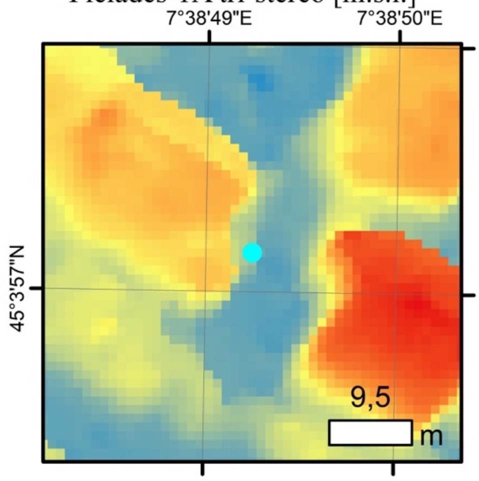

ArcMap basemap GeoEye

Sample point 9 (height difference = -0.11 m)

Pléiades-1A tri-stereo [m.s.l.]

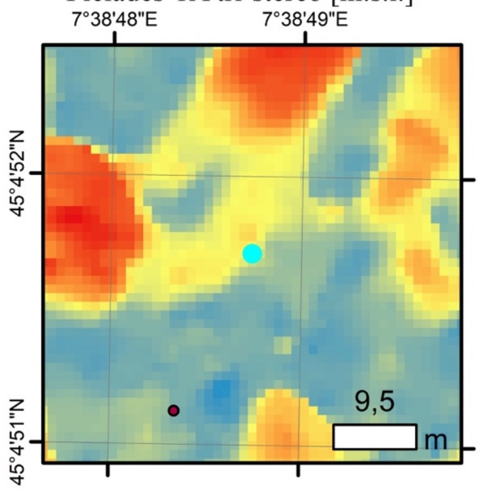

ArcMap basemap GeoEye

After these ascertainments, it was decided to restrict the sample in an acceptance range between -10 m and 10 m. In this way, delating the systematic errors from the sample, it was obtained a more representative one. From a first look at the new samples statistics *(Fig. 64 - 65 - 66, Tab. 12)* the model with the better distribution of the values in the range, presenting a Gaussian trend, is Pléiades-1A tri-stereo. It is also the model with mayor number of sample points falling in the acceptance range (76%), followed by WorldView-3 with 64% and Pléiades-1A two-stereo with 54%. As it is possible to see the mean of the tri-stereo DSM is negative, this mean that the effect showed in the focus 1 is minimized. This minimization is imputed to the tri-stereo mode which, as said before, reduce the perspective geometric distortions.

In WorldView-3 and even more in Pléiades two-stereo the distribution is concentrated on positive values, meaning that these models reduce the foreshortening effect. This confirm the reduction better processing of the canyon saw for Pléiades two stereo in the qualitative analysis.

At the end of this assessment of the ground differences is legitimate to evaluate Pléiades-1A tri-stereo DSM as the best product.

Table 12 - Summary table of the statistics referred to the height ground differences in the range [-10,10]

	WorldView-3	**Pléiades-1A two-stereo**	**Pléiades-1A tri-stereo**
Count	1740	515	751
Percentage of falling sample over the total	64%	54%	76%
Min [m]	-10	-10	-10
Max [m]	10	10	10
Sum [m]	448.56	2263.8	-2215.9
Mean [m]	0.25	4.3	-2.9
St. deviation [m]	5	2.8	5.4

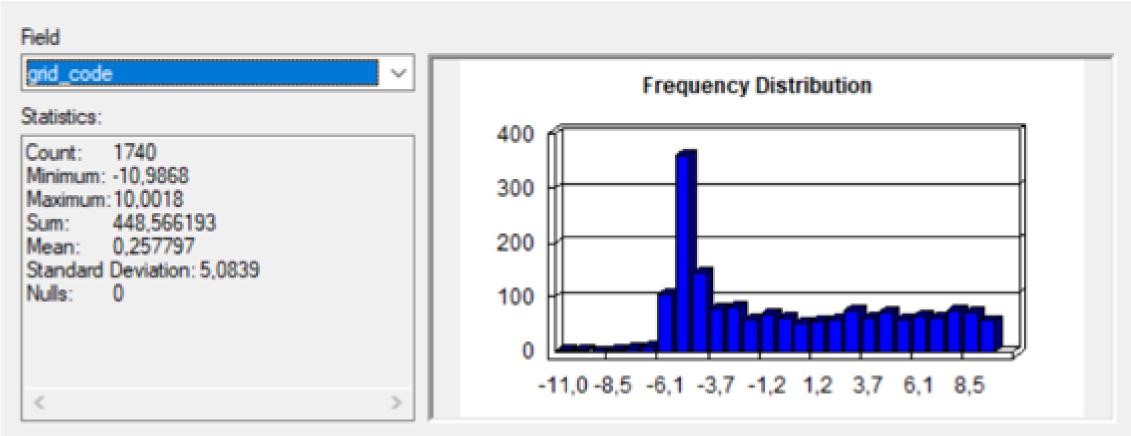

Figure 63 - Statistics in the range [-10,10] ground heights WorldView-3 DSM minus "ground raster" (ArcMap)

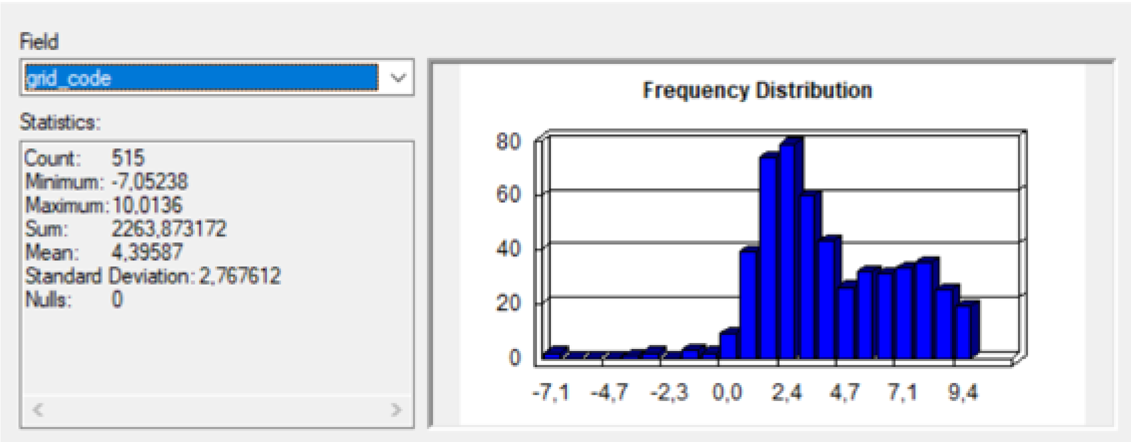

Figure 64 - Statistics in the range [-10,10] ground heights Pléiades-1A two-stereo DSM minus "ground raster" (ArcMap)

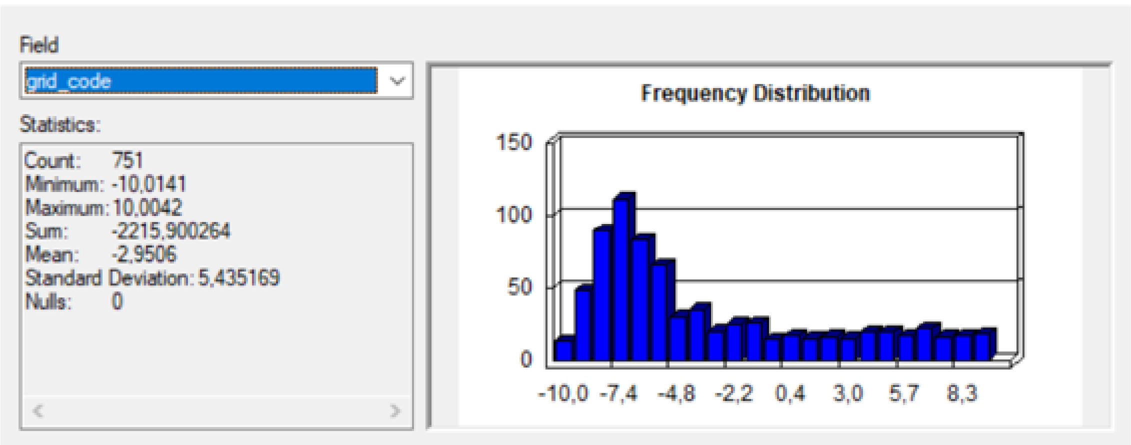

Figure 65 - Statistics in the range [-10,10] ground heights Pléiades-1A tri-stereo DSM minus "ground raster" (ArcMap)

5.2.2.2. Results using gutter heights benchmarks

As seen for the ground heights assessment, we have subtracted to the DSMs the benchmarks raster referred to the gutter heights (“gutter raster”), obtaining the raster representing the difference in heights “difference gutter raster” and transformed it in a vector product “difference gutter vector”. From these files, through a “select by location” command, there were selected the points falling in the test area. From these points there were extracted the statistics, reporting their count, the minimum and the maximum, mean, sum and standard deviation above all their heights *(Fig. 67 - 68 - 69).*

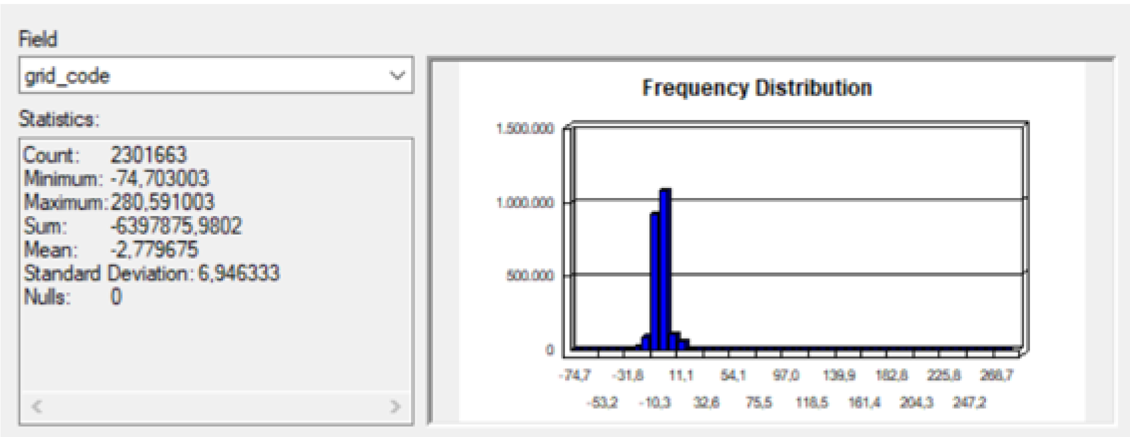

Figure 66 - Statistics gutter heights WorldView-3 DSM minus "gutter raster" (ArcMap)

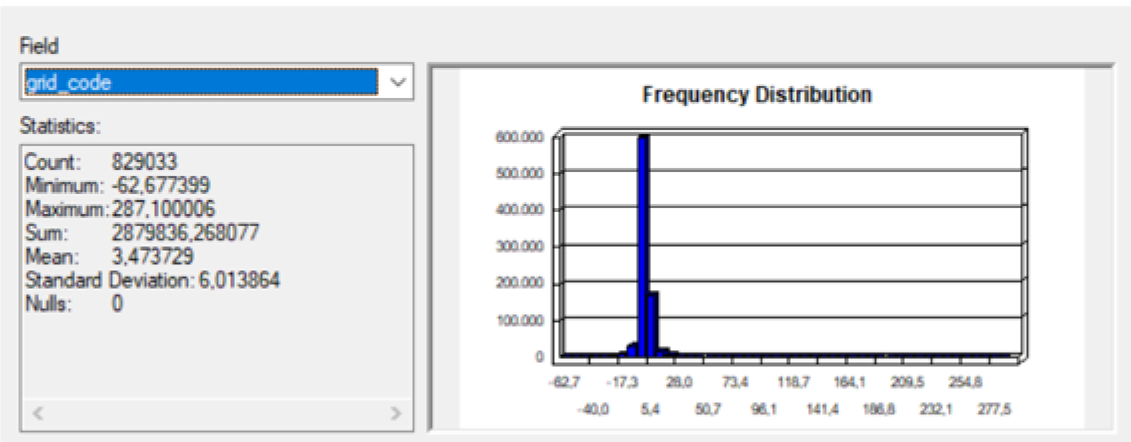

Figure 67 - Statistics gutter heights Pléiades-1A two-stereo DSM minus "gutter raster" (ArcMap)

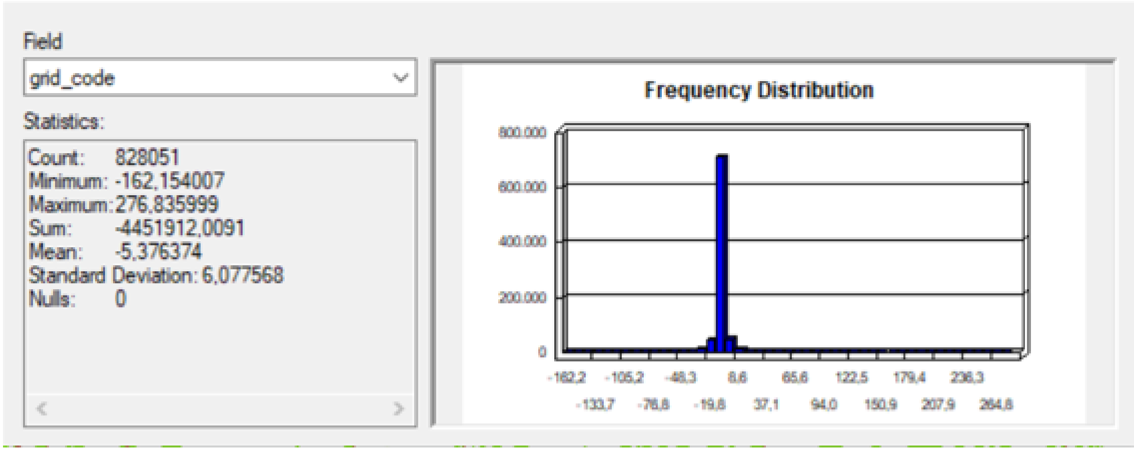

Figure 68 - Statistics gutter heights Pléiades-1A tri-stereo DSM minus "gutter raster" (ArcMap)

In this case the sample is constitute by a really high number of points. For this reason, the assessment of the gutter heights starts with a visual evaluation of three thematic rasters *(Fig. 70 - 71 - 72)*, which classify for each DSM the gutter heights in 8 ranges of values (as it is showed in the legend). From a first analysis of those emerge that the best prediction of the roofs heights is done by Pléiades-1A tri-stereo DSM, followed by WorldView-3 and Pléiades-1A two-stereo one.

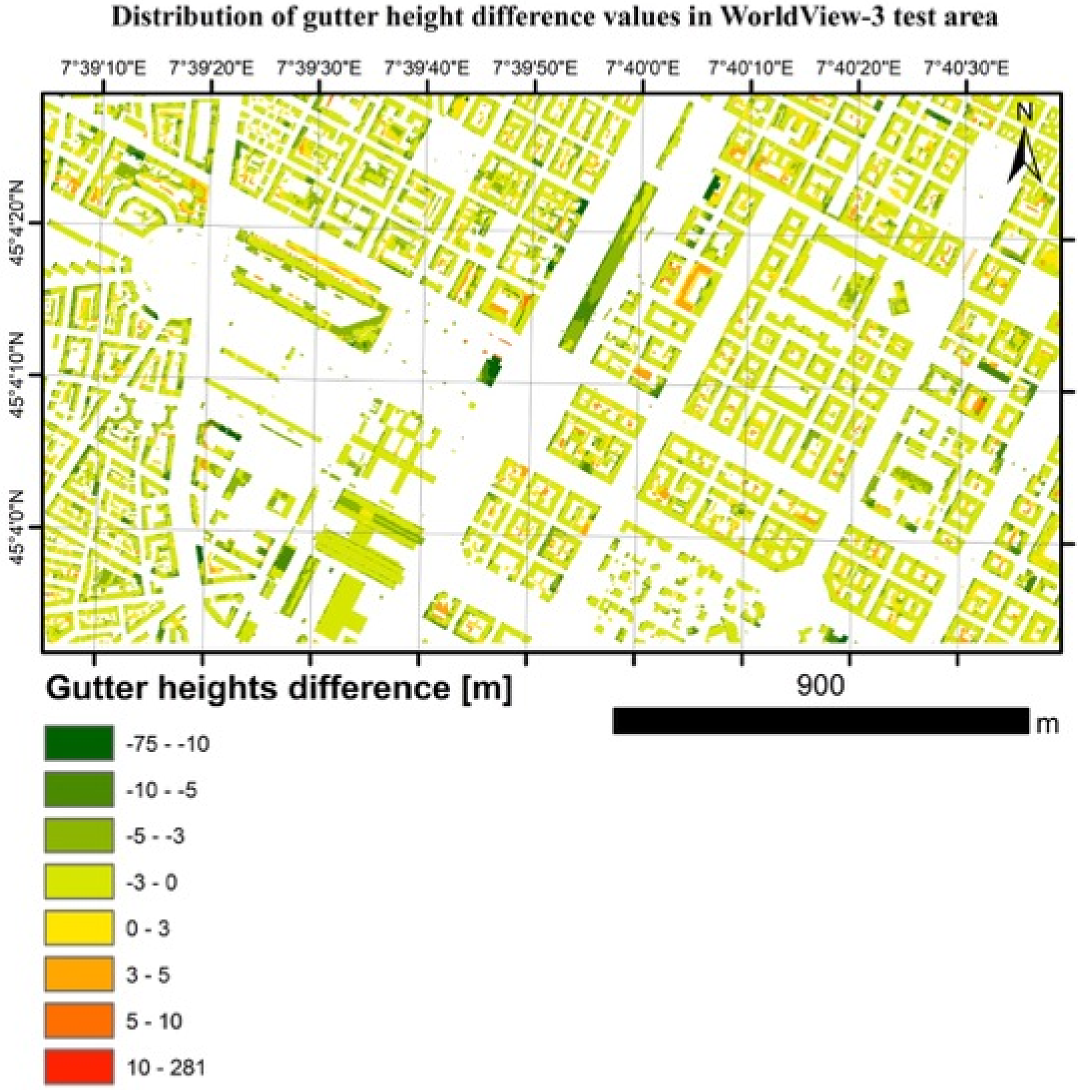

Figure 69 - Distribution of gutter height difference values in WorldView-3 test area (ArcMap)

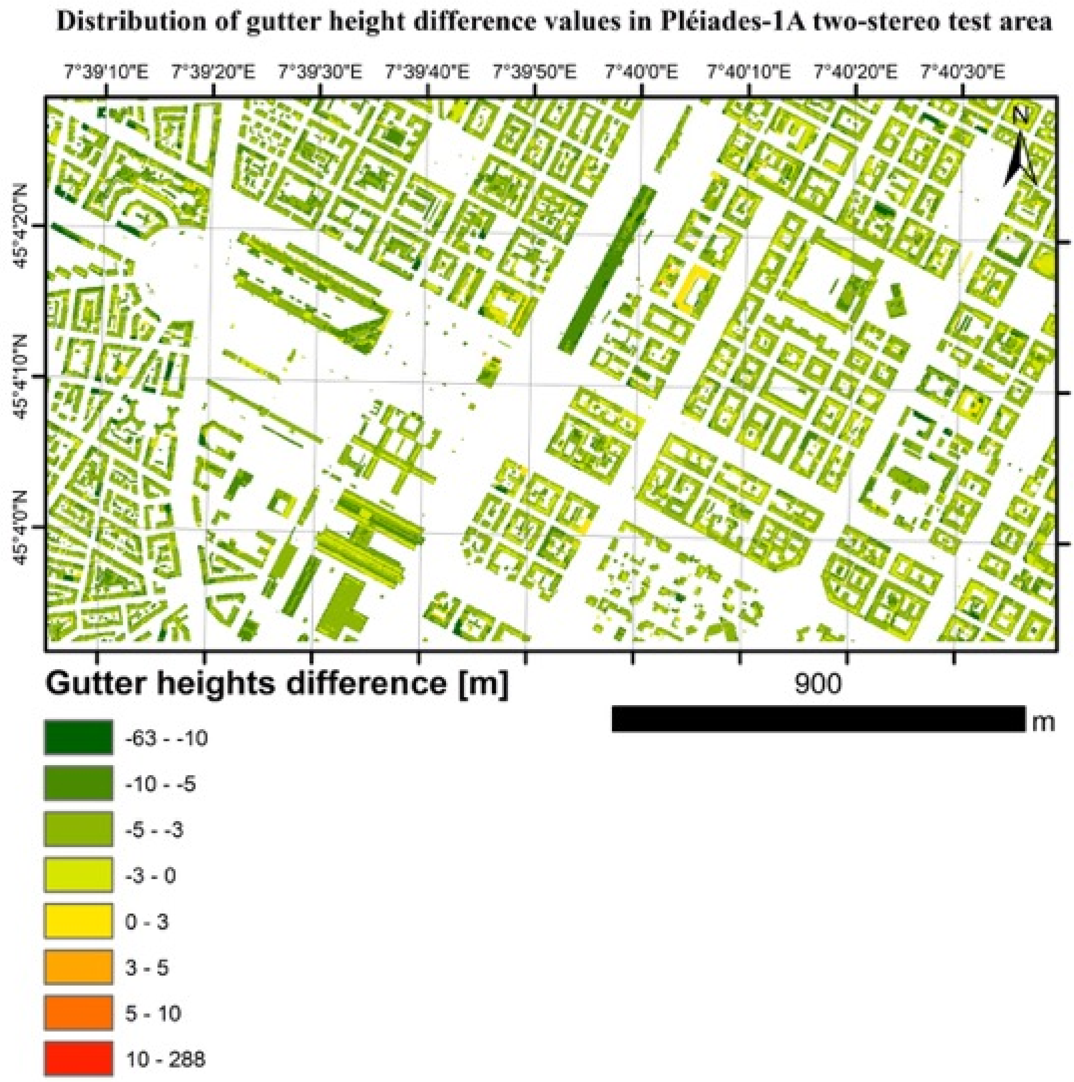

Figure 70 - Distribution of gutter height difference values in Pléiades-1A two-stereo test are (ArcMap)

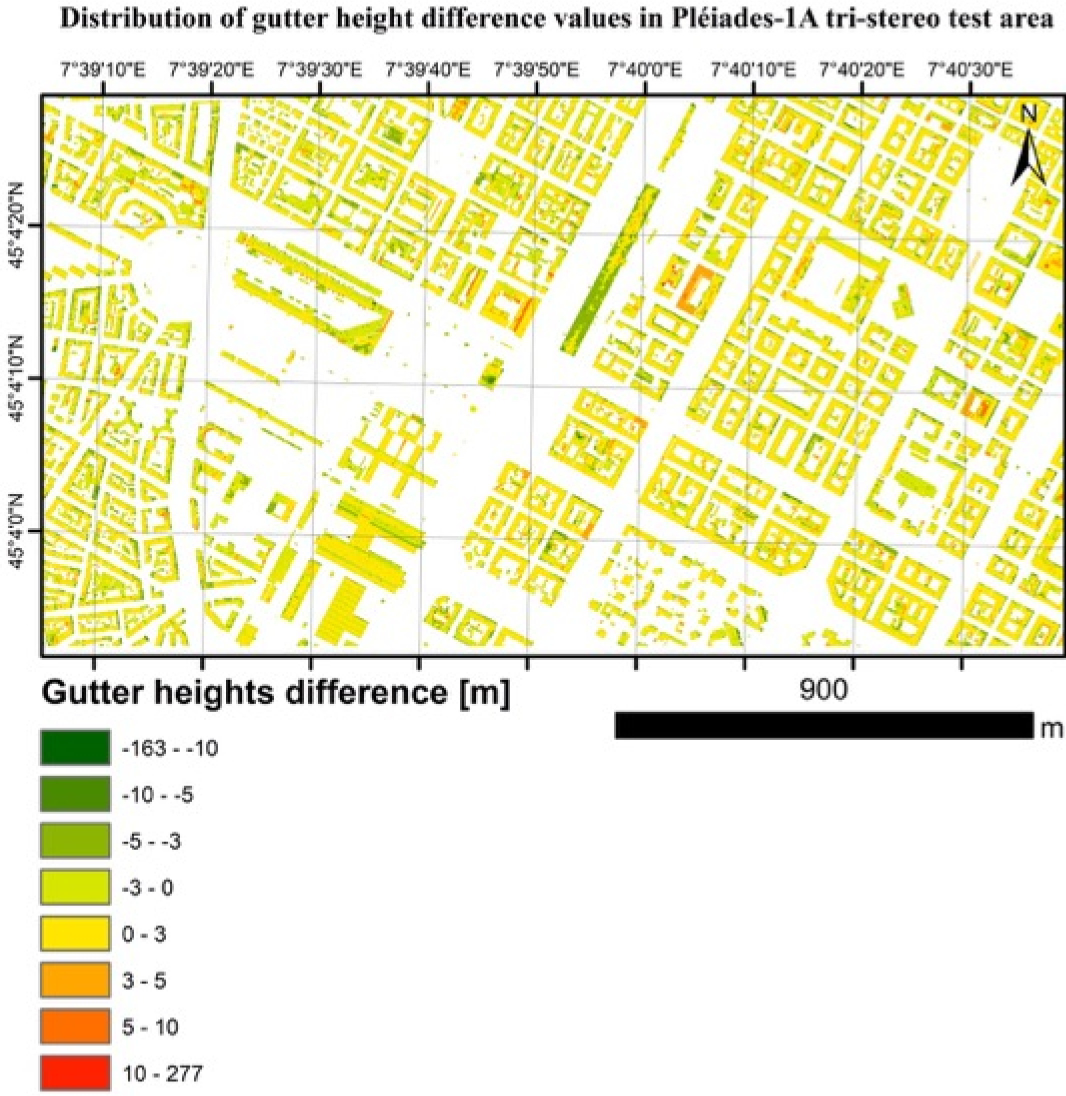

Figure 71 - Distribution of gutter height difference values in Pléiades-1A tri-stereo test area (ArcMap)

Despite in this case the models are not affected by the problems saw for ground height differences evaluation, there are other issues coming from the gutter benchmark *(Focus 10)*. It was extracted from a volumetric raster, which report for each roof a constant value of height corresponding to the higher part of it, i.e. transforming all the roofs in flat ones. This can bring to high values of the gutter height differences (from 1 m to 5 m) in cases of pitched roofs *(Sample point 3, focus 10)*. This bring to the conclusion that for this evaluation a model with a distribution oriented on negative values can be more reliable than one with a negative mean.

Other issues in the models are related to:

a) High negative difference values (Focus 10, sample point 1), found where a point of the raster (which in the reality is on the roof) fall in the DSM on the ground area, then the point present the height of the roof and the DSM the ground one. This evidence affects mainly buildings borders;
b) High positive difference values *(Focus 10, sample point 2),* found where point present a false null value of height or when there is a new construction not yet included in the database. The result of the subtraction is yet the height of the DSM. This kind of errors are restricted to two buildings and belong to human mistakes or not updated cartography.

Focus 10 - Sample points that present height difference abnormal values in Pléiades-1A tri-stereo

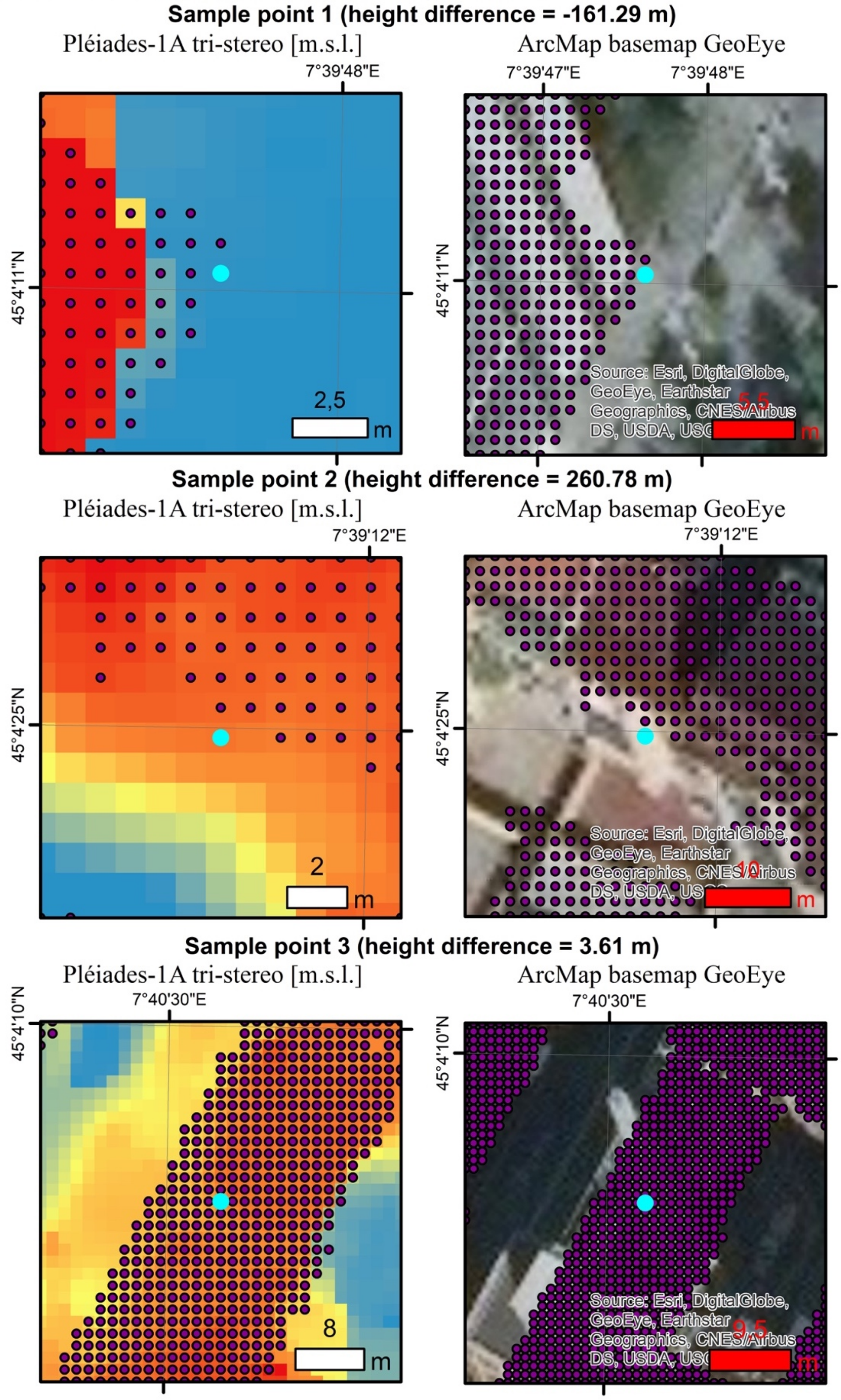

Although the sample is numerous, most of the points, deleting the ones with errors previously seen, are concentrated in the range [-20,10]. Ascertained that the majority of the negative values are correlated to the case in which the point of the raster (which in the reality is on the roof) fall in the DSM on the ground area, it was preferred to reduce the acceptance range from -10 to 10. All the models present a Gaussian distribution.

Looking at the percentage of sample points falling in this range (all around 90%) *(Tab. 13),* it is possible to conclude that in the city the DSMs better defines the roofs than the streets, due to the foreshortening and inclination. The number of points affected by the problems (delineated before) is very low if compared to the total sample. As found in the qualitative analysis Pléiades-1A two-stereo DSM better outline the roof heights. Observing better also the thematic rasters and their legends *(Fig. 73 - 74 -75)*: the values in Pléiades-1A tri-stereo are concentred in the range [0, 3], the two-stereo one instead distributes the values from [-3, 0] and [-3, -6]. As said before, due to the benchmark systematic error, if the distribution is oriented on negative values, that means that the model better shapes the pitched roofs. At the end of this assessment of the roof heights differences is legitimate to evaluate Pléiades-1A two-stereo DSM as the best product, confirming the conclusion of the qualitative analyzes.

Table 13 - Summary table of the statistics referred to the height gutter differences in the range [-10,10]

	WorldView-3	**Pléiades-1A two-stereo**	**Pléiades-1A tri-stereo**
Percentage of falling sample over the total	90,5%	94,63%	91,18%
Min [m]	-10	-10	-10
Max [m]	10	10	10
Sum [m]	448.56	2263.8	-2215.9
Mean [m]	0.25	4.3	-2.9
St. deviation [m]	5	2.8	5.4

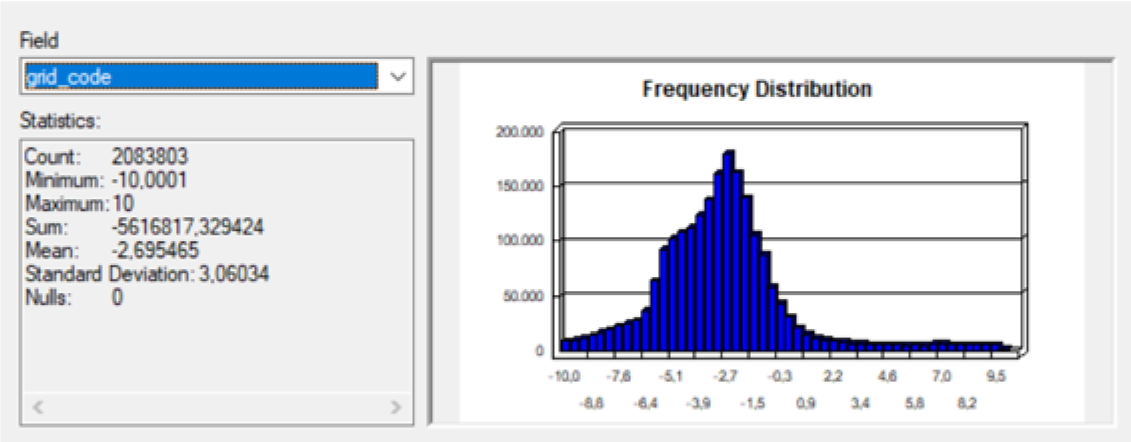

Figure 72 - Statistics in the range [-10,10] gutter heights WorldView-3 DSM minus "gutter raster" (ArcMap)

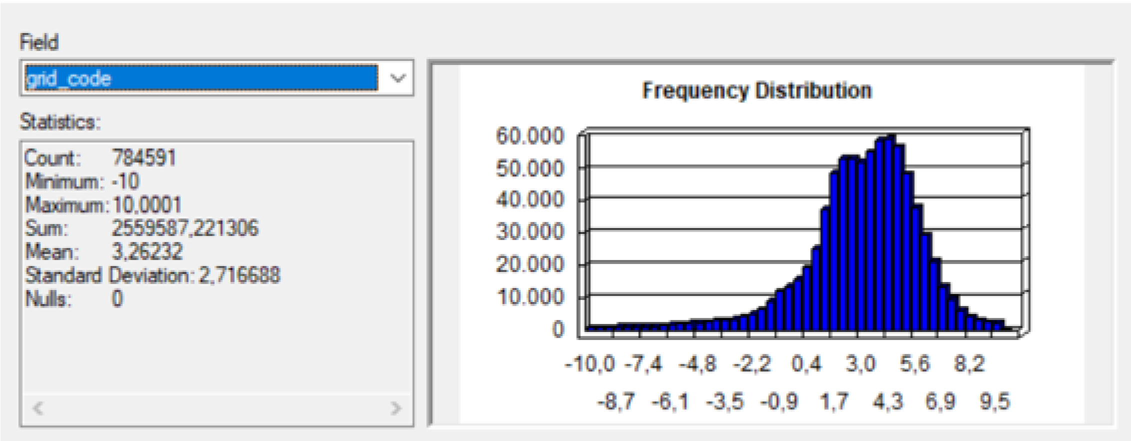

Figure 73 - Statistics in the range [-10,10] gutter heights Pléiades-1A two-stereo DSM minus "gutter raster" (ArcMap)

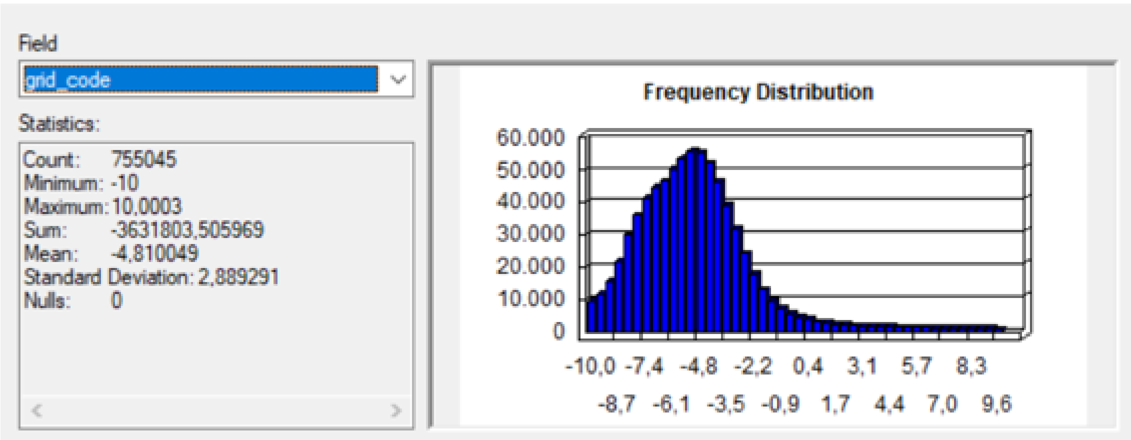

Figure 74 - Statistics in the range [-10,10] gutter heights Pléiades-1A tri-stereo DSM minus "gutter raster" (ArcMap)

6. Application of the models

As seen in Chapter 2.3, the DSMs have a wide ranges of uses, focused in particular on urban planning, bringing important benefits for the sectors in which they are used. Their analysis is mostly based on a visual approach that can be improved by performing basic GIS 3D analysis steps ((Moser, Albrecht and Kosar, 2010). Therefore, in this chapter we want to give an overview of the analyses which can be applied to subsequent DSM: existing cartography update, soil consumption analysis, urban green classification, evaluation on mobile network antenna positioning, emergency management and telephony coverage planning, building damage assessment, roof slope and solar incoming radiation assessment.

6.1. Application based on orthorectification of images based on VHR DSM

The ortho-rectified images, combining the properties of the DSM (rapid display of the heights of each object on the surface) with the orthophoto one (possibility of understanding the properties of the soil and of the framed objects, in particular the materials and the texture of the buildings), is presented as the perfect product to carry on this type of analysis. For the orthorectification was used the special command Ortho Generation of OrthoEngine PCI Geomatic program *(Fig. 76 - 77).*

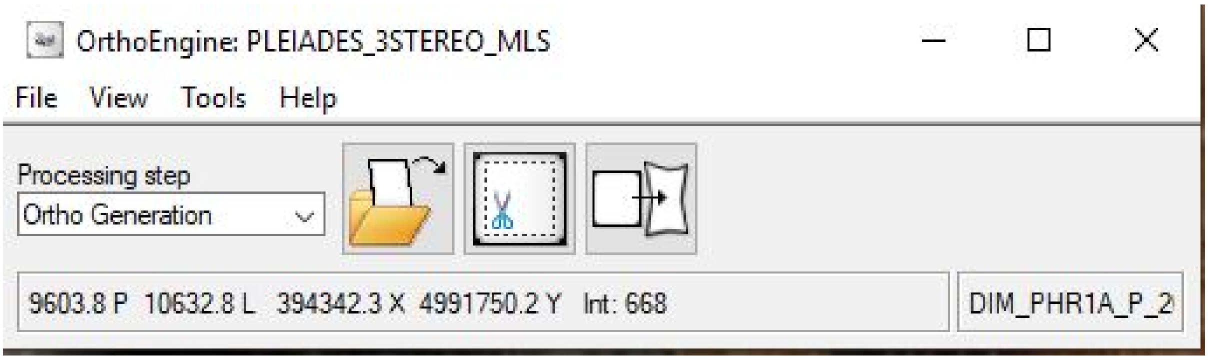

Figure 75 - OrthoEngine PCI, Ortho Generation tool

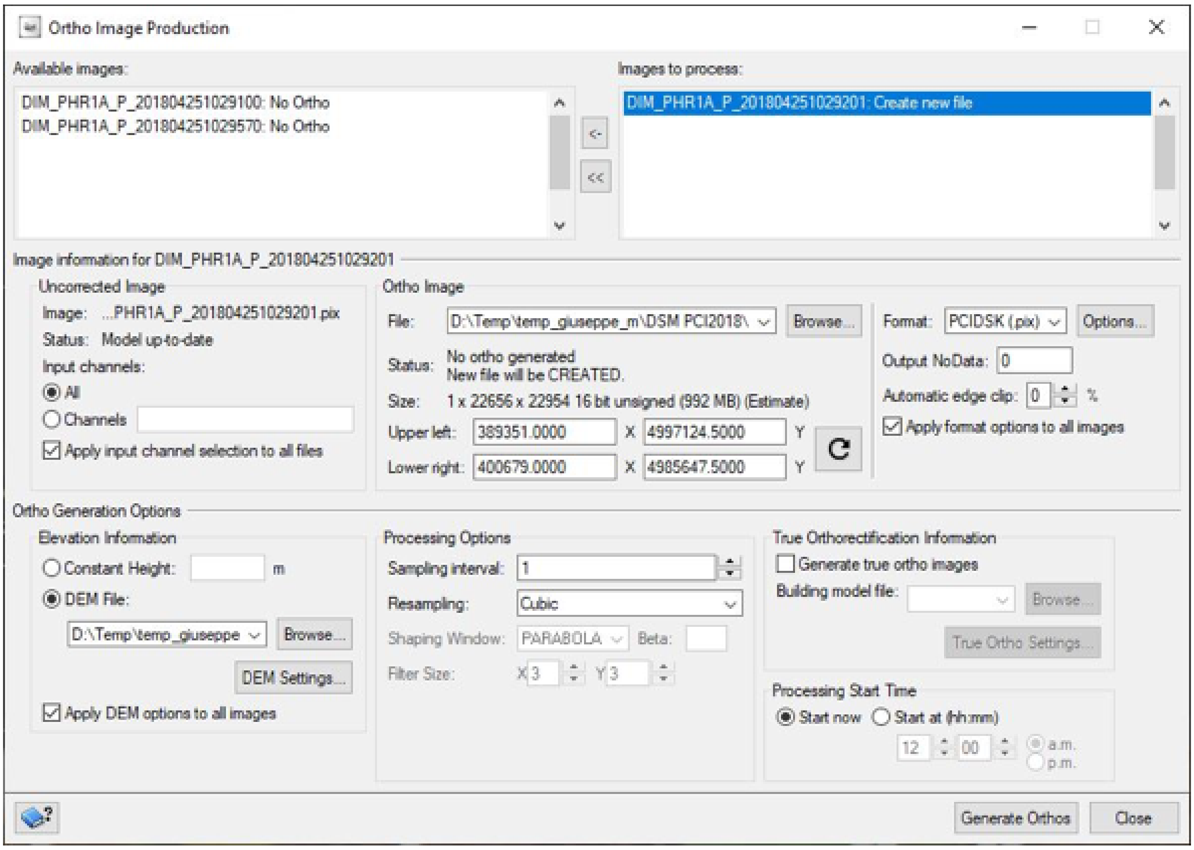

Figure 76 - OrthoEngine PCI, Ortho Generation tool, Ortho Image Generation setting window

In the displayed case, the operation was carried on using Pléiades-1A tri-stereo mean sea level referred DSM and one multispectral image of the same area acquired by Plèiades-1A. The processed ortho-rectified image *(Fig. 80)* present a low resolution (because use a multispectral image as base). For this reason it was generated a second ortho-rectified image *(Fig. 82)* using the DSM and a panchromatic image (higher resolution) *(Fig. 81),* in order to subsequently perform a Pan-sharpening with ArcMap

(Fig. 78). The Pan-sharpening function "uses a higher-resolution panchromatic image (raster band) to fuse with a lower-resolution, multiband raster dataset. The result produces a multiband raster with the resolution of the panchromatic raster where the two layers fully overlap" *(Fig. 79)* (ArcMap Help). The used algorithm is the IHS, this method "converts the multispectral image from RGB to intensity, hue, and saturation. The low-resolution intensity is replaced with the high-resolution panchromatic image. If the multispectral image contains an infrared band, it is taken into account by subtracting it using a weighting factor. Then the image is bac-transformed from HIS to RGB in the higher resolution" (ArcMap 10.5.1 Help).

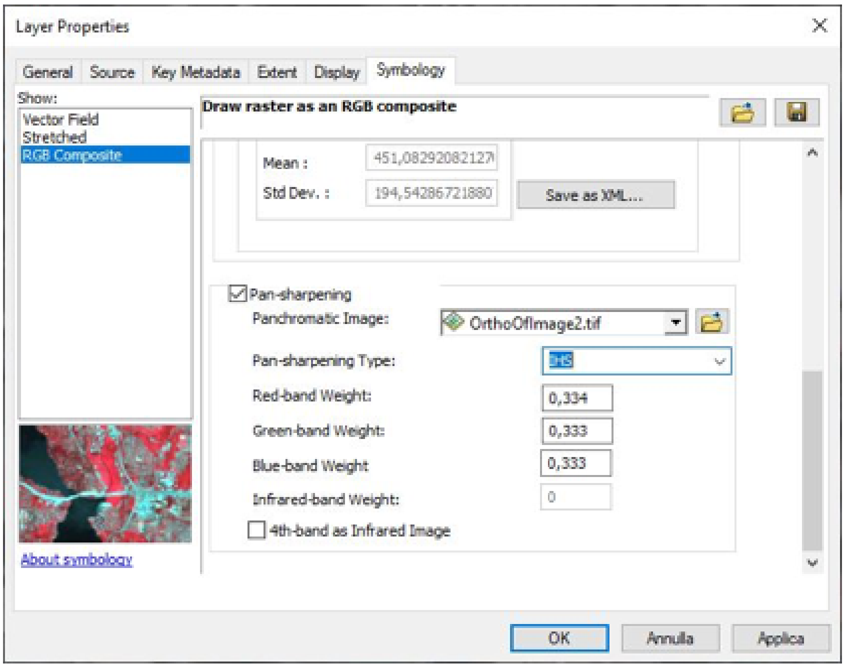

Figure 77 - ArcMap, Pan-sharpening setting window

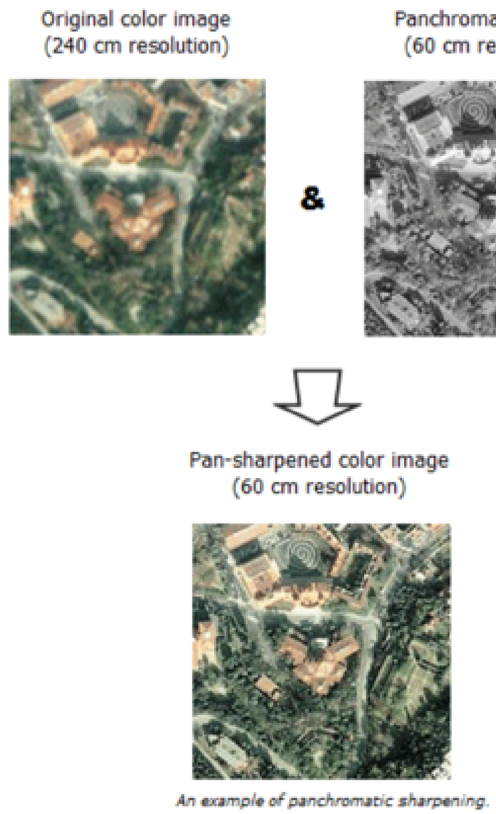

Figure 78 - Example of Pan-sharpening raster processing

Figure 79 - Ortho-rectified multispectral image

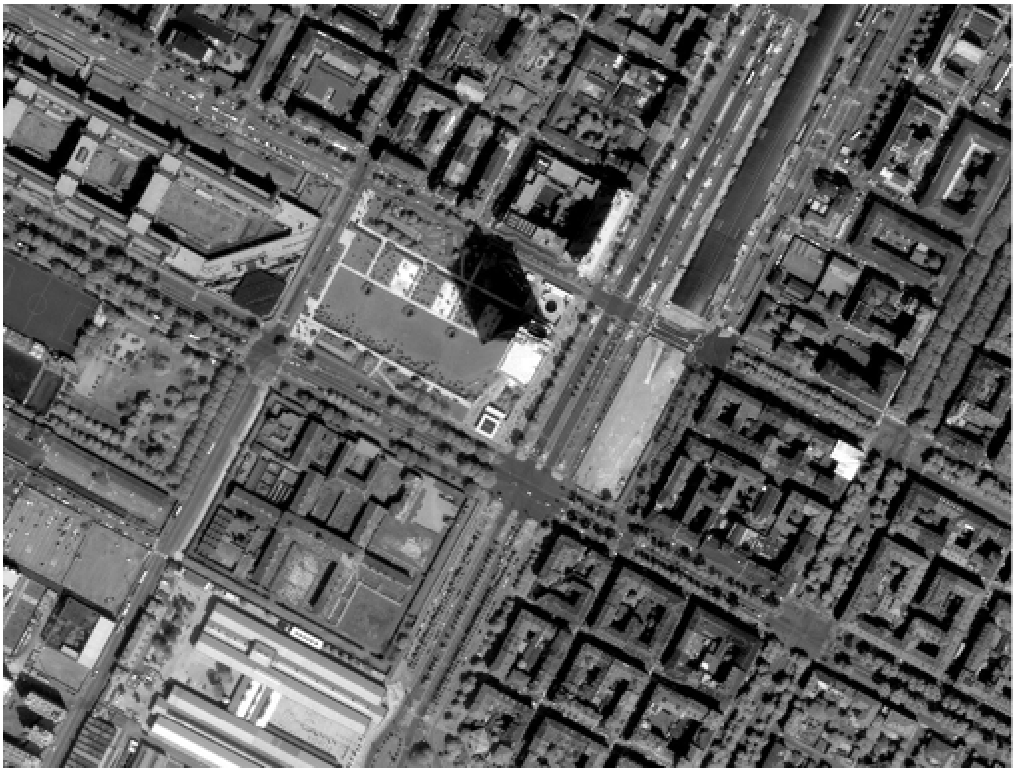

Figure 80 - Ortho-rectified panchromatic image

Figure 81 - Pan-sharpening of the two Ortho-rectified images

Those ortho-rectified images can be used for many purposes related to the city planning. The first one, the most obvious, is the existing cartography update, adding for example heights of new buildings and artefacts or land consumption areas. The new building can be identified for example overlapping a vector data, as the one used as benchmark. Concerning the land consumption analysis in Piedmont (region in which Turin is located), it provides to picturing the transformation processes of the territory, thanks to the updated cartography of the National System for Environmental Protection (SNPA), analysing the evolution of land consumption within a broader framework of territorial transformations at different levels, putting attention on the mapping and evaluation of soil ecosystem services (Isprambiente.com). The process carried on with orthorectified images is almost the same of the normal: having different images acquired in a different time it is possible to appreciate the changes of the soil and the rise of new buildings. The difference is that with the orthorectification the inclination of the buildings disappear, facilitating and improving the quality of the area measurements.

Orthorectified images generated with infrared multispectral one can be very useful for the urban green classification, which precedes a correct analysis of maintenance and disposal costs of it.

6.1.1. Evaluation of potential mobile network antenna positions

The condition of propagation of electromagnetic waves in an urbanized environment is the most difficult to determine, since the portion of electromagnetic energy radiated by the antenna of the transmitting station reaches the receiver propagating itself through different possibilities of paths. The multi-ray fields emitted by the station are subject to propagation mechanisms *(Fig. 83)*: reflection on large flat surfaces, diffraction on surfaces with small irregularities or small objects, transmission and absorption by buildings, vegetation (arboreal and grassy), water, etc..., which lead to a significant variation in the amplitude and phase of the wave (Blaunstein, 1998).

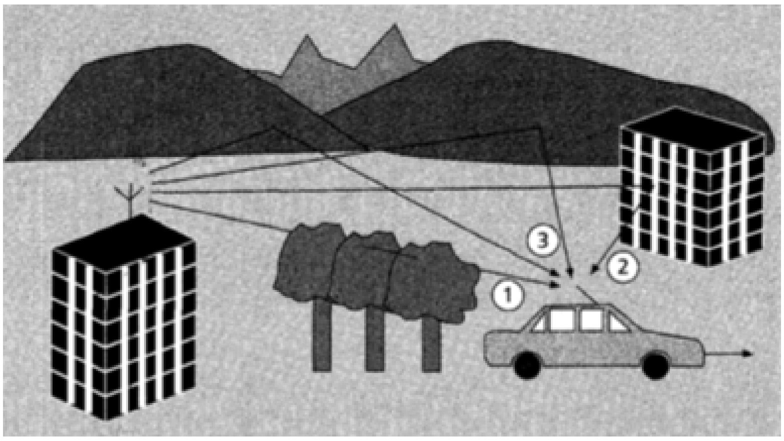

Figure 82 - Propagation electromagnetic waves mechanism in urban environment (Fleury and Leuthold, 1996)

Radio environments can be extremely different (for example, indoor and outdoor environments). As can be seen in table *(Fig. 84),* depending on the type of cell and the position of the base transmission antenna, the propagation scenarios may differ substantially. A decrease in the coverage area is observed as the positioning height and the size of the transmission antenna cell decrease.

Cell types	Base station antenna location	Cell dimension in km
Macrocell	Above rooftop level	1 – 30
Large cell (urban)	Above rooftop level	3 – 30
Small cell (urban)	Above rooftop level	1 – 3
Microcell	Below rooftop level or at about the same level	0.1 – 1
Picocell	Below rooftop level or in a building	0.01 – 0.1

Figure 83 - Main geometric characteristics of radio cells (Fleury and Leuthold, 1996)

The characteristics of a specific environment in a given category usually cannot be described completely as they are subject to random variables, such as the electrical properties of buildings in the urban area, which can be determined up to a certain level of accuracy, and factors which lead to temporal variations of the wave (Fleury and Leuthold, 1996).

Many experimental investigations have shown that the diffusion of the wave decreases in the case in which the transmitting station and the receiver are both on the ground level (at the same level), below the roofs of the buildings. This is due to the fact that the buildings, even depending on the thickness of the walls, appear as insuperable obstacles for the wave, increasing reflection and diffraction (on the edges) and generating a great diffidence between areas of shadow and areas illuminated by the signal (Blaunstein, 1998).

These evidences imply, for the purpose of the correct positioning of the transmitting antenna and an improvement of the signal: a soaring point, an analysis of the surrounding ground cover, preferring areas with simplified land cover, and an evaluation of the weaving and materials constituting the buildings in the area of interest. A DSM can be used for the definition of the positioning points of the antennas for the transmission of mobile network signals (electromagnetic waves). The analysis can be compared to a "visibility analysis". These identify points or areas visible to a specific observer located at a specific point within the cityscape *(Fig. 85)*. Comparing the position of an antenna for the transmission of the mobile network signal to an observer, it is possible to determine from the DSM information related to the area seen by each observing station, that is the quality of each potential position of the observer and the combination of visible points from every position.

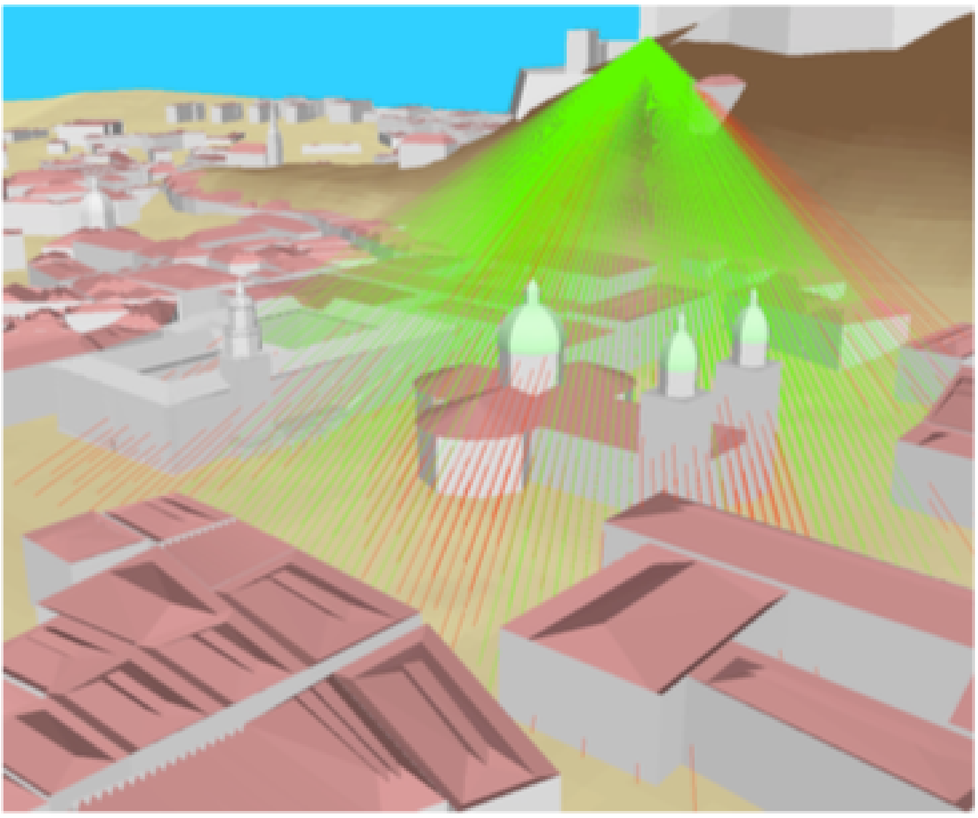

Figure 84 - Iterative line-of-sight-analysis applied to lines from one observer point to a number of evenly distributed target points (Moser, Albrecht and Kosar, 2010)

For a safe positioning measure the system must ensure that each position is visible from at least four observation points, i.e. that each position is covered by at least 4 antennas. If an antenna becomes inactive, the receiver can still rely on another 3 points. This information forms the basis for choosing the optimal combination of observation stations to position the antennas (Moser, Albrecht and Kosar, 2010).

It is wanted to report as example the position of the Polytechnic of Turin antennas. The analysis was conducted using images ortho-rectified on the DSMs of the city previously generated, for the determination of the exposure of a specific antenna position. As it is possible to see from the figure 86, in a first analysis, the rooftop of the building (Polytechnic's part crossing Corso Castel Fidardo) is flat, perfect for the installation of the antennas. In the figure 87, instead, it is showed up the area around the transmitting points. All the buildings and the threes result smaller than the one chose and there is not many low vegetation around it, this implies a minimum absorption and reflection effect on the waves. Moreover, thanks to the multispectral images it is possible to distinguish the rooftops materials of the other buildings.

Figure 85 - Part of polytechnic buildings crossing Corso Castel Fidardo, point of the antennas installation

Figure 86 - Area around the antennas

6.2. Emergency management and telephony coverage planning

Although very different, all these fields of application require the respective analysis of the data concerning the density of the 3D population: the first problem of this datum to predict the movement of masses, possible escape routes and rescue areas, the second he needs it to calculate the telephone network that will require a private area. The population data are normally collected per housing unit, which is why the density related to each building is calculated per floor, considering the relative intended use (commercial, residential, industrial, ...), adding the previous one to the canyons between them (road and pedestrian traffic). In addition to the temporal distribution, for a correct analysis, it will also be necessary to take into account the temporal one going to consider the difference of distribution of the day and night population, taking into consideration factors such as rush hour and weekend traffic. Following the analysis it will therefore be possible to identify the danger zones, which will be more important during the drafting of the civil protection plan, and the telephone network needs (deriving from the cellular transmitters) (Moser, Albrecht and Kosar, 2010).

6.3. Building damage assessment

Each year disasters and calamitous events (earthquakes, floods, hurricanes,…) crashing on different areas of the planet causing loss in terms of human lives and economic damages (public and private buildings, agriculture, businesses,...). The estimates closed from 1980 to 2011, the world trend shows a growth higher than double.

As a result of each event, a damage analysis is therefore necessary and in particular a classification of the buildings in the area concerned ("Destroyed", "Severe Damage" and "Moderate Damage"). This operation in recent years has been facilitated by the use of satellite images and the drafting of "emergency maps", to support emergency response operations. Two of the major services able to provide post-event information about disasters are Copernicus (European Union, 2012-2018, Copernicus EMS) and UNOSAT (Program of satellite operational applications). Both base their analysis on vertical VHR satellite images, comparing the pre and post event dataset of the affected region (Cotrufo, Sandu, Tonolo, Boccardo, 2018).

In some cases, however, it is not very easy to think of a building being damaged by simple observation of vertical images. Instead, the acquisition of a pair of stereoscopic images and, for a further and more detailed analysis, the generation of DSM permit a double exposure visualization for the evaluation of architecture and 3D geometry of damaged buildings. In the figure 88 there were reported as example two different representation of a damaged building in Turin (in the intersection of Corso Vercelli and Via Cuneo). The one on the right is a normal satellite multispectral image acquired by GeoEye, which can be compared with the dataset used by emergency services. On the left the building, represented in Pléiades-1A tri-stereo DSM, report the heights of each point of the building, pointing out the real damage on it. Figure 89 shows the real state of the building thanks to a 3D detailed rendering of Google Earth. It is possible to increase the accuracy of building damage assessment putting beside the use of a satellite VHR, the availment of digital surface models. Already today and more in the future this technology will be essential for areas in which there is not an updated reference cartography.

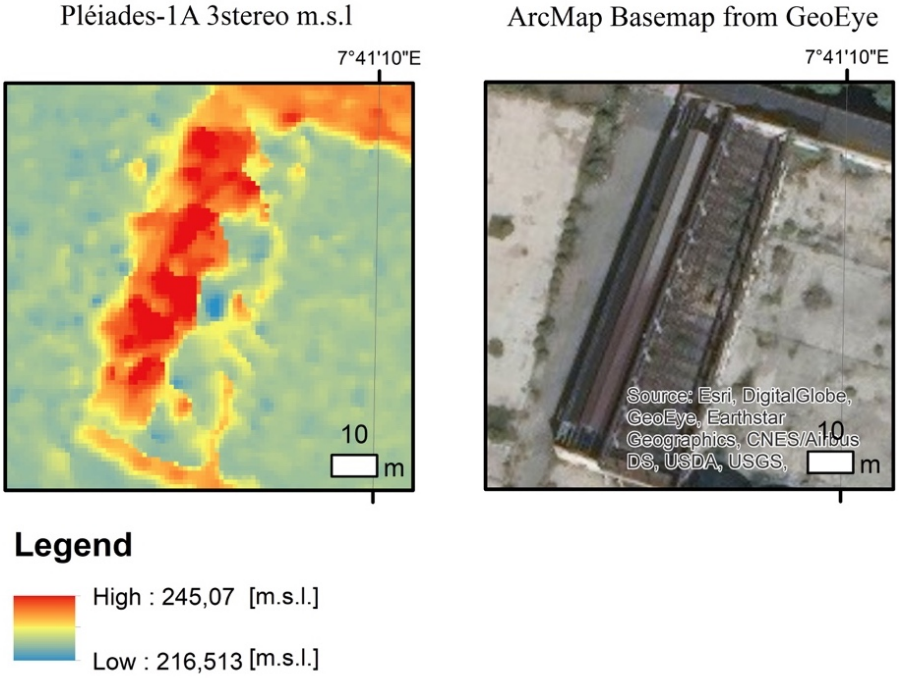

Figure 87 - Damaged building in Turin area, Pléiades-1A tri-stereo (left) and GeoEye satellite image (right)

Figure 88 - Google Chrome 3D view, damaged building (Corso Vercelli and Via Cuneo intersection, Turin)

6.4. Roofs slope ad solar incoming radiation assessment

The model can also be applied to assess roofs slope and the solar incoming radiation on them. It was decided to carry on the evaluation circumscribing the tested area to the “Officine Grandi Riparazioni” and other two adjacent building roofs *(Frame 1, fig. 94)*. On one of these are already installed solar panels. The tested area was extracted using the “Extract by mask” ArcMap tool *(Fig. 90)*.

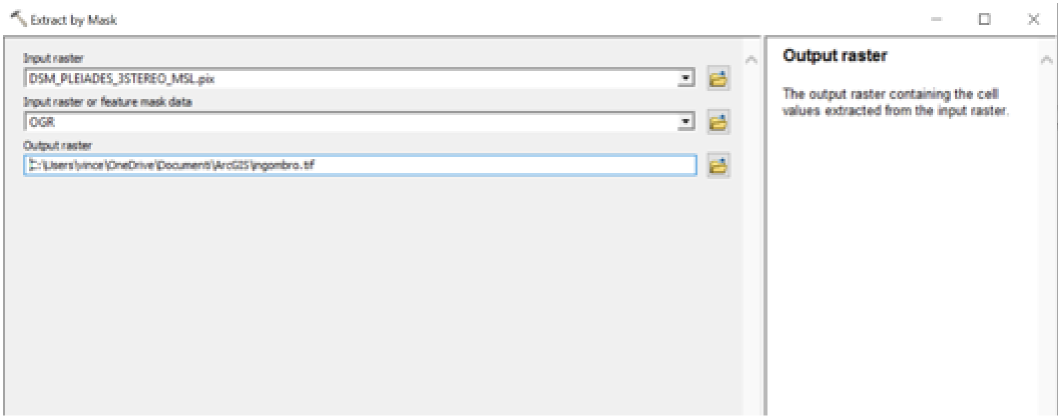

Figure 89 - Extract by mask ArcMap tool

For the slope determination was used the “Slope” ArcMap tool *(Fig. 91),* fixing the output values of the slope in degrees and the z factor, which “adjusts the units of measure for the z-units when they are different from the x,y units of the input surface” (ArcMap 10.5.1 Help) to 0,1. As it is possible to appreciate in the frame 2 of the figure 94 the slope goes from a maximum value of 45,53° to 0,02°. The tool calculates the slope considering the difference in height, thus the value 45 is not representative because represent the drop between two pieces of roof without connection solution. Moreover, the panels seem, from a first visual analysis, to have the same slope of the OGR roof. This aspect could be very interesting, if there will be in the future intinction to install plane solar panels on the OGR roofs.

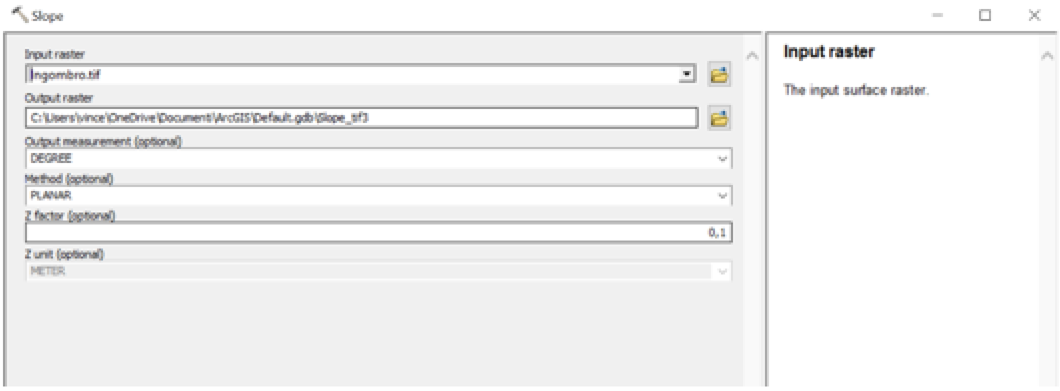

Figure 90 - Slope ArcMap tool

Afterwards, in the interest of assess the “compass direction that the downhill slope faces for each building face location” (ArcMap Help), was carried on an “Aspect” *(Fig. 92)*. The product raster *(Frame 3, fig. 94)* highlight as the supposed possibility of panels installation is confirmed, as the solar direction exposition of those part of the OGR roof is the same of the solar panels (South-SouthWest). In Europe the ideal orientation for photovoltaic panels is in the South (Riccò, 2013).

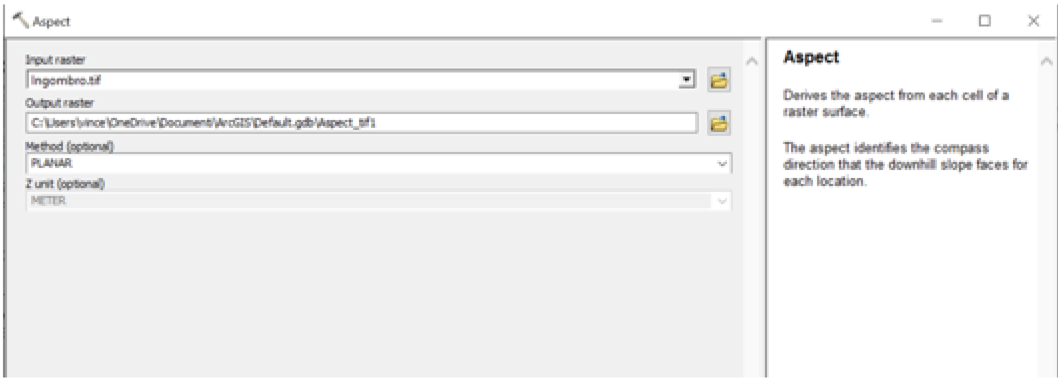

Figure 91 - Aspect ArcMap tool

Thus, it was decided to determine the solar radiation incoming on the OGR roof *(Frame 5, fig. 94)*. It was possible thanks to the employ of “Area Solar Radiation” ArcMap tool *(Fig. 93),* which “derives the incoming solar radiation from a raster surface” (ArcMap Help). In the settings it was also fixed the time period of calculation (multiple days in a year, “performing calculations for a specific multiple-day period within a year" (ArcMap 10.5.1 Help)) to the default time configuration: starts on day 5 and ends on day 160 of the current Julian year.

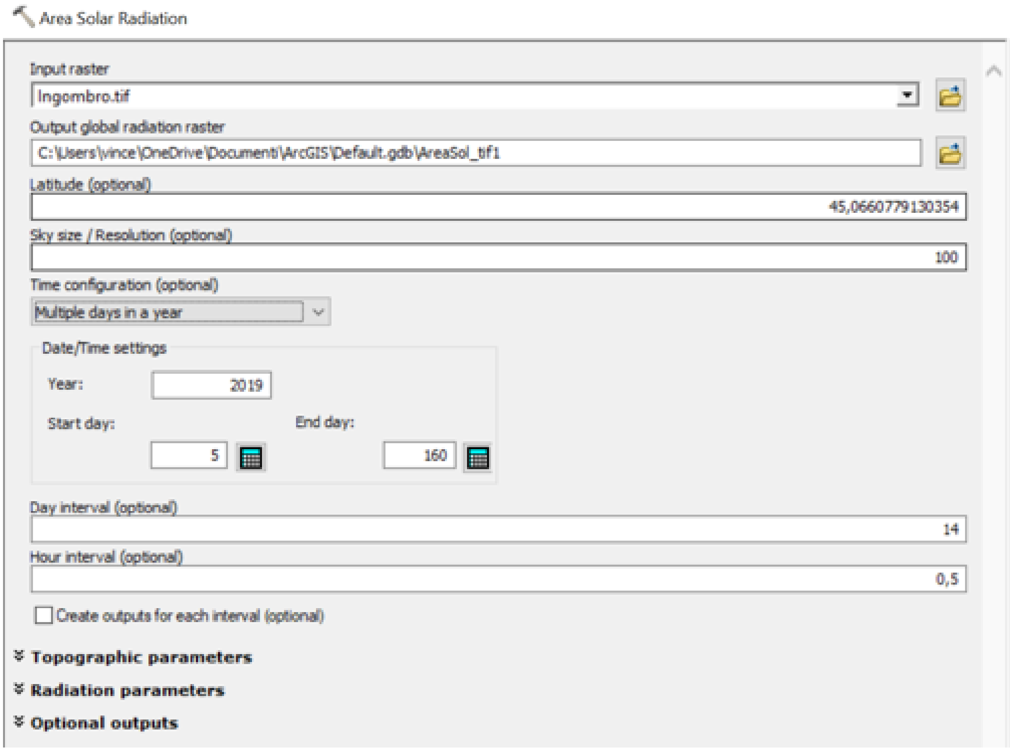

Figure 92 - Area Solar Radiation ArcMap tool

The generated raster *(Frames 4 - 6, fig. 94)* shows that maximum solar incoming radiation in the framed area is 2579 W/m^2 and that on the OGR rooftop it is almost the same of the solar panels or even higher in some points. This mean that these hypothetical solar panels installed on that roof would lead to more generated power.

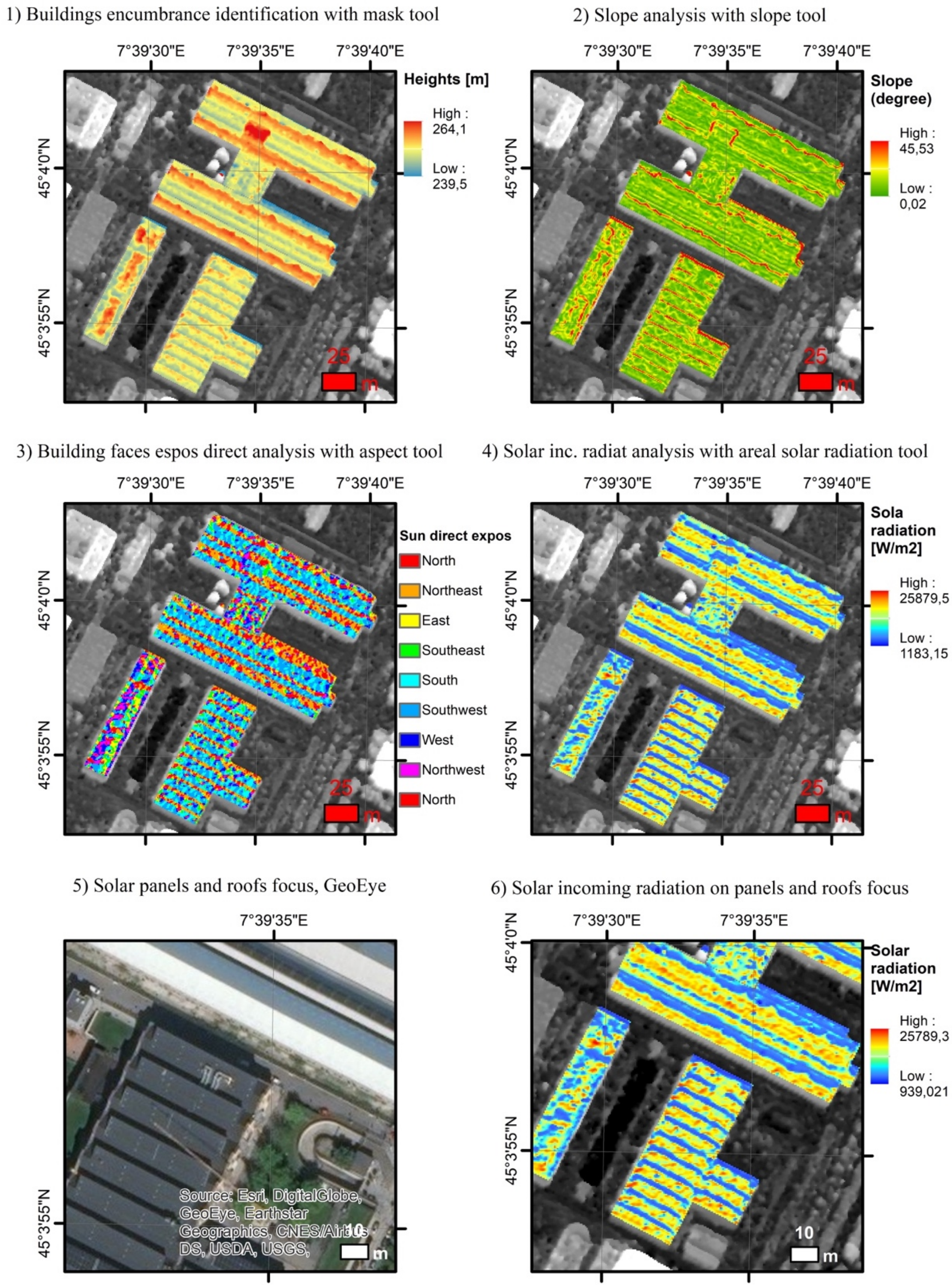

Figure 93 - 1) Buildings encumbrance identification, 2) slope analysis, 3) building faces exposition direction analysis, 4) solar incoming radiation analysis, 5) solar panels and roof focus, 6) solar incoming radiation on panels and roofs focus (From Pléiades-1A two-stereo DSM)

It was searched in literature (Riccò, 2013) the formula related to the calculation of the photovoltaic panels yield:

$$Yield\ (\%) = \frac{Photovoltaic\ module\ power\ [W/m^2]}{Solar\ power\ incident\ in\ the\ area\ of\ panel\ module\ [W/m^2]} \cdot 100$$

Other factors affect the efficiency of the production of a photovoltaic system can be grouped into 2 macro sections:

- external factors that represent the context that is the surrounding environment (temperature and cleanliness) and the position (orientation, shading and inclination)
- internal factors all the products and components that must be installed with their guarantees (quality and obsolescence time).

Returning to the slope determination, the extracted data can also be used to enrich the municipal database, transforming with a "Raster to point" operation the raster data in vector and then calculating the average slope of the buildings roofs.

7. Conclusion and future development

The paper investigated DSMs extracted by different stereo pairs VHR images acquired from Deimos-2, Pléiades-1A and WorldView-3, acquired over the area of the city of Torino in the North-West of Italy used as testfield. The aim of the paper was to address the differences in visual characteristics, resolution and accuracy of the generated digital surface models. In order to collimate the stereo pairs (or triplet for Pléiades-1A) there were generated DSM both with the use of TPs only and adding GCPs to them. It was found that the use of TPs only better collimate the block, showing a better geometries shaping and reducing the noises in narrow streets or near close buildings. The geoid referred DSM were subsequently characterized and asses evaluating them from a qualitative and quantitative point of view. The first one, consisting in a qualitative analysis of the data, evaluating noise, sharpness in city canyons, ability in shaping the geometries and identification of details (vegetation, small objects on the ground). From this assessment emerged that Deimos-2 model (with a resolution of 2 m) results very poor, showing an elevation accuracy that does not permit to identify or distinguish the shape of the object on the ground and presenting a lot of issues related to noise and false elevation spikes. Despite to what expected, concerning the other DSM it was found that for WorldView-3, even if presents an high GSD in the acquisition, the generated DSM results inferior in comparison to Pléiades-1A one, showing in particular some problems in the canyon shaping. Focusing on Pléiades-1A models, the one generated in tri-stereo mode exhibit higher capacities in the identification of details (vegetation, small objects on the ground), which in some case can turn into noise; the model generated in two-stereo mode instead demonstrate an improved sharpness in city canyons and roofs geometries shaping.

The qualitative output were double checked with the quantitative analysis of the data, concerned the evaluation of the altimetric accuracy of the models through the use of two different benchmarks. The DSMs accuracy was assessed quantitatively using a cadastral points vector file, reporting for each point ground height values, and a cadastral volumetric raster, reporting the roofs gutter heights. The comparison in terms of difference height values (between the DSM and the benchmark), calculated on a set of sample points, returned what had arisen from the qualitative investigation: Pléiades-1A DSMs exceed also in height accuracy level WorldView-3 product. In particular the two-stereo mode result more efficient in ground height calculation and the tri-stereo one in the calculation of the buildings heights.

The extracted models were then employed in different domain of applications: existing cartography update, soil consumption analysis, urban green classification, evaluation on mobile network antenna positioning, emergency management, building damage assessment, roof slope and solar incoming radiation assessment.

The present study showed the efficiency of Pléiades dataset and the great contribution that a DSM can cast in the urban planning, energy, emergency management, raising the possibility of services improvements in megacities in under developed areas (e.g., China, India). Already today and more in the future this technology will be essential for areas in which there is not an updated reference cartography.

It was established that the quality of a DSM has not a resolution dependence only. If in the next future more stereo pairs will be available over the area of Turin, it could be very interesting to investigate on them in order to find other discriminating factors, testing them with different blending techniques and more advanced benchmarks (LIDAR) for the quantitative assessment.

8. Attachments

8.1. Attachment 1 - Satellites features comparative table

N. of satellite	WORLDVIEW-3	DEIMOS-2	PLEIADES-1A
Launch date	August 13th, 2014	June 19th, 2014	December 16th 2011 and December 2nd 2012
Lifetime	Minimum 7.3 years; est. 10 to 12 years	est. 7 years	
Orbit type	Sun-Sync, 10:30 AM desc. Node Altitude: 617 km	Sun-Sync, 10:30 AM desc. node Altitude: 620 Km	Sun-Sync Altitude: 694 Km
Orbit inclin.	Not found	Not found	180°
Spectral bands	Pan: 450 - 800 nm Coastal: 400 - 450 nm Red Edge: 705 - 745 nm Near - IR2: 860 - 1040 nm Near - IR1: 770 - 895 nm Green: 510 - 580 nm Yellow: 585 - 625 nm Red: 630 - 690 nm Blue: 450 - 510 nm	Pan: 560-900 nm; Blue: 466-525 nm, Green: 532-599 nm, Red: 640-697 nm, Near Infrared (NIR): 770-892 nm	Pan: 480-830 nm Blue: 430-550 nm Green: 490-610 nm Red: 600-720 nm Near Infrared (NIR): 750-950 nm
Detectors	Not found	Not found	Not found
Dynamic range	11-bits per pixel Pan and MS; 14-bits per pixel SWIR	10 - bits per pixel	
Optical system	Not found	Not found	High resolution optical Multispectral; 5 VNIR channels, 4 multi-spectral (MS), one panchromatic (PAN)

GSD (nadir)	Pan Nadir: 0.31 m 20° off-nadir: 0.34 m Multispectral Nadir: 1.24 m 20° off-nadir: 1.38 m	Pan: 1 m Pan sharped after ground processing 0.75 m Multispectral: 4 m	50-cm panchromatic 50-cm color (pansharpened) 2-meter multispectral Bundle: 50-cm panchromatic and 2-meter multispectral
Swath (nadir)	13.1 km	12 Km	20 km
Onboard Storage	2199 Gb solid state with EDAC	256 Gbit - Equivalent to 1400 km observation strip	Not found
Capacity	680,000 km2 per day	Up to 200,000 km2 per day	1M km2 per day, per satellite
Geolocation Accuracy (CE90)	Predicted <3.5 m CE90 without ground control	100 m CE90 without GCP	With ground control points: 1m Without ground control points: 3m (CE90)

8.2. Attachment 2 - GCPs used for Pléiades-1A two and tri stereo DSMs generation

GCP1 (393156.000 E, 4995764.000 N - WGS84 UTM 32N, 258 m.s.l)

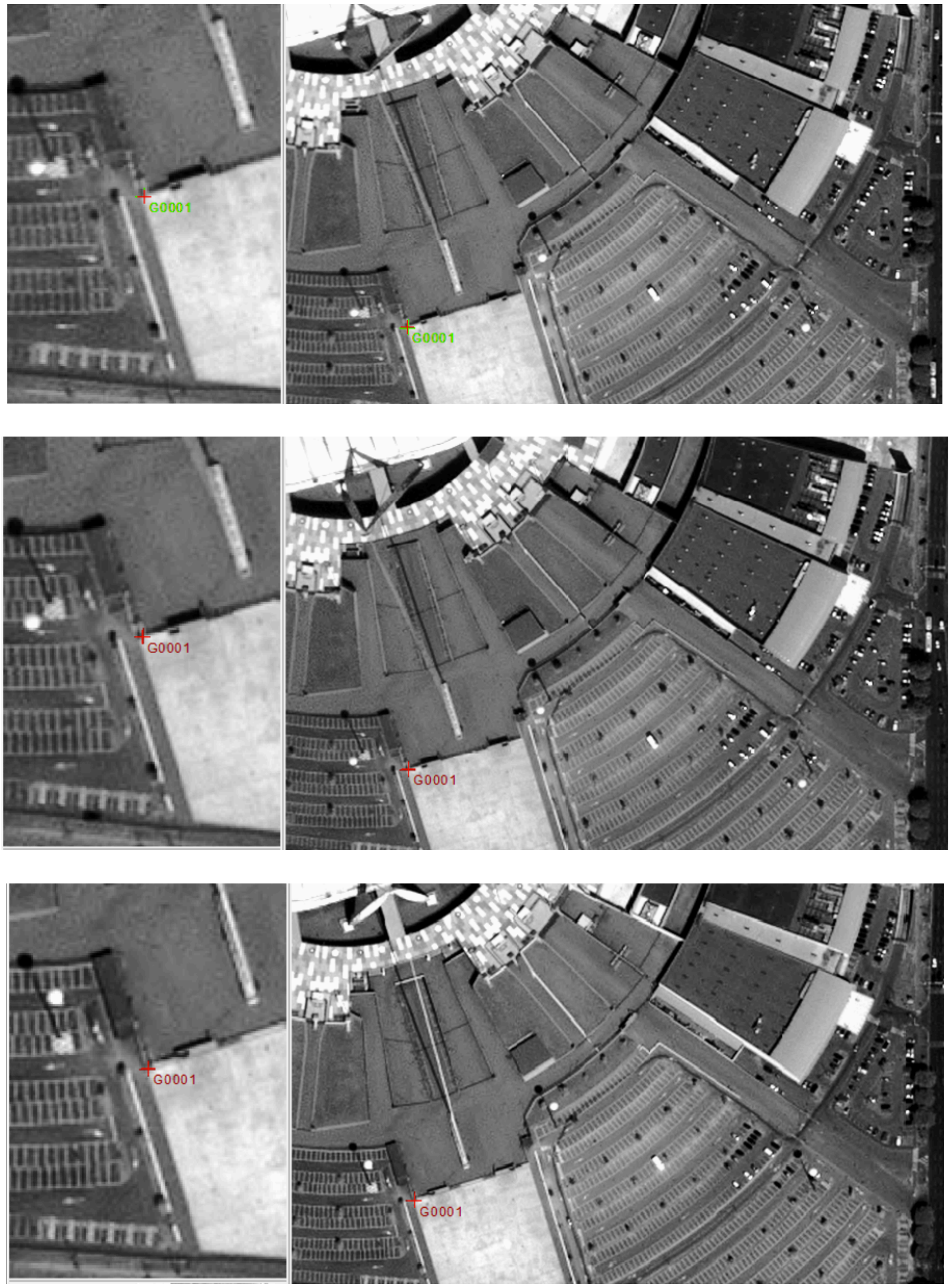

GCP2 (399011.000 E, 4992201.000 N - WGS84 UTM 32N, 217 m.s.l.)

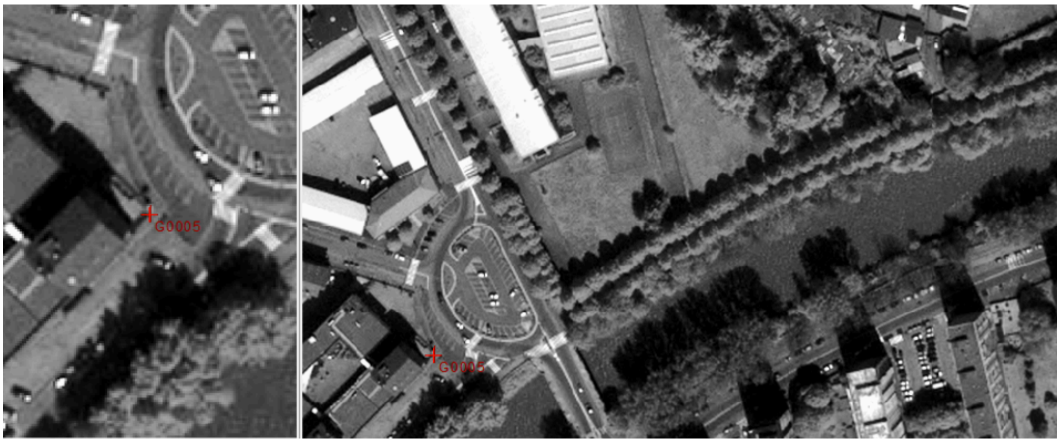

GCP3 (395506.000 E, 4993403.000 N - WGS84 UTM 32N, 236 m.s.l.)

GCP4 (390640.000 E, 4986993.000 N - WGS84 UTM 32N, 257 m.s.l.)

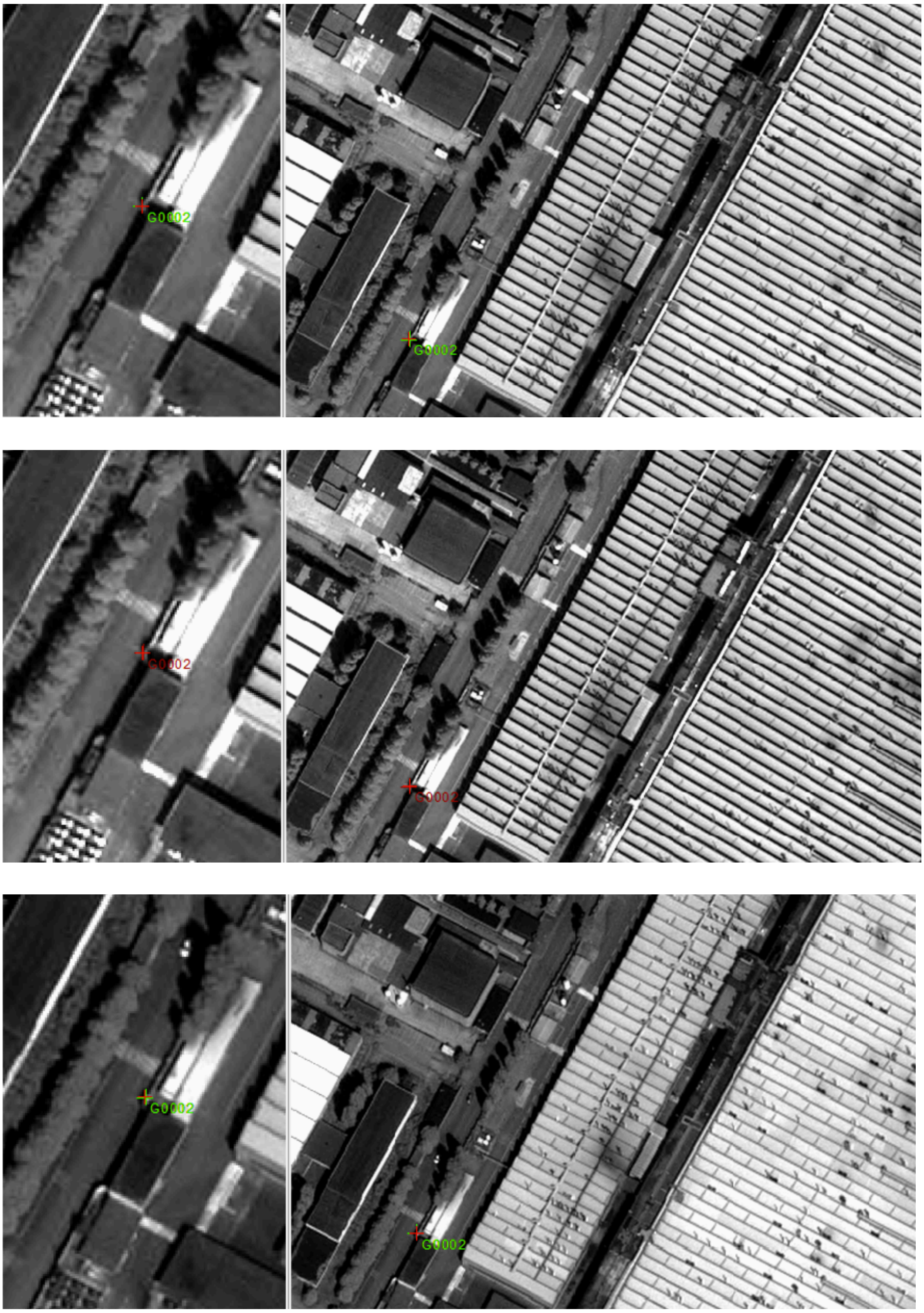

8.3. Attachment 3 - GCPs used for WorldView-3 DSMs generation

GCP1 (396534 E, 4995153 N - WGS84 UTM 32N, 237 m.s.l.)

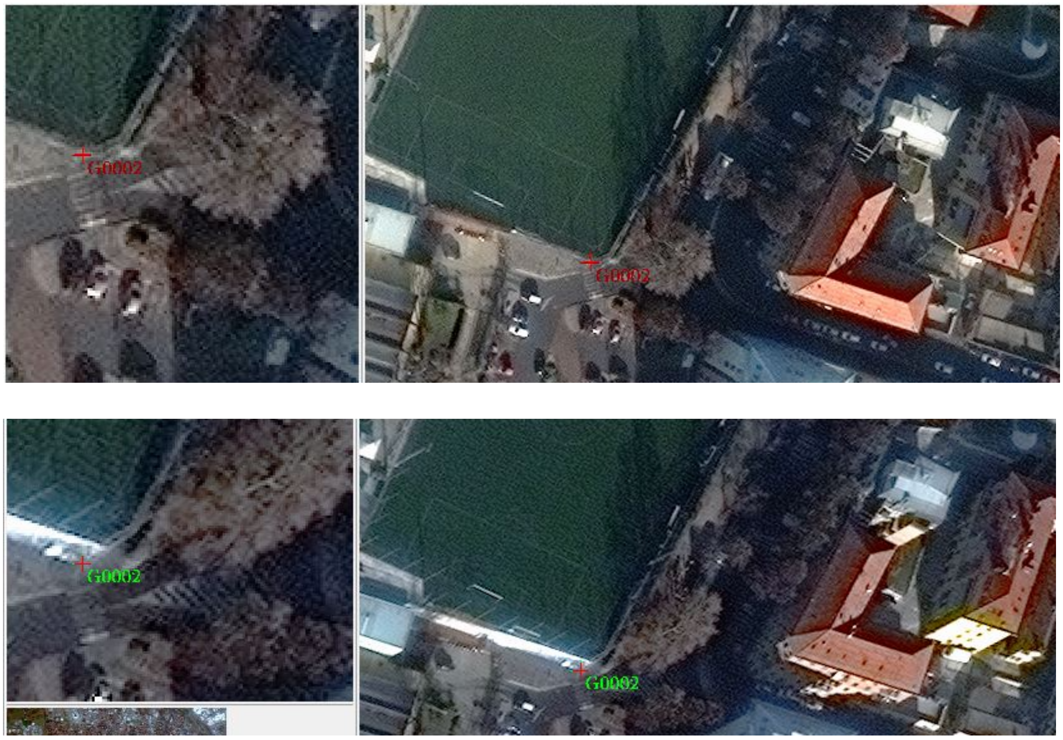

GCP2 (396004 E, 4987953 N - WGS84 UTM 32N, 219 m.s.l.)

GCP3 (395427 E, 4993113 N - WGS84 UTM 32N, 234 m.s.l.)

GCP4 (394350 E, 4991557 N - WGS84 UTM 32N, 250 m.s.l.)

9. Bibliography

- Airbus Defence & Space (2013) *Pléiades Spot the Detail*, *Geo-Intelligence Fact Sheet*. Available at: https://www.intelligence-airbusds.com/files/pmedia/public/r49228_9_pleiades_product.pdf.
- Amato, L. (2015) 'Rilievo del territorio mediante tecniche lidar terrestri ed aeree', (March).
- Amela, R., Agostino, M. De and Soffia, C. (2011) 'Modellazione numerica degli alvei fluviali mediante l'uso di DSM', *Atti 15a Conferenza Nazionale ASITA*, (2008), pp. 71–83. Available at: http://www.attiasita.it/ASITA2011/Pdf/129.pdf.
- Archeologica, N. D., Studio, E. N. and Edilizia, D. (2017) 'open area', pp. 219–238.
- Barilotti, A. *et al.* (2014) 'Confronto Tra Tecniche Classiche E Metodi Diretti Multirisoluzione Per La Produzione Di Modelli Digitali Del Terreno Da Scansioni Lidar', (June).
- Berry, P. A. M., Garlick, J. D. and Smith, R. G. (2007) 'Near-global validation of the SRTM DEM using satellite radar altimetry', *Remote Sensing of Environment*, 106(1), pp. 17–27. doi: 10.1016/j.rse.2006.07.011.
- Blaunstein, N. (1998) 'Average field attenuation in the nonregular impedance street waveguide', *IEEE Transactions on Antennas and Propagation*, 46(12), pp. 1782–1789. doi: 10.1109/8.743813.
- Codou, G. *et al.* (2016) 'Operational scheduling of Direct Tasking innovative concept to improve reactivity on earth observation system', in *SpaceOps 2016 Conference*. Reston, Virginia: American Institute of Aeronautics and Astronautics. doi: 10.2514/6.2016-2357.
- Dicar, M. F. (2015) 'Come si orienta un blocco fotogrammetrico'.
- Fleury, B. H. and Leuthold, P. E. (1996) 'Radiowave propagation in mobile communications: An overview of European research', *IEEE Communications Magazine*, 34(2), pp. 70–81. doi: 10.1109/35.481300.
- Galileo, E. *et al.* (2015) *DEIMOS-2 Imagery User Guide*.
- Gao, C., Zhu, H. and Guo, Y. (2012) 'Analysis and improvement of SUSAN algorithm', *Signal Processing*. Elsevier, 92(10), pp. 2552–2559. doi: 10.1016/j.sigpro.2012.03.002.

- Geomatica (no date) ‘Geomatica Training Guide’.
- Hu, F. *et al.* (2016) ‘DEM extraction from worldview-3 stereo-images and accuracy evaluation’, *International Archives of the Photogrammetry, Remote Sensing and Spatial Information Sciences - ISPRS Archives*, 2016–Janua(July), pp. 327–332. doi: 10.5194/isprsarchives-XLI-B1-327-2016.
- Ita, E. N. G. *et al.* (2019) ‘Geoeye-1’, pp. 1–2.
- Kruse, F. A., Baugh, W. M. and Perry, S. L. (2015) ‘Validation of DigitalGlobe WorldView-3 Earth imaging satellite shortwave infrared bands for mineral mapping’, *Journal of Applied Remote Sensing*, 9(1), p. 096044. doi: 10.1117/1.jrs.9.096044.
- *Latitude and longitude / GPS-coordinates* (no date). Available at: https://www.gps-latitude-longitude.com/ (Accessed: 19 April 2019).
- *Personal notes from Geomatica course, M. Caprioli, Polytechnicof Bari.*
- Led, U. and Diode, L. E. (2018) ‘LED: principio di funzionamento (I)’.
- M. Thompson et al. (2017) ‘HIGH RESOLUTION LANDCOVER MODELLING WITH PLÉIADES IMAGERY AND DEM DATA IN SUPPORT OF FINE SCALE LANDSCAPE THERMAL MODELLING’.
- *Personal notes from Remote sensing course, P. Boccardo, Polytechnicof Turin.*
- Manuel Ángel Aguilar et al. (2013) ‘DSM extraction from worldview.pdf’.
- Mason, M. and Data, A. (2008) ‘Cartografia Territorio’.
- Maune, D. F. (2011) ‘Digital Elevation Model (DEM) Whitepaper NRCS High Resolution Elevation Data’, p. 120.
- Moser, J., Albrecht, F. and Kosar, B. (2010) ‘Beyond visualisation - 3D GIS Analyses for virtual city models’, *International Archives of Photogrammetric, Remote Sensing and Spatial Information Sciences*, XXXVIII(4/W5), pp. 143–146.
- Nascetti (2011) ‘Generazione di DSM da stereo coppie satellitari.pdf’.
- Panagiotakis, E. *et al.* (2018) ‘Validation of Pleiades Tri-Stereo DSM in Urban Areas’, *ISPRS International Journal of Geo-Information*, 7(3), p. 118. doi: 10.3390/ijgi7030118.
- PCI (2013) ‘Geomatica OrthoEngine Pleiades 1A data – DEM extraction and DSM to DTM conversion’, pp. 1–12. Available at: http://www.pcigeomatics.com/pdf/Pleiades_DEM_extraction_and_DSM_to_DTM_conversion.pdf.

- PCIGeomatics (2019) ‘Tie points explained’, pp. 1–2.
- Poon, J. *et al.* (2005) ‘Quality assessment of digital surface models generated from ikonos imagery’, *Photogrammetric Record*, 20(110), pp. 162–171. doi: 10.1111/j.1477-9730.2005.00312.x.
- Queija, V. R., Stoker, J. M. and Kosovich, J. J. (2005) ‘Recent U.S. Geological Survey Applications of Lidar’, *Photogrammetric Engineering & Remote Sensing*, (January), pp. 5–9.
- Riccò, F. (2013) ‘Stima del rendimento effettivo (Performance Ratio) di moduli fotovoltaici con e senza modelli matematici’.
- Roggero, M. (2014) ‘Cartografia’.
- Saha, K. (2014) ‘DSM extraction and evaluation from Cartosat-1 stereo data for Bhopal city , Madhya Pradesh’, *International Journal of Scientific and Research Publications*, 4(5), pp. 4–8.
- Sandu, P. B. C. (2018) ‘Building_damage_assessment_scale_tailored_to_remot.pdf’.
- Satellite imaging corporation (2016a) ‘CARTOSAT-1’, 1, pp. 8–11.
- Satellite imaging corporation (2016b) ‘Geoeye-1’, pp. 8–11.
- Satellite imaging corporation (no date) *Pleiades-1A Satellite Sensor | Satellite Imaging Corp*. Available at: https://www.satimagingcorp.com/satellite-sensors/pleiades-1/ (Accessed: 19 April 2019).
- Shi, W., Zheng, S. and Tian, Y. (2009) ‘Adaptive mapped least squares SVM-based smooth fitting method for DSM generation of LIDAR data’, *International Journal of Remote Sensing*, 30(21), pp. 5669–5683. doi: 10.1080/01431160802709237.
- Shortridge, A. (2006) ‘Shuttle Radar Topography Mission Elevation Data Error and Its Relationship to Land Cover’, *Cartography and Geographic Information Science*, 33(1), pp. 65–75. doi: 10.1559/152304006777323172.
- ArcMap 10.5.1 Helper
- ISPRA http://www.isprambiente.gov.it/it/banche-dati/repertorio-dello-stato-di-attuazione-dei-piani-per-il-parco-nei-parchi-nazionali/regione-piemonte